Republic of Iraq
Ministry of Higher Education and Scientific Research
University of Babylon
College of Education for Pure Sciences
Department of Physics

Preparation of Silicon Rubber-Polyurethane-lead Composite for Attenuation the Nuclear Radiation

A thesis
Submitted to the Council of the College of Education for Pure Sciences of University of Babylon in Partial Fulfillment of the Requirements for the Degree of Doctor of Philosophy in Education / Physics

By

Mousa Hawan Naeem

B. Sc. in Physics
(University of Baghdad, 2003)

M. E. Sc. in Physics
(University of Babylon, 2019)

Supervised by

Prof. Dr. Sameer Hassan H. Al-Nesrawy
Department of Physics College of Education for Pure Sciences

Prof. Dr. Mohammed H. Al-Maamori
Department of Bio-Medical Engineering College of Al-Mustaqbal

2023 A.D **1445 A.H.**

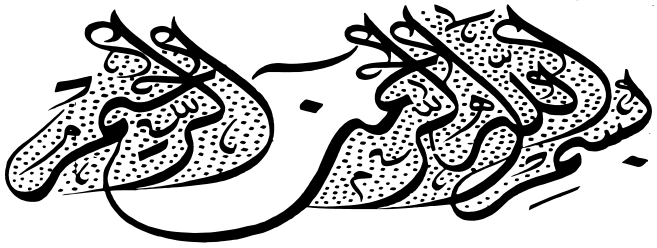

((قالوا سبحانك لا علم لنا إلا ما
علمتنا إنك أنت العليم الحكيم))

صدق الله العلي العظيم

سورة البقرة (الآية ٣٢)

Supervisor Certification

We certify that this Thesis entitled **"Preparation of Silicon Rubber-Polyurethane-lead Composite for Attenuation the Nuclear Radiation"** is prepared by the student (**Mousa Hawan Naeem**) under our supervision at the College of Education for Pure Sciences, University of Babylon as partial fulfillment of the requirement for the degree doctor of philosophy education / physics.

Signature:
Name: **Sameer Hassan Al-Nesrawy**
Title: Professor
Date: / / 2023

Signature:
Name: **Mohammed H. Al-Maamori**
Title: Professor
Date: / / 2023

Head of the Department Certificate

In view of the available recommendations, I forward this Thesis for debate by the examining committee.

Signature:
Name: **Dr. Khalid Haneen Abass**
Title: Professor
(Head of Physics Department)
Date: / / 2023

Dedication

To the Great Prophet of Good the Seal of Prophets "Mohammed"

To the owner of the age and time,

"Imam Al-Mahdi"

To my late father and mother

To my brother the martyr (Sadiq)

To the best of my life, my children

To my dear wife

To my teachers, Dr. Sameer Hassan Hade Al-Nesrawy and Dr. Mohammed H. Al-Maamori

To all my dear teachers and friends

To everyone who helped me with this work

Mousa ... ✍

ACKNOWLEDGEMENTS

In the name of Allah, the most merciful the most compassionate all praise be to Allah the lord of the worlds and prayers and peace be upon Mohamed his servant and messenger and to his good and pure household.

First and foremost, I thank the Almighty Allah for helping and giving me the ability to complete this thesis. Our thanks go to Prophet Mohammed and AhlulBayt (blessings of Allah be upon them all). As I finish my thesis, I cannot but extend my sincere thanks and great gratitude to my dear supervisors Dr. Sameer Hassan Hadi Al-Nesrawy and Dr. Mohammed H. Al-Maamori for his distinguished efforts, valuable advice and continuous directions. Many Thanks to the Deanship of the College of Education for Pure Sciences / University of Babylon and the Department of Physics.

Finally, I extend my heartfelt thanks to those who supported me and alleviate the difficulties I encountered during my work and to everyone who helped me in one way or another while working. I wish success to everyone.

Mousa ..

Abstract

This study includes the preparation of a rubbery-polymeric batches that is mainly used in the production of a protective suit for radiation shielding. Silicone rubber (SiR) was chosen as a basic material in the work with polyurethane (PU) in different weight ratios of (100:0, 90:10, 80:20, 70:30, 60:40, 50:50, 40:60, 30:70, 20:80, and 0:100) pphr With hardeners a ratio 1:1

The mechanical properties such as tensile strength, elongation, hardness, and modulus of elasticity were examined of the (SiR:PU) rubber blend. Hardness was measured using stand ASTM-D1415 (Shore A), and tensile testing was done used stand ASTM-D 412-88 (T10-Tensometer). Sample (SiR_{80}:PU_{20}) was the most suitable for mechanical properties.

The micro lead powder was added to (SiR_{80}:PU_{20}) rubber blend as a reinforcement material in different loading ratios of (0, 20, 40, 60, 80, 100, 150, 200, 250, and 300) pphr for each (SiR_{80}:PU_{20}) rubber blend.

Infrared spectrometry (FTIR) was performed on the rubber blends, as was scanning electron microscopy (SEM), where the lead was equally distributed on the SiR:PU/micro-Pb composites. Then the mechanical properties represent of hardness, tensile strength, elongation, and modulus of elasticity were examined. The samples were presented to examine the properties of the radiation by using a Geiger counter using two radiation elements (Cs^{137}) and Co^{60}. The sample SiR_{80}:PU_{20}/micro-Pb_{300} was selected as the most suitable.

Rubber composites (SiR_{80}:PU_{20}/micro-Pb_{300}) were cast using a casting method, and then nano-lead material was used as a support material at several weight ratios of (0, 0.2, 0.4, 0.6, and 0.8) pphr. The samples were characterized by FTIR and SEM. The samples were also examined for mechanical properties and radiation properties by using a Geiger counter using two radiation elements (Cs^{137}) and (Co^{60}). According to the results of linear absorption coefficient (μ),

mass absorption coefficient (μ_m), and half thickness ($X_{1/2}$), the loading ratio of nano and micro lead powder in hexane increases the linear and mass absorption coefficients and decreases the half thickness. This holds for all radioactive sources.

The nanocomposite of (SiR_{80}:PU_{20}/micro-Pb_{300}:nano-$Pb_{0.8}$) was demonstrated high radiation attenuation efficiency compared to other samples , which makes it suitable for use in shielding applications as an armored suit to protect medical and industrial fields.

List of Contents

Chapter Three: Materials and experimental techniques

Chapter Four: Results and Discussion

List of Figures

List of Tables

List of Symbols

Symbol	Physical Meanings	Unites
ΔL	Length Difference	cm
A	Area	cm^2
C	Velocity of Light	$m.s^{-1}$
D	dimeter of indenter	cm
d	depth resulting from the penetration of the test body into the water	cm
E	Elastic Modulus (Young's Modulus))	MPa
E_{ph}	Photon Energy	eV
F	Force	N
g	acceleration due to gravity	cm/s^2
I	The intensity of the transmitted radiation	-
I_0	The intensity of the incident radiation	-
K	Thermal Conductivity	W/m.°C
L	Length	cm
L_0	Initial Length	cm
N	number read from the test device after performing the test	pphr
P	applied load	N/cm^2
t	Thickness	cm
T_g	Glass transition temperature	°C
T_m	Melting temperature	°C
$X_{1/2}$	Half thickness	cm
α	angle of indenter	degree
ε	Strain	Unit less
λ	Wavelength of Light	nm
μ	Linear absorption coefficient	cm^{-1}
μ_m	Mass absorption coefficient	$g^{-1}. cm^2$

ρ	Rubber density	g/cm^3
Σ	Stress	N/m^2
υ	Photon Frequency	Hz
h	Planck's constant	J.s

List of Abbreviations

Abbreviations	Physical Meanings
ASTM	American Society for Testing and Materials
BR	Butadiene Rubber
CB	Carbon black
CMC_S	Ceramic Matrix Composite
CNMs	Carbon Nano Matrix
CNT_S	Carbon nanotubes
EHV	Extremely High Voltage
FTIR	Fourier transform infrared
G_nP_S	Graphene platelets
HVL	Half Value Layer
IIR	Isobutylene isoprene rubber
IMC_S	Intermetallic Matrix Composite
IRHD	International Rubber Hardness Degree
MAC	Mass Attenuation Coefficient
Micro-Pb	Micro-lead
MMC_S	Metal Matrix Composite
Nano-Pb	Nano-lead
NPs	Nano Particles
NR	Natural rubber
PMC_S	Polymer Matrix Composite
pphr	Part Per Hundred of Rubber
psi	Pounds per square inch
PU	Polyurethane
SBR	Synthetic rubber (Styrene-Butadiene Rubber)
SEM	scanning electron microscope
SiR	Silicon Rubber
TIM_s	Thermal Interface Materials

Chapter One Introduction and Literature Review

Chapter One: Introduction and Literature Review

1.1 Introduction

Historically, "rubber" has been used for any material that deforms under stress with a relatively modest load or deflection ratio and then snaps back into place with surprising vigor. There is no longer any external pressure. Different materials may be roughly separated into natural and synthetic rubber categories based on these criteria [1] .

Silicon rubber (SiR) is a unique rubber that exhibits remarkable durability under extreme conditions. SiR-based conductive composites are popular in wearable electronics [2**]**.

Polymers have rapid growth in recent years at the cost of more conventional materials in both traditional uses and emerging applications and markets. This increase may be attributed to many useful characteristics of materials', including their low weight, resistance to corrosion, simplicity of processing, and cost-effectiveness. Elastomers, a class of natural and synthetic polymers, are valued for their widespread use in the production of elastic bands, tires, seals, hoses, etc., as well as for their capacity to recover entirely from significant deformations while maintaining instantaneous elasticity [3]. The mechanical characteristics of the blend of BR: SBR and EPDM was sought by conducting compression resistance and shore hardness tests to determine the variation in properties as a function of the amount of synthetic rubber present in the sample. This is necessary because the market is flooded with elastomers, each possessing unique mechanical properties [3].

1.2 Liquid Silicon Rubber

It is a synthetic rubber manufactured in China from a silicone compound composed of silicon, carbon, hydrogen and oxygen [4]. A Variety of Silicone Rubber Compositions Silicone rubber, which finds widespread

use in manufacturing, often consists of a dual polymer composition, with the addition of fillers for either improved qualities or lower costs, calling this material “silicon” is misleading. Chemists use the suffix to refer to substances in which an oxygen atom forms a double bond with another atom in the main chain. For a while after the discovery of silicon, scientists believed that its oxygen atoms were linked in this way, the appropriate technical word for many silicone rubber formulations is dimethyl, polysiloxane, and silicone rubber [5].

Silicon dioxide, also referred to as silica, is abundant in large quantities within quartz sand. Several techniques involve applying heat to a blend of silicone and methyl chloride. Polydimethylsiloxane, the resulting polymer, may be subjected to additional polymerization methods, which vary based on the desired application. In the context of injection or extrusion molding processes, it is common to include a catalyst, along with other additives such as colors, in the raw silicone compound. The manufacturing process ends with the curing stage[6]. Table (1-1) presents some properties of silicone rubber [7].

Table. (1-1): Some properties of liquid Silicon Rubber [7]

Property	**Value**
Chemical formula	$[\text{-Si-O-}]_n$
Chemical symbol	SiR
Color	Liquid white
Density	(0.95 - 1.20) g/cm^3
Molecular Weight	28.085 g/mole
Melting point	1410 °C
Boiling point	2355 °C
Glass transition temperature (T_g)	-125 ˚C
Melting temperature (T_m)	450 ˚C

1.3 Liquid Silicon Rubber Properties (L-SiR)

The L-SiR exhibits consistent performance across a temperature range of 100 to 300, showing remarkable resistance to extreme cold and heat [8]. In addition to its resilience, elasticity, and resistance to creep, repetitive bending, rupture, and deformation under pressure, silicon rubber is also a superb thermal insulator and a good electrical (high voltage) insulator. Tensile strength at high temperatures surpasses even organic rubber materials, and it may be used as a fireproofing measure in certain cases. These properties make silicone rubber the material of choice for initial shape retention and mechanical strength under extreme conditions of heat or cold [9].

1.3.1 Liquid Silicon Rubber Applications

One of the primary distinguishing characteristics of this particular category is its inherent safety, as shown by medical equipment, blood vessels, and other related entities. The food industry encompasses it [10]. Certain businesses need materials that can survive high temperatures. In these sectors, the backside of rubber and printing modules is used to create certain forms. For instance, gypsum molding is employed in decorative works, while shapes for jewelry, buttons, and other industries are also produced using this method [11]. Liquid silicone rubber is also manufactured for biosciences applications (syringe pistons, closures for dispensing system, respirator masks), cosmetic products (mascara brushes, makeup packaging, make-up applicators, lipstick molds) and optics products (circular lenses, apparatus for producing collimated rays, Fresnel lenses and the free form lenses [12]. Freeze-tolerant solar water heating panels use the flexibility of silicone to accommodate expansion of water when repeatedly frozen [13].

1.3.2 Peroxide Treatment System

The silicon rubber industry makes extensive use of peroxide treatment. By-products from the curing process may be unsafe in food contact and medicinal settings. However, the peroxide breakdown products are considerably reduced when these products are treated in the (Postcure) furnace [14]. Dicumyl peroxide, one of the two most common organic peroxides, dissociates mostly into acetophenone and phenyl-2-propanol. There's also dichlorobenzene peroxide, which breaks down mostly into dichlorobenzoic acid and dichlorobenzene [15].

1.4 Polyurethane

Any long-chain organic composite with a urethane backbone is called polyurethane [16]. PU is a typical shorthand for it acts as an insulator to keep whatever it's covering safe from extreme temperatures or corrosive environments [17].

The composition is comprised of a sequence of organic entities that are chemically linked to a urethane moiety [18]. polyurethane (PU) to give durability and protection to the objects it covers from heat, cold, due to extensive uses [19, 20]. Polyurethane is the product of the reaction between an isocyanate with two or more isocyanate groups per molecule [$R(N=C=O)_n$] and a polyol with two or more hydroxyl groups per molecule $(R' - (OH))_n$ [21]. When an activator or catalyst is [22, 23].

The isocyanates and polyols employed in its production significantly impact the material's final qualities. Polyols' lengthy, pliable segments make for a supple polymer, whereas extensive chemical crosslinking makes something stiffer. Flexible polymers are produced by using elongated chains that possess a limited number of interconnections. Conversely, strong polymers are derived from shorter chains that exhibit a higher density of crosslinks. Additionally, foam polymers that are deemed beneficial

are created by employing elongated chains with intermediate networks [24]. Due to its crosslinks, polyurethane has a substantial molecular weight and three-dimensional network structure. Some industries treat polyurethane as a single, massive molecule; thus, ordinary polyurethanes don't melt or discolors when heated. These polymers are known as "thermoplastic polymers." Polyurethane's adaptability stems from the fact that its qualities may be tailored by adding various additives and manufacturing conditions, in addition to the chemistry of polyols and isocyanates [25].During production, small amounts of foaming agents can be added to polyurethane foam (including foam rubber), resulting in a lower-density foam with improved energy absorption and thermal insulation. This, along with the many other additives and processing conditions, gives polyurethane its wide range of properties, making it a polymer with many applications [26]. The molecular units of the polyurethane, shown as [-NH-(C = O)-O-] in the Figure (1-1), are urethane groups. Table (1-2) represents some of the properties of polyurethane [24].

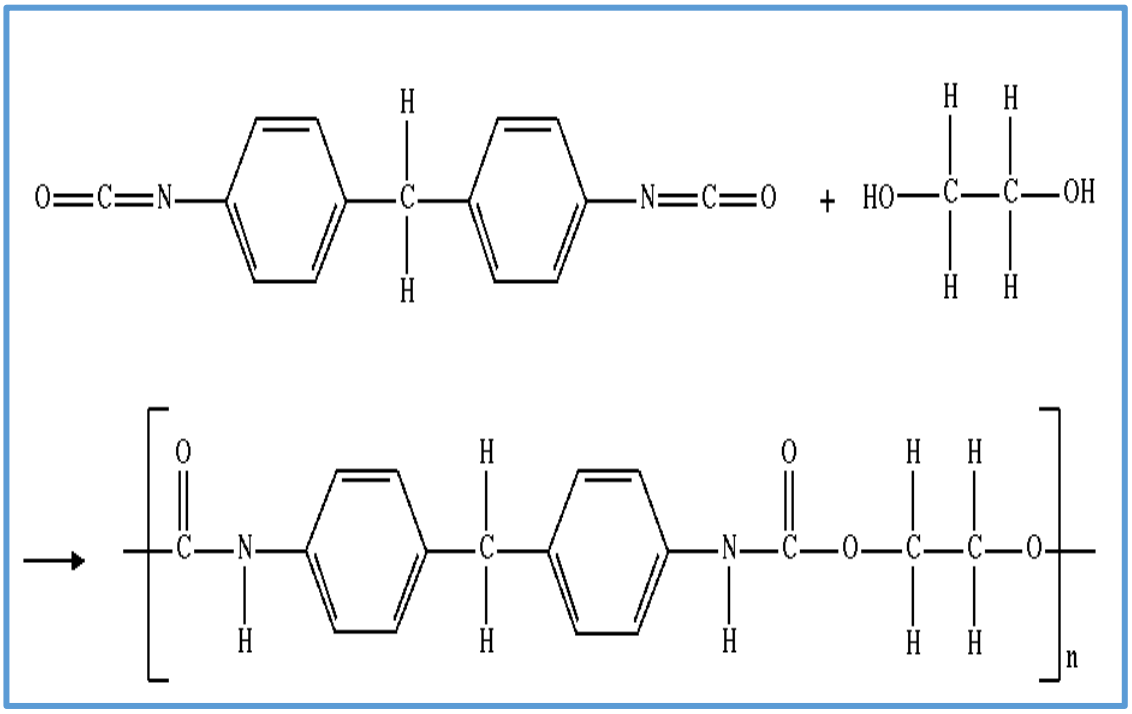

Fig. (1-1): The chemical formula of polyurethane [27]**.**

Table. (1-2): Some properties of polyurethane [28]

Property	Value
Chemical formula	$C_{17}O_4H_{16}N_2$
Chemical symbol	PU
Color	yellow
Density	1.005 g/cm^3
Molecular Weight	548.59 g/mol
Melting point	48-50 °C
Boiling point	(182-184) °C
Glass transition temperature (T_g)	200 °C
Melting temperature (T_m)	163 °C

1.4.1 Polyurethane Applications

The PU material used in parking garage floors is not easily removed because it prevents water leakage and has strong abrasion resistance, quartz grains (sand) are added to the coating to give it a rough surface and enhance the anti-slip property, which extends the life of the coating from 8 to 10 years with regular maintenance. which in general protects the concrete surfaces and closes the pores of the concrete. It is also used in the manufacture of skateboard wheels and is also used in sleeping mattresses with various degrees of density, some of which are formed by the temperature of the human body for more comfort [29, 30].

1.5 Hexane

Hexane is a byproduct of petroleum refining and crude oil. It is a transparent liquid with a slight smell of gasoline. The flammability of hexane is very high. However, it is included in a wide range of everyday products, including stain removers. Due to its toxicity, proper handling and storage of this chemical is extremely important. Of industrial and chemical applications, Plastic and rubber industry, Organic Chemistry, Paint Industry Scientific research [31, 32]. Table (1-3) represents some of the properties of hexane.

Table. (1-3): Some properties of Hexane [24]

Property	Value
Chemical Formula	C_6H_{14}
Chemical Symbol	HS
Color	colorless
Density	kg/m^3
Molecular Weight	86.18 g/mol
Boiling Point	68.7 °C
Melting Point	275 °C

1.6 Lead

Lead, denoted by the chemical formula (Pb) with atomic number 82, The fourth group's fourteenth table (based on the overall grouping system's designations). Lead, a heavy metal with a high specific gravity, is a dense metal often found in a blue silver that rapidly loses its shine to an opaque gray upon exposure to air [33]. Several alloys include lead as an ingredient. It is also a soft, malleable metal that is ductile and malleable. Its value was in the chain of radioactive integrity decay chain. The distinctive properties of lead, from its dense, melts at a low temperature, and is chemically inert to oxidation; to its high relative abundance and low price, helped it to be used in many applications that included, for example, construction, radiation protection, plumbing, the manufacture of batteries, bullets, projectiles, weights and various alloys such as alloys welding, pewter and eutectic alloys; In addition to its previous use in the field of paints and its addition to car fuels (in the form of tetraethyl lead) . Where the volume of micro-lead is (249.307). As for the volume of nano-lead (86.483), according to the information recorded within the lead cans [34].

Lead is a toxic metal, which led to the limitation of its applications in most countries after the discovery of its toxicity. Lead negatively affects biological bodies, where its effect is similar to neurotoxins in terms of the ability to damage the nervous system and disrupt the functional performance of the some vital enzymes, the causing neurological

and the movement disorders [35]. Table (1-4) represents the physical properties of lead in general.

Table (1-4): Represents the physical properties of lead [34]**.**

Property	Value (unit)
Atomic Number	82
Chemical Symbol	Pb
Color	Silvery bluish, gray exposed to air
Density at Room Temperature	11.34 $g.cm^{-1}$
Melting Temperature(Tm)	4.77 K. J. $mole^{-1}$
Glass Transition Temperature(Tg)	(140-370) °C
Molecular Weight	207g/mole

1.7 Literature Review

In 2014, G. Ossola, and A. Wojcik [36]**,** they used rubber in concrete to reduce the compressive and flexural strength, where the surface treatment of the reanimated rubber with concrete was carried out with ultraviolet light by changing the energy of the surface exposure to radiation and the strength of cohesion between cement and rubber, where the water retention method was used to determine the length The most effective wavelength, the samples were exposed to UV rays for different periods of time, and a flexion test was performed. It was found that the samples that were not exposed to radiation gave low values compared to the samples that were exposed to radiation. Also, the samples that do not contain recycled rubber are weaker by 6% than the samples treated with rubber.

In 2014, S. H. AL-Nesrawy *et. al.* [37], studied the effect of adding some industrial waste, which is cement kiln dust and recycled rubber as fillers, in addition to carbon black (N375) to support rubber kneaders consisting of synthetic rubber (styrene-butadiene) (SBR 1502) and (BR cis) in addition to natural rubber (NR SMR 20), to fabricated is SBR/NR/BRCIS,

SBR/NR SBR/BRCIS used in the manufacture of fenders for ships, where the mechanical properties of hardness, tensile strength, elongation, tear resistance, compressibility, and wear were studied.

In 2016, G. Shi *et. al* [38]**,** Graphene platelets (GnPs) and silicon rubber may be utilized to make high-performance strain sensors and stretchable conductors quickly, cheaply, and scalable. GnPs with changeable gauge factors of 27.7–164.5 have increased piezoresistivity, determined from experimental data. The composite film's excellent linear and reproducible sensitivity tensile stresses are due to it. Health monitoring applications like finger bending and pulse detection perform well with hybrid sensors built on different days. Their functions include electronic skin, vibration sensors, and HMI controller. Equivalent Pb shielding. Shielding tests should be done independently for each new lab or hospital radioisotope.

In 2016, S. A. Seyedmehdi*, et. al* [39]**,** Manufacturing method, silicon fluid, rubber type, and coating thickness affect the hydrophobic properties of silicon rubber coatings for high voltage insulators. Silicon rubber and nanofluidic particles were mixed and cured at room temperature to make these coatings. The manufacturing procedure might increase coatings' contact angle and minimize slide angle. Silicon fluid reduced coating hydrophobicity. Silicon rubber layers with silica filler had lower contact angles and higher sliding angles. Hydrophobicity and surface roughness depend on coating thickness. A command unit with an HMI provides Pb-like protection. The shielding test should be done before using any new radioisotope in the lab or hospital..

In 2017, A. Hashim and A. Had [40], studied research several uses for polymer nanocomposites have been researched, including constructing containment structures for people and equipment in nuclear power plants and hospitals.This article focuses on preparing new polymer nanocomposites

with excellent linear attenuation coefficients for nuclear radiation shielding. Synthesized and analyzed the optical characteristics of nanocomposites comprised of polyvinyl alcohol, polyacrylic acid, and lead oxide nanoparticles of varying component concentrations. The absorbance of a polymer mix and the optical constants both rise with increasing concentrations of PbO_2 nanoparticles while the energy band gap narrows. Testing of the nanocomposite for gamma radiation shielding revealed very high attenuation coefficients.

In 2018, H. Yang *et. al* [41]**,** used systematic approach to examining the electromechanical characteristics of graphene-silicon rubber nanocomposites. In the first step, conductive nanocomposites are made by co-coagulating graphene and silicon rubber, which results in a decreased percolation threshold at 1.87 wt.% (0.94 vol%). Rubber nanocomposites with varying amounts of graphene show excellent strain sensitivity (gauge factor > 143), a broader strain sensing range (>170%), and strong recoverability and repeatability through repeated loading and unloading. For a full description of the electromechanical characteristics and an explanation of the shoulder peak phenomena, an analytical model is created based on the connection of the graphene nanosheets and the viscoelasticity of the rubber matrix.

In 2018, A. E. Ersundu *et. al* [42]**,** used a melt quenching process, a novel series of heavy metal oxide (HMO) glasses with the composition 10WO3-xMoO3-(90-x)TeO_2 with x = 10-40 mol% has created and examined for their possible use in radiation shielding.Examined gamma attenuation characteristics such as the mass attenuation coefficient (MAC) and the half value layer (HVL) in an optimal transmission architecture. After determining the ranges in which electron, proton, and alpha particle interactions occur and the macroscopic removal cross sections for fast neutrons, the produced

glasses' shielding abilities against fast neutron and charged particle radiation were examined. Normal concrete and glass made with lead (Pb) were used as comparisons wherever feasible. When compared to other glasses, as well as concrete and Pb-based shielding glass, it was determined that the $10WO_3$-$10MoO_3$-$80TeO_2$ glass sample exhibited good shielding qualities.

In 2018, D. Toyen, *et. al* [43]**,** This paper examined potential alternatives to soft lead (Pb). Oxides like iron (II and III) oxide (Fe_3O_4), tungsten (III) oxide (W_2O_3), and bismuth (III) oxide (Bi_2O_3) were introduced as gamma-shielding materials to improve the properties of the natural rubber (NR) system and reduce the risks associated with Pb. The results showed that the gamma attenuation coefficients, tensile modulus at 100% elongation, and hardness (Shore A) all improved with increasing oxide content from 0 to 100, 300, and 500 parts/100 parts of rubber by weight (pphr), despite a decrease in tensile strength and elongation-at-break.

In 2019, F. Cataldo and M. Prata [44], synthesized a castable polyurethane (PU) with soft segment made by polytetrahydrofuran polyol derived from renewable sources was used as polymer matrix to prepare neutron shields. Both the linear μ and massic attenuation coefficient μ/ρ of the two PU composites were determined. FT-IR spectroscopy and DSC before and after neutron processing with a total dose of 1.5×10^{13} cm^{-2}. No significant changes were detected neither in the FT-IR spectra behaviour confirming the excellent radiation resistance of PU and its suitability as polymer matrix for neutrons and more in general radiation shielding.

In 2020, M. Wortmann *et. al* [45], studied the vacuum casting technique using silicon molds is one of the most common uses of quick tooling. It is widely used to produce polyurethane prototypes for manufacturing. The isocyanate in the polyurethane resin diffuses into the surface of the mold cavity during the casting process, reducing

the mold's longevity over time. This article provides the first detailed account of the molecular-level chemical and physical processes at work. Inside the polydimethylsiloxane matrix, the isocyanate is shown to polymerize with water to produce polyurea. Under mechanical demolding pressures, polyurea clusters that arise from the ensuing interpenetrating polymer network due to prolonged exposure to isocyanate encourage fissure formation.

In 2021, J. Liu, *et. al* [46]**,** Introduces a new nanoparticle-reinforced silicone rubber compound that is both strong and sticky. The novel composite has a tensile strength of up to 10.4 MPa and an adhesive sheer force of up to 90 kPa, much more than that of the well-known silicon rubber product Sylgard184. In addition, the composite's high adhesion capability is remarkably stable after many hours of usage or after being attached and detached repeatedly. As an adhesive material, the present composite seems superior to current silicon rubber goods. It also has prospective uses in producing sophisticated adhesive devices, such as wearable electronics.

In 2021, F. I. El-Agawany, *et. al* [47]**,** Examined the physical properties, neutron and gamma-ray shielding abilities of a lead (Pb)-silicate glass system doped with sodium oxide (Na_2O), from 32.70 to 76.93, with the greatest value in the NSP_{50} glass sample. The estimated exposure buildup factor values for all glasses examined were higher than the energy absorption buildup factor at constant energy and penetration depth.

In 2022, H. Aboud, *et. al* [48], they effected of lead (Pb) activation on certain properties of recently discovered bismuth (Bi)-cadmium (Cd)-barium (Ba)-borate (B_2O_3) glasses is discussed. Melt-quenching was used to make mirrors with the formula B_2O_3-Bi_2O3-CdO-BaO-PbO with different amounts of PbO doping (from 0 to 20% mol) and to describe them. XRD determined that the as-quenched samples were indeed glassy. There

was an analysis of the glasses' molar volume, density, and band gap energy versus Pb concentration. The glasses Raman and Fourier transform infrared spectra revealed distinct effects of PbO on the structures of the various glasses based on their compositions. There was a positive correlation between the amount of PbO in the samples and their attenuation coefficients. There was a significant shift in the removal cross sections for fast neutrons, and the best-ray shielding property was observed in glass samples containing the most Pb.

In 2022, O. Kilicoglu *et. al* [49], This paper contains Microlead (Pb) loaded polymer composites. They were investigated for potential use in radioprotective applications, such as shielding construction. The data show that the composites' mass attenuation coefficients for various photon energy scales linearly with the filler loading. For nuclear radiation shielding, the Pb (20%) micro composite was shown to were very high attenuation coefficients for photon radiation.

In 2023, Z. Rajabimashhadi, *et. al* [50], Investigated this research Microlead (Pb)-loaded polymer composites were investigated for potential use in radioprotective applications, such as shielding construction. The data show that the composites' mass attenuation coefficients for various photon energy scales linearly with the filler loading. Simulation of transmission tests using FLUKA and GEANT4 Monte Carlo software, the Pb (20%) micro composite was shown to was very high attenuation coefficients for photon radiation.

In 2023, H. A. Al-Samed, *et. al* [51]**,** They focused on the socket, which is the top part of the prosthesis that touches the severed limb. Friction between the skin and the socket, local pressure, and germs cause skin irritation and an unpleasant odor. Silicone rubber lining can compress customization, absorb moisture, and be antibacterial to fix this. The silicone

rubber was reinforced with certain percentages of polyurethane foam (0, 10, 15, 20, 25, 30, and 35%) and the percentage was (20%) showing the best result. PU was used as a filler to improve the silicone rubber properties, it can have a direct effect on the tensile strength, modulus of elasticity, percentage of elongation as well as hardness. The molecular structure was evaluated by FTIR.

1.8 Aim of This Study

Impact of micro and nano lead on structural, morphological, and mechanical properties of silicone-polyurethane composite for radiation shielding Applications.

Chapter Two

Theoretical Background

Chapter Two: Theoretical Background

2.1 Introduction

This chapter provides a comprehensive overview of the theoretical ideas, scientific explanations, and mathematical relationships pertaining to the qualities under investigation. These attributes include mechanical, structural, and radiation characteristics that have been attained.

Silicone rubber's special features such as ''organosiloxanes polymer'' has been originated from its unique molecular structure that they carry both inorganic and organic properties unlike other organic rubbers. In other words, due to the Si–O bond of silicone rubber and its inorganic properties, silicone rubber was superior to ordinary organic rubbers in terms of heat resistance, chemical stability, electrical insulating, abrasion resistance, weatherability and ozone resistance. With these unique characteristics, silicone rubber has been widely used to replace petrochemical products in various industries like aerospace, munitions industry, automobile, construction, electric and electronics, medical and food processing industry. Recently, these scopes of silicone applications have been expanding at a great speed by the demand of industries that want more reliable elastomer [52].

Natural rubber (NR) and styrene butadiene rubber (SBR) are both types of large hydrocarbon molecules. These molecules consist of various components and can be modified by incorporating different materials such as carbon black (CB) to enhance their physical properties. Additionally, chemical substances can be added to facilitate the kneading process, reduce costs, or improve the rubber's performance under different weather conditions. Vulcanizing agents, particularly sulfur (S), are commonly used in rubber samples. These agents undergo a chemical reaction with the rubber molecules at the double bond sites [53].

2.2 Polymer Blends

Polymer blends have been a focus for research and development in polymer science and technology for decades. Polymer blends' improved characteristics and cost-effectiveness make them useful across many industries. For a long time, scientists have experimented with combining polymers with different properties [54].

Blending two or more polymer types is a valuable method for creating new materials with improved qualities over their separate components. From an industrial standpoint, controlling the mixing condition of polymer blends is of utmost importance [55].

Several motivating factors have elevated polymer mixing to the forefront of polymer science, one is that polymer blends make innovative polymeric materials quickly and cheaply, these materials have different properties depending on their composition [56].

Although combining synthetic and natural rubbers is not new, technological advances over the last five years have made it possible to put them to good use. These composites may create a chemical bond between the two rubbers, creating a more technologically friendly blend. Selecting an appropriate SBR: NR ratio results in blended vulcanizates with improved physical qualities [57].

There has been prior research into the performance of styrene butadiene rubber (SBR) blends and other forms of rubber. An appropriate compatibilizer may greatly enhance the blends' physical and mechanical qualities [58]. SBR and (BRcis) rubber composites need a thorough understanding of the impact of black carbon loading and cement waste on tensile set, compression set, and fatigue [59].

2.3 Composites

Composite materials are systems made from two or more components that differ in shape or composition to create new materials with better properties for industrial applications [61]. The composite material's characteristics are determined by three types: the base material, the filling material, and their interaction through a bonding surface called the interface [62]. A system's most fundamental constituent is the basic material, which serves as a protective shell for the other pieces, promotes elemental cohesion, and forges connections between them [63].

The base material is characterized by light weight and high durability, and it must protect the reinforcing material from wear and tear and the environment, even if it contributes to transferring the load imposed on it to the reinforcing material, and that the composite materials possess a certain property due to the nature of the base material or the type of reinforcement used Composites are multi-part materials that can't be separated into their parts due to their different chemical and physical properties [60, 61]. Reinforcements (such as fibers, particles, whiskers, lamination, flakes, or fillers) and a binder are often the second components [62].

Increasing the rubber composite's modulus and so-called ultimate qualities like tensile strength, tear resistance, and abrasion resistance leads to better end-use performance, which is what the name "reinforcement" to Particulate materials used to improve rubber's tensile strength, rip strength, and abrasion resistance are known as reinforcement fillers. Semi-reinforcing fillers may boost (1) tensile strength and (2) tear strength without affecting the material's resistance to abrasion. Adding a filler that does not reinforce the material cannot improve these qualities and functions [63]. Matrixes may be made of metals, polymers, or ceramics, and they encase the composite and give it its bulky shape. The matrix is a structural component that determines

the internal structure of the composite. For many purposes in medicine, civil engineering, and the armed forces, contemporary composites have largely replaced traditional materials owing to their superior strength and stiffness [64, 65].

The mechanics of the composite material is higher than the mechanical properties of its components if it is single, and the strength-to-weight ratio is high, as well as the resistance-to-weight ratio is high, and the possibility of flexibility for specific design requirements is possible [66]. Composites' weaknesses include rapid variations in mechanical and physical properties as a function of environmental conditions, a shorter lifespan than conventional materials, and a lack of thermal resistance (although there are ongoing studies in this area, it is sufficient to note that the space shuttle's nose cone is made of composite materials and bears the largest part of the weight from the shuttle's thrusters) [67].

2.3.1 Classification of Composites

Composites can be classified depending on many factors, such as material composition, base materials used, type of reinforcement used, and intended purpose. The classification method divides buildings into four main groups according to the shape of the structural element, as shown in Figure (2-1) [68].

1. Particulate composites, composed of particles with the matrix.
2. Flake composites, comprised of flat flakes with the matrix.
3. Fiber composites composed of fiber with the matrix.
4. Laminate composites, composed of layer with the matrix.

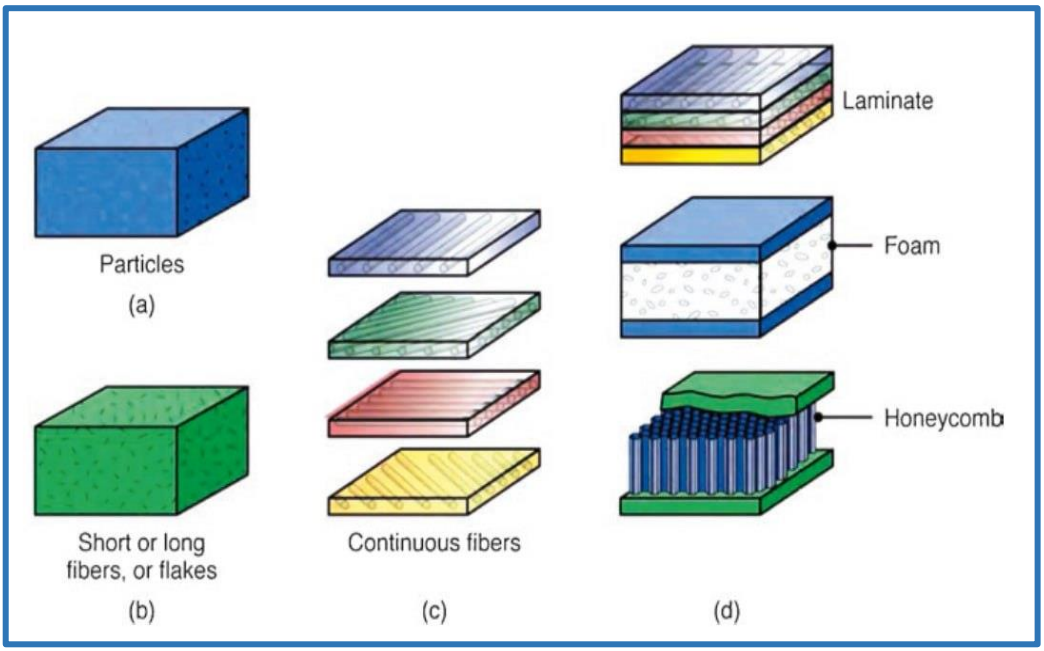

Fig. (2-1): Schematic illustration of methods of reinforcing plastics (matrix) with (a) particles; (b) short or long fibres or flakes; and (c) continuous fibres. The laminate structures in (d) can be manufactured from the layers of continuous fibres or sandwich structures [71].

So the classification according to the matrix system are [69, 70].

1. Metal matrix composite (MMCs) These materials can be used where high strength is required at temperatures up to 1250 °C. coupled with ductility and toughness for example boron fiber in aluminum basis or carbon fiber in magnesium basis.

2. Polymer matrix composite (PMC_s) the most common aerospace and military applications have been major drivers in developing polymer composites, including composites whose matrices are made of thermosetting thermoplastic, elastomer, and plastic reinforced with carbon fibers or glass fibers.

3. Ceramic matrix composite (CMCs) such as silicon nitride reinforcing with silicon carbide, lightweight, high temperature strength Along with excellent dimensional and environmental stability. The matrix is resistant to extreme temperatures. Glass matrices can function at temperatures as high as 1500 degrees Celsius. Carbon –carbon composite (CCCs)

Graphite fibers in carbon matrix offer the possibility of a heat resistance material that could operate at temperatures up to (3300°C), with high strength and light.

4. Intermetallic composites (IMCs), are a fourth option. Aluminides of iron, titanium, nickel, and niobium have fiber compositions (SiC, Al_2O_3, and Ti_3Al) that don't bend well at low temperatures (1000 °C) and don't resist oxidation well at high temperatures.

2.4 Rubber Composites

Goodyear and Hancock first developed rubber composite, it continues to evolve as novel materials are developed [71]. The market is flooded with fresh iterations of old products. Everyday rubber, such as found in tires and erasers, and a combination of many distinct substances. Raw gum elastomer is used at the outset; this might come from the plantation owner as NR or from the petrochemical complex as bales or chips of BR, SBR, NBR, or CR rubbery polymers. It is sent to a rubber producer, who then incorporates it into a larger batch. Raw gum elastomer has few use beyond adhesives. Most cannot hold their molded form because they are mechanically weak and expand significantly when exposed to liquids [72].

The expanding usage of rubber in engineering applications derives from its unique qualities, including high extensibility, high strength, high energy absorption, and high resilience to fatigue. Increased resilience and resistance to the effects of the environment are two more distinguishing features. You may find engineered rubber goods that are entirely rubber or that blend rubber with other materials. Products might be as basic as a rubber band or as complicated as radial tires or rubber-metal bearings for use in aircraft [73].

Composites are commonly made by combining rubber with other materials, such as steel, aluminum, plastics, cloth, or cables. In most cases, these substances are used to bolster durability, reduce distortion, or do both [74].

Compression set behavior, loss of resilience, and the capacity to preserve elastic characteristics under sustained action of compressive loads are only a few of the phenomena seen in rubber composites. For a particular deflection and temperature, a material has a higher permanent deformation resistance if its compression set % is smaller. Choice of rubber composites for engineering applications [75].

Tire transportation belts, pipelines for fluids and oils transfer, mobile phone damping and support components, and diaphragms are some of the many rubber industry uses that rely heavily on high-elastic polymer composites. Dampers and supports made from rubber composites employ many types of rubber. Because rubber is well characterized by the high elastic strain damping derived from the abrupt impact loading that occurs due to varied accelerations in the system, this study offers a broad scope. As a result, blended polymers like (NBR, SBR, NR, CR, etc., have been developed to provide increased resistance to mechanical loads and to account for factors like environmental effects at high temperatures in the presence of oils and friction [37, 76].

2.5 Nanomaterials

The fascinating new class of materials known as nanomaterials it is in strong demand for various uses. For reference, five silicon atoms or ten hydrogen atoms aligned would equal one nanometer in length. Nanomaterials are those sizes, or at least one of their dimensions, fall between 1 and 100 nm. It's not easy to trace back the precise origins of human use of nanoscale items. However, the usage of nanomaterials has a long and illustrious history, these tools were probably used effectively by humans across a diverse range of applications, even prior to their recognition and understanding. Approximately 4500 years ago, individuals used asbestos nanofibers to enhance the structural integrity of ceramic compositions [77].

Greece is the cradle of nanotechnology. A nanometer (nm) is a unit of measurement equal to a billionth of a meter. Nanoscience and nanotechnology have a special role in the technological applications of the modern world as all measurements are now made at the nanoscale. Nanoscience and nanotechnology have received a lot of attention and importance since quantum phenomena began at the nanoscale, truly leading to revolutionary advances in science and industry [78].

The difference between nanomaterials and non-nanomaterials is the size i.e., < 100 nm in 1D are referred to as a nanomaterial and > 100 nm in all dimensions are non-nanomaterials. Besides, nanomaterial cannot be seen by naked eyes, whereas non-nanomaterials are visible through a simple microscope. In contrast to non-nanomaterials, nanomaterials display a higher surface/volume ratio which allows good performance and applies them to be used in various applications such as nano sensors, nano-sorbents, and fuel cells [75].

Furthermore, nanomaterials have shown higher adsorption capacity in both gas and liquid phases [79]. These nanomaterials are synthesized through methods, depending upon the end-user property demand. Synthesis of nanomaterials has two major approaches, one is top-down, in which the size of larger molecules makes smaller to nanoscale and the other is a bottom-up approach, in which small molecules or atoms are combined to produce nanomaterials. These approaches involve several synthesis methods and four major categories like chemical, physical, mechanical, and biological. Generally, the top-down approach involves methods like high-energy ball milling, severe plastic deformation, etching, mechanical alloying, lithography, reactive milling, and micromachining methods. Whereas, bottom-up includes molecular self-assembly, sol-gel, electron (or ion) beams, metal-organic chemical vapor deposition, vacuum arc deposition, inert gas condensation, molecular beam

epitaxy, electrodeposition, physical/chemical vapor deposition, and ultrasonic dispersion [80].

The geometry of nanomaterials divides them into three categories, as depicted in Figure (2-2) [81]. Nanomaterials applications in industry such as Engineering, Medicine, Cosmetic, Sports, Chemical, and Electronic [82].

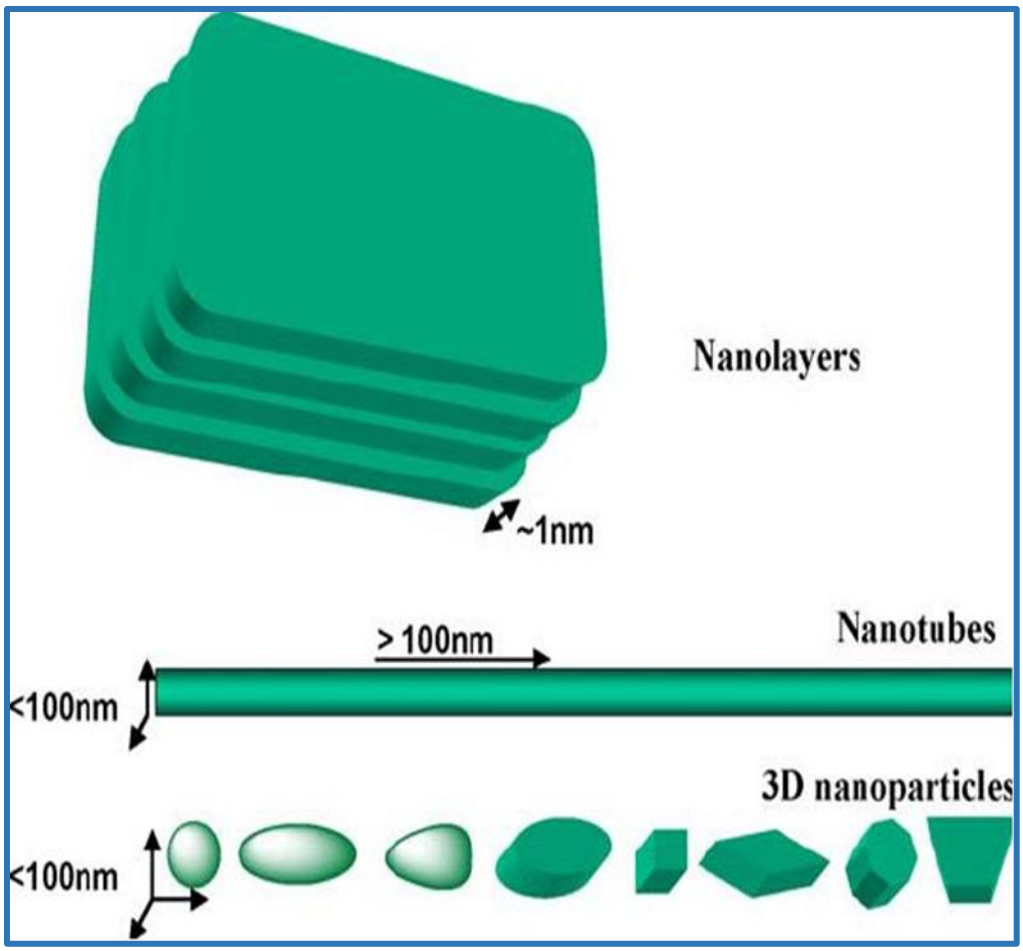

Fig. (2-2): Various types of nanoscale materials [83].

2.5.1 Approaches for the Synthesis of Nanomaterials

Nanomaterial's research takes a materials science-based approach to nanotechnology, leveraging advances in materials metrology and synthesis which have been developed in support of microfabrication research. Materials with structure at the nanoscale often have unique optical, electronic, thermo-physical or mechanical properties. Nanomaterials are slowly becoming commercialized and beginning to emerge as commodities [83]. Obviously, there

are two approaches to the synthesis of nanomaterials and the fabrication of nanostructures: top-down and bottom-up. Figure (2-3) shows the two approaches. Attrition or milling is a typical top-down method in making nanomaterials [84].

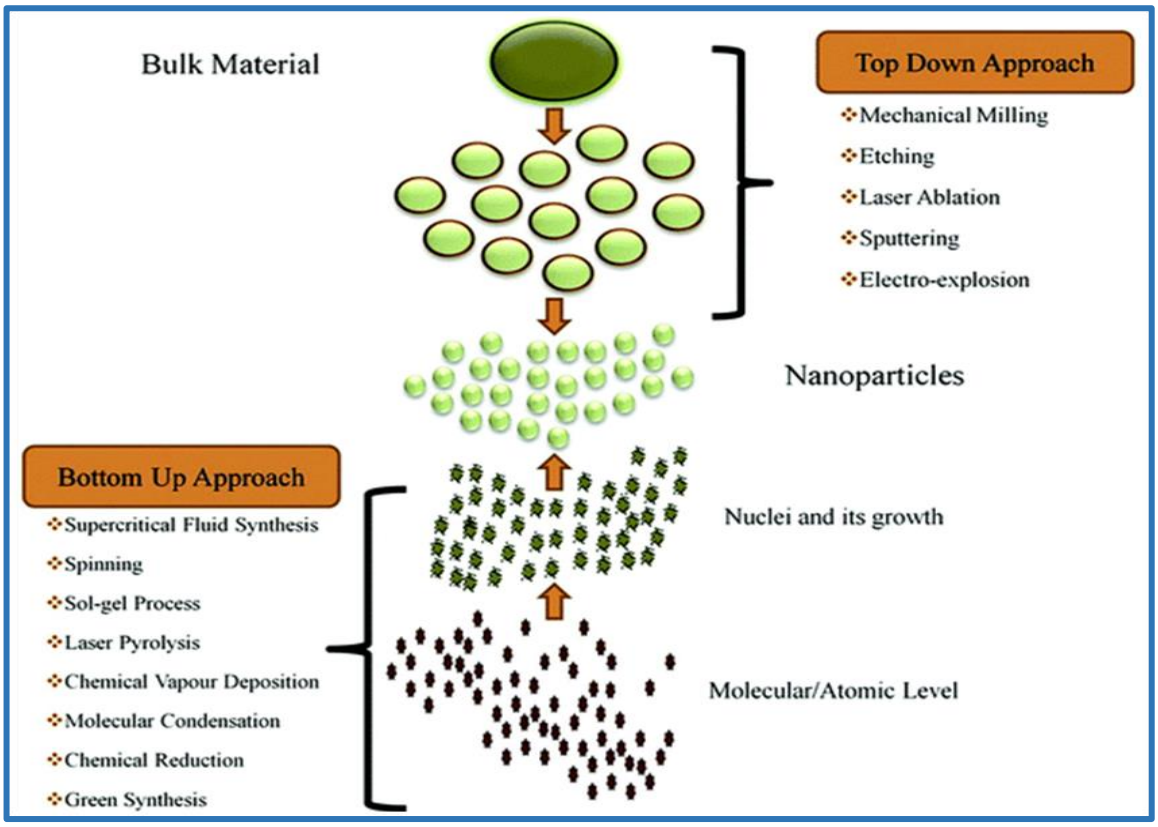

Fig. (2-3): Synthesis of nanomaterials *via* top-down and bottom-up approaches [85]**.**

2.5.2 Properties of Bio nanomaterials

Nanoscale materials vary from conventional macromolecules in many ways, including their unusual optical, magnetic, and electrical characteristics. High surface-to-volume ratio, improved electrical conductivity, superparamagnetic behavior, spectrum shift of optical absorption, and distinctive fluorescence properties are all features shared by most nanomaterials [86]. Nanomaterials have potential uses in the medical sector, including medication delivery and controlled release. Other distinguishing characteristics include increased permeability that allows for the traversal of biological barriers and enhanced biocompatibility [87]. In bio-imaging

and drug delivery, metallic nanoparticles have been widely explored due to their unique optical, magnetic, and photothermal properties. Metals may be conjugated to various carriers, including NPs, liposomes, dendrimers, and CNMs. MRI imaging is the primary field of use for magnetic nanoparticles. Magnetic nanoparticles (NPs) guided by an external magnetic field may deliver chemical medications to cancer cells, mitigating some of the negative effects of standard chemotherapy [88].

2.5.3 Classification of Nanomaterial's Based on Dimensions

Figure (4-2) illustrates how the number of dimensions is used to categorize nanomaterials. Siegel defines four distinct dimensions for nanostructured materials: zero dimensions (0D), one dimension (1D), two dimensions (2D), and three dimensions (3D) [89].

(i) **Zero-dimensional nanomaterials:** Here, all dimensions (x, y, and z) are nanoscale, i.e., none of the sizes exceeds 100 nm. There are nanospheres and nanoclusters present [90].

(ii) **One-dimensional nanomaterials:** Here, two dimensions (x, y) are nanoscale, and the remaining is not. This results in nanomaterials shaped like needles. It consists of nanofibres, nanotubes, and nanorods [90].

(iii) **Two-dimensional nanomaterials**: Here, one dimension (x) is at the nanoscale and the other two are outside the nanoscale. The 2D nanomaterials exhibit platelike shapes. It includes nanofilms, nanolayers and nanocoatings with nanometer thickness [90].

(iv) **Three-dimensional nanomaterials:** These nanomaterials can be made at any size, not only the nanoscale. Three dimensions of this substance are more than one hundred nanometers. Many nanoscale crystals in various orientations comprise bulk (3D) nanomaterials. The 0D, 1D, and 2D structural components are near and form interfaces and this

category includes nanoparticle dispersions, nanowire and nanotube bundles, and multi-nanolayers (polycrystals) [90].

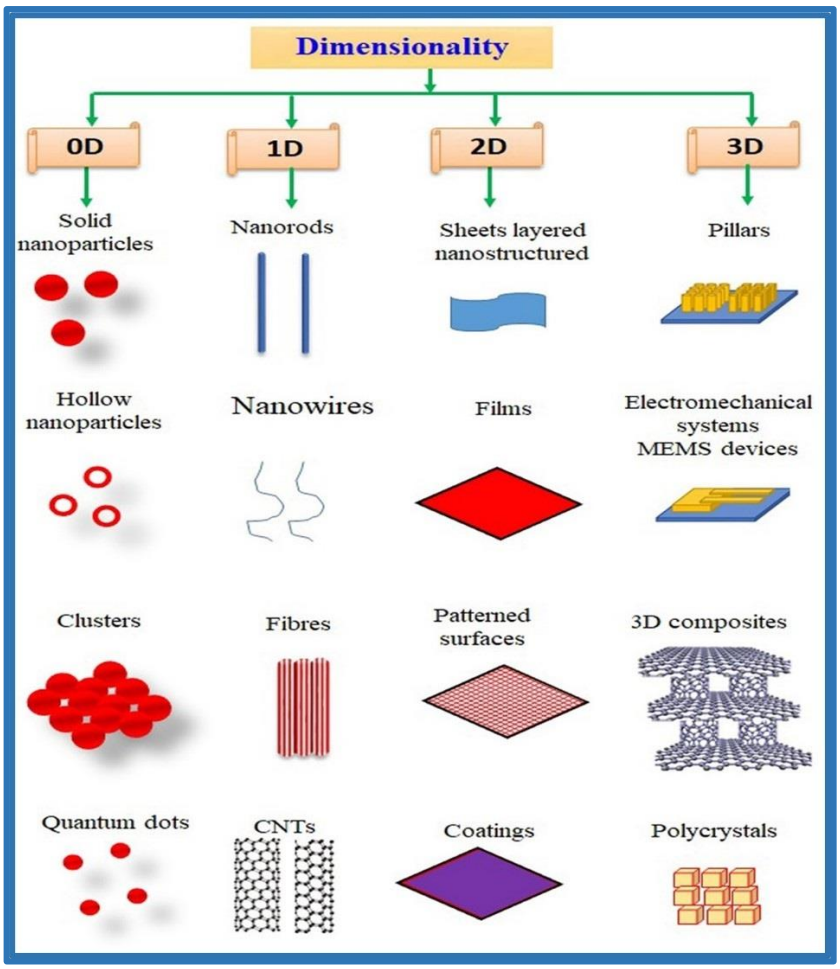

Fig. (2-4): Classification of nanomaterials [90].

2.6 Nanocomposites

Nanocomposite combines two or more materials of which at least one is a nanomaterial with different physical and chemical properties. Nanocomposite materials are designed to exhibit properties that exceed, sometimes drastically, the capabilities of the sum of their constituent parts [82].

When at least one filler characteristic size is lowered to the nanometer scale, a much larger interface is established between the nanofillers and the polymers, according to a new idea from nanocomposites. When sphere-shaped fillers have their radii shrunk from micrometres to nanometers, the contact area rises by 10^{-6} [91]. Polymers placed at the interface

significantly impact the macroscopic material characteristics of the nanocomposites due to the huge increase in the interface area between nanofillers and polymer chains [92]. In this context, the interphase refers to the region of the polymer close to the nanofiller surface where its characteristics deviate from those of the bulk polymer.

2.6.1 Polymer Nanocomposites

Polymeric nanocomposites – materials incorporating nanosized inclusions into the polymer matrices – represent a major area in the field of nanocomposites. They exhibit excellent mechanical properties, enhanced modulus and dimensional stability, flame retardancy, improved scratch and mar resistance, superior thermal and processing properties, reduced warpage of components and enhanced impact resistance making them suitable to replace metals in various industrial applications [93]. The exponential growth of polymeric nanocomposites began with the discovery of fullerenes (also known as C-60 atom or buck balls). This discovery paved the road for discovery of carbon nanotubes (CNTs) and later graphene, all of which have become important filler materials for nanocomposites. Some of the most major improvements achieved from the introduction of nano fillers into polymeric matrices are enhancement of mechanical properties, improvements in thermal and electrical properties from the incorporation of CNTs, flame retardant properties in the case of the introduction of nanoclays and metal hydroxides, thermal stability, gas permeability, and so on [94] . Moreover, the organic origins of some nanofillers, such as nano cellulose, allow the usage of these materials for medical purposes due to their biocompatibility.

2.6.2 Nanocomposites in Food Packaging

Nanoclays, which are added to, for example, polypropylene or polylactic acid packaging films, prevent the diffusion of oxygen or flavorings and thus prolong the shelf life of foods. Nanosilver has an antimicrobial effect and can

be used in plastics composites, for example to manufacture food packaging such as films or containers to protect food from spoilage [95].

Particle fillers used and proposed in the literature include the nanoclays montmorillonite (MMT) and kaolinite, carbon nanotubes, and graphene nanosheets [96]. Most materials currently used for food packaging are non-degradable, generating environmental problems. Several biopolymers have been exploited to develop materials for eco-friendly food packaging. However, the use of biopolymers has been limited because of their usually poor mechanical and barrier properties, which may be improved by adding reinforcing composites (fillers), forming composites. Most reinforced materials present poor matrix–filler interactions, which tend to improve with decreasing filler dimension [97].

2.7 Mechanical Properties

Mechanical properties are of particular importance for composites because they reveal the materials' responses to external loads.

2.7.1 Hardness

The definition of hardness is the resistance of a material's surface to abrasion, furrowing, or penetration of the pressure applied to the sample surface. There are four methods for calculating the hardness of the material, all of which depend on the same principle, but they differ in the method of examination [98], where we used Shore hardness. Perhaps the most widely used test in the rubber industry is the hardness measurement, as workers in the rubber technology field use hardness as a preferred method for classifying rubber materials [98].

It is possible to compare the hardness of two surfaces by measuring the rebound of the metal ball from both surfaces. The higher hardness gives higher rebound, Durometer ASTMD-2240, the American Standard Specifications (ASS). It can tell how hard anything is by putting bump against

the notch and reading the scale, which runs from 0 (very soft) to 100 (very hard) [99]. The unit of hardness is the international rubber hardness degree (IRHD), and the accuracy of the reading of the test devices depends on the extent of the loading rate and the duration of the load [100].

There are several hardness measurement systems:

1- The shore hardness measurement methodology is divided into types:
   a- Shore A is a hardness measurement metric used for flexible soft rubber.
   b- Shore B is used for measuring the hardness of softer rubber materials and elastomers that have a relatively low hardness.
   c- Shore D is a hardness measurement system used for polymeric materials.
   d- Shore H is a hardness measurement system used for rubber industry.

Vickers hardness number (HV) equations are;

$$HV = \frac{2F\ Sin(\alpha/2)}{g\ d^2} \quad (2\text{-}1)$$

Where (F) is a force, (α) is an angle of indenter, commonly taken as (α=136°), (g) is an acceleration due to gravity, and (d) is the depth resulting from the penetration of the test body into the water.

Brinell hardness number (HB) equations are;

$$HB = \frac{2P}{\pi D(D-\sqrt{D^2-d^2})} \quad (2\text{-}2)$$

Where (P) is an applied load, and (D) is a dimeter of indenter.

Rockwell hardness number (HR) equations are;

$$HR = N - d \quad (2\text{-}3)$$

Where (N) is the number read from the test device after performing the test.

And Shore test are;

$$HS = 100 - d \quad (2\text{-}4)$$

2- Type of hardness measurement system (IRHD) and range (0-100) IRHD.

Figure (2-5) depicts the quantity of rubber surface penetration or furrowing induced by the hardness devices (Shore A and IRHD) [101].

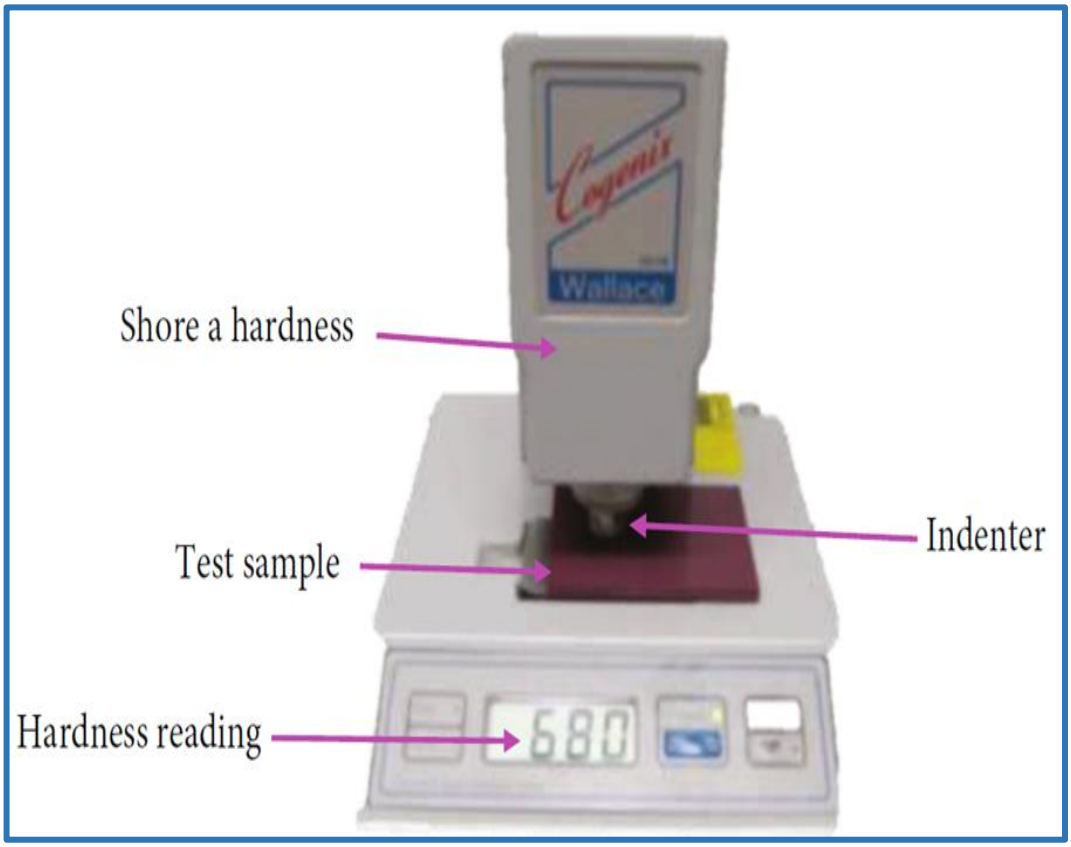

Fig. (2-5): The amount of penetration or indentation of the rubber surface caused by the hardness devices represented by (Shore A) [104].

2.7.2 Stress–Strain Curve

The stress-strain curve illustrate how various materials respond to stress and strain. The angle for a given material is determined by subjecting a material sample to a tensile or pressure test and keeping track of the deformation it experiences over a certain period. These curves show many material characteristics [102]. A material's strength, stiffness, elasticity, and failure limitations may be gained by examining its stress-strain curve. In contrast to a rubber ball, which may bounce back to its original form after being placed on the ground, a glass marble would instantly shatter into shards. Stress-strain curves provide a full explanation for why a glass marble and a rubber ball behave so differently [103]. Figure (2-6) represents stress–strain.

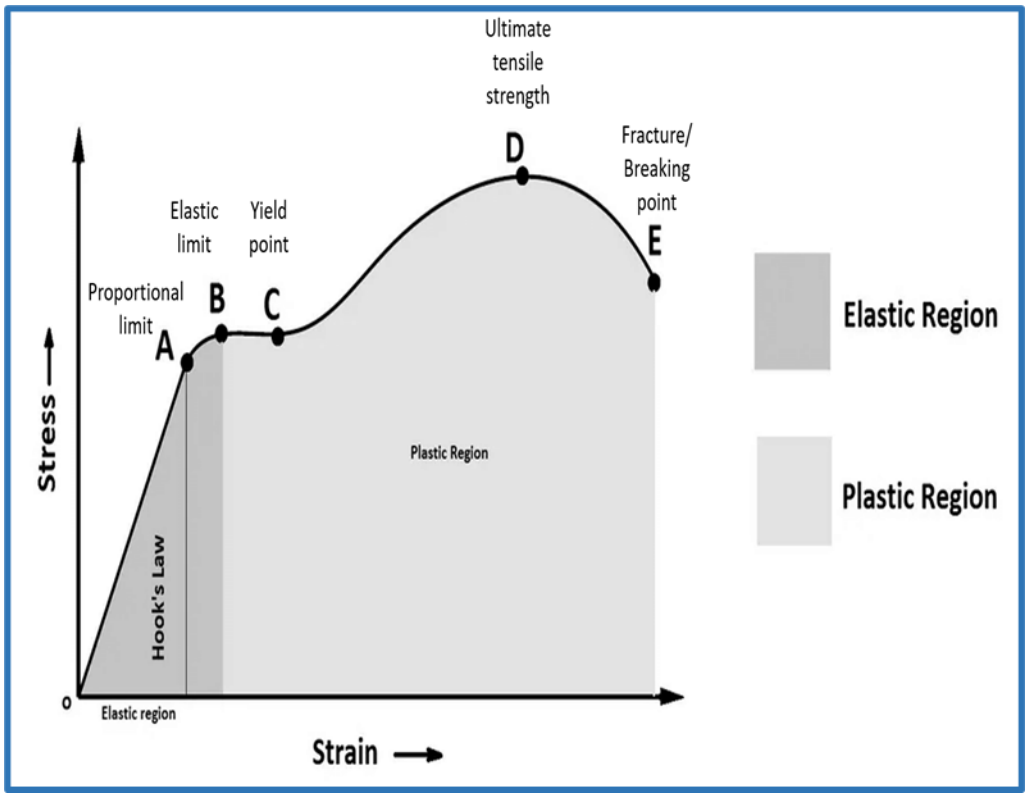

Fig. (2-6): The stress-strain curve [102].

2.7.3 Tensile Strength

Tensile strength, also known as the force exerted per unit area of a sample section during the rupture phase of a standard sample, is one of the essential physical qualities of vulcanized rubber [104]. Good mechanical qualities, such as the rubber body's resilience to abrasion and pressure and its ability to regain its size and form once the influence is removed, are associated with a tensile strength higher than 20.7 MPa, testing this attribute may determine the maximum elongation and the material's resistance. The stress used to test the rubber sample is the longitudinal stress, , as shown in Figure (2-7), described by the following relationship based on the stress-strain curve [105].

$$\sigma = \frac{F}{A} \qquad (2\text{-}5)$$

where F is the applied force (N) and A is the cross-sectional area of the assay sample (m^2).

The strain ε used in the above curve is expressed by the following relationship:

$$\varepsilon = \frac{\Delta L}{L_{\circ}} \quad (2\text{-}6)$$

where $\Delta L = L - L_0$ is the final length (m) and L_0 is the original length (m).

The (Stress–Strain) curve may be used to determine the stress-resistance property at the fracture, which is expressed in megapascals (MPa), and modulus of elasticity in (MPa), represented by Mod100, Mod200, and Mod300, respectively, and also the percentage of elongation when cutting , elongation is defined as the ability of rubber to be stretched without breaking the rupture until it stretches to its limit; values are expressed as a fraction of the starting length [106].

Since elongation decreases with increasing hardness and tensile strength, a greater elongation force is required for harder and stronger materials. Modulus of elasticity, also known as the "pulling force per square meter of the test sample to give the elongation," or "stretching resistance," is the force (stress) needed to produce a certain elongation (strain) in the test sample, and is expressed in pounds per square inch (psi). The first is the most common, although the other two and possibly the third are possible [107].

Since the modulus of elasticity measures tensile strength at a given elongation, a more rigid composite will have a higher value. Thus, Yonk's modulus, denoted by the symbol (E) in the connection, is the ratio between stress and strain and defines the modulus of elasticity as the effort exerted divided by the pressure produced in the elastic area of equation (2-7) and (2-8), it can be written in terms of (σ) as in the relationship (2-9), and equation (2-10) resulting change in height after dropping the load [108].

$$E = \frac{F/A}{\Delta L/L_0} \quad (2\text{-}7)$$

$$E = \frac{\sigma L_{\circ}}{\Delta L} \quad (2\text{-}8)$$

where (E) is the modulus of elasticity, (F/A) represents tensile strength, and whereas $\Delta L/L_0$ represents elongation, where $\Delta L = L - L_0$.

The tensile device (Tansometer 10) made by the English business (Monsanto) tests these characteristics by ASTM D412-68 [109].

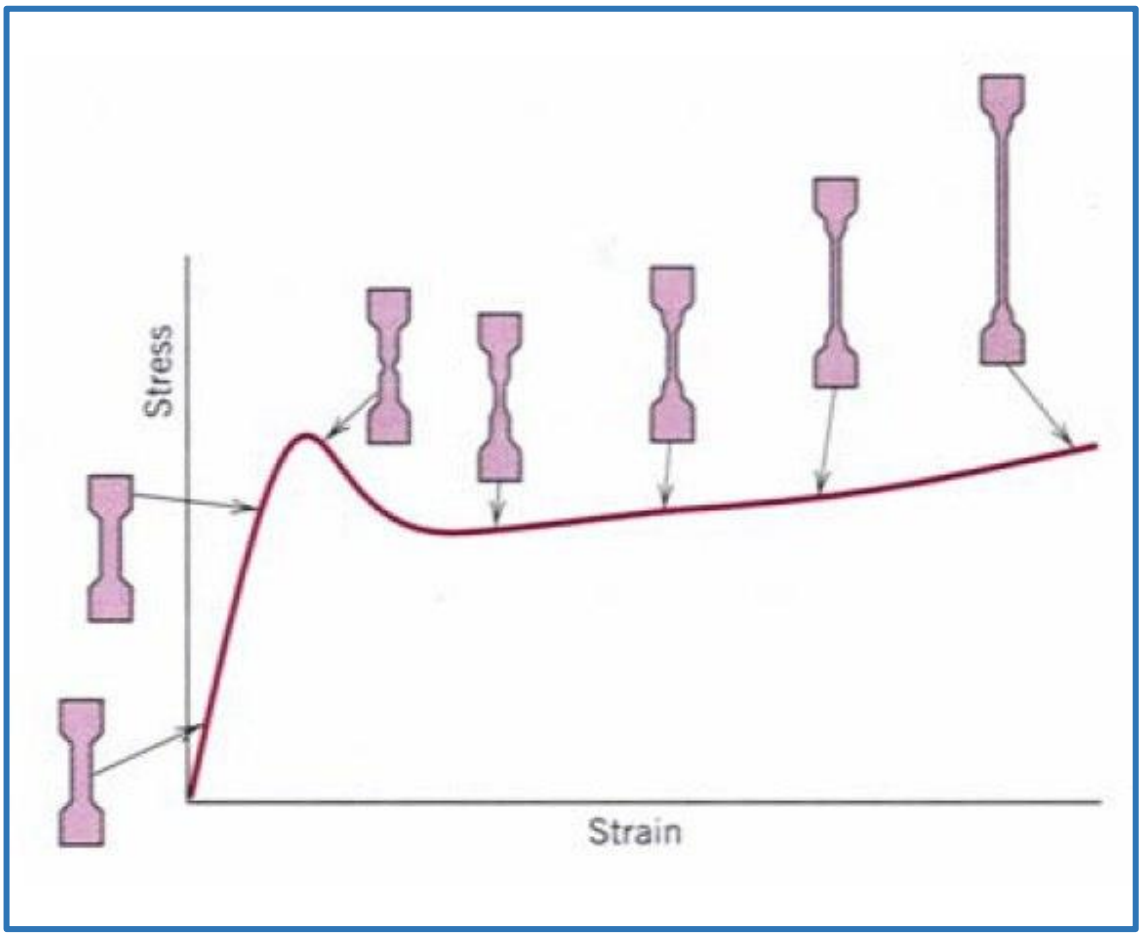

Fig. (2-7): The sample length changes with the applied stress [110].

2.7.4 Elongation

Elongation is the change in length due to tension relative to the original length before the cut occurred [111].

$$\varepsilon = \frac{\Delta L}{L_0} = \frac{L - L_0}{L_0} \qquad (2\text{-}9)$$

The result is also shown in the Tensometer -10 for the same model used to find the tensile strength, cut-off point and modulus of elasticity.

2.7.5 Modulus of Elasticity

It is the tensile stress at a certain elongation, as it appears with the previous results in the tensile examination on the same model. In rubber, stress is used to a certain elongation, to clarify the elasticity of the rubber model. When the coefficient at 300%, the stress required to cause an elongation of 300% of the original body length [112].

2.7.6 Specific Gravity

Density is defined as the mass of a unit volume of a substance, while the specific weight can be defined as the ratio between a known volume mass of a substance to the mass of the same volume of water at the same temperature. submerged in a liquid to the weight of the liquid displaced when the weight of the substance is a known weight equal to the volume of water. Therefore, the specific weight can be determined by taking the weight of the sample in the air and its weight while it is in the water, and the specific gravity is calculated according to the following equation (2-10) [113].

$$\text{Specific gravity} = \frac{Weight\ in\ \ air}{Weight\ in\ air - weight\ in\ water} \times Specific\ gravity\ in\ water \quad (2\text{-}10)$$

The specific weight is checked within the specification ASTM D1817-66 [56], so the specific weight of any substance is measured using the relationship (2-8), so this method includes the weight of the substance and means the substance being tested in air and its weight in water [114].

2.8 Radiation

There are several types of radiation, and each radiation has energy, and the effect of radiation on materials is according to the energy of the radiation [115]. There are two types of radiation: ionizing radiation, which ionizes the atoms it passes through, and non-ionizing radiation, which does not ionize the atoms it encounters. Atoms and the surrounding medium are ionized as a result. it passes through, but causes its atoms to be excited,

and it includes ionizing radiation (gamma rays and X-rays). Minutes, alpha rays, beta particles, and neutrons [116].

2.9 Radiation Shielding

Shielding is one of the most important factors adopted in the principles of radiation protection to reduce the risks of radiation exposure for workers in the radiation field. These shields are divided into two parts [117].

1- Single layer shields, which in turn are divided into two parts:

A - pure single shields.

B - homogeneous blend.

2- multi-layered shields.

The issue of radiation protection by some radiation-absorbing materials that prevent the passage of radiation and its spread in the area surrounding the radioactive source is one of the useful and practical methods in reducing the danger caused by radiation [118]. A present, lead is used in the manufacture of protective shields from X-rays, as it is placed in the form of sheets in the path of the rays and absorbs them through the photoelectric interaction between photons and lead atoms. Polymeric materials have been shown to have a high absorption efficiency, making them a popular choice for use as radiation shields thanks to advances in science [119]. Researchers have been inspired to identify novel multi-use materials with high engineering and synthetic specifications in response to the revived human propensity towards a lavish lifestyle made possible by the world's fast industrial growth and advancements in technology. By studying the properties of engineering materials (metals, ceramics, polymers), the researchers found a discrepancy between the properties of these materials, withstands high temperatures and high forces (above 400°C), and Plasticity. Ceramic materials are characterized by their ability to withstand high temperatures, thermal and electrical insulation, high

hardness, and tolerance to compressive forces; however, they are also characterized by their brittleness, fragility, propensity to fracture, and insensitivity to impact and tensile strengths. As for metals, they are distinguished by their capacity to withstand high burdens, resistance, durability, and susceptibility to oxidation due to exposure to the elements [120]. Consequently, these materials may be appropriate for one discipline but not another. Numerous modern technologies and industries necessitate using materials with a combination of uncommon properties. Rubber is a natural or synthetic polymeric material distinguished from other engineering materials by its high elongation, resilience, good damping properties, and ability to withstand high shock, lightweight, and resistance to different environmental conditions. These characteristics make rubber economical and suitable for industrial and engineering applications, which is a reason for the search for so-called composite materials [121]. While rubber's coefficient of friction is high while dry, it rapidly drops as it becomes wet. Because it lacks charge carriers and has covalent bonds, it is a poor electrical conductor. It has a glass transition temperature (Tg) that is typically lower than the operating temperature. It is a poor heat conductor, has damping properties, and can change its external shape under pressure and then return to its original state. It appears from the historical information that the residents of Mesopotamia were the first to know the overlapping materials, so they armed the building layers with reed fibers to build ziggurats and make arches. The Babylonians used asphalt and straw to pave roads and asphalt in building boats [122].

As for the Sumerians, they used reeds and papyrus with bitumen in building boats, and the ancient Egyptians sewed the mummy with cotton fibers. In the manufacture of bricks, as well as their use of resinous plant resins for various purposes [123].

Since 1960, the space and transportation industries have had a growing need for a material that meets the requirements of high resistance, stiffness, and lightweight. Finding materials meeting these criteria has required extensive research into composites, including a deep understanding of the relationships between material properties. Materials came into being with each other and the ratios of their addiction. Composite polymeric materials, which overlap, provide superior mechanical qualities relative to density and are simple to produce [124].

2.10 Radiation Interactions with Matter

Radiation, whether in the form of particles such as neutrons, protons, and alpha and beta particles, or in the form of electromagnetic radiation such as gamma rays and X-rays, has a described energy in addition to other specifications such as mass, kinetic energy and charge, which in total determine the nature of the interaction of these radiations with matter. In general, all interactions that occur with radiation with matter whether it leads to full or partial absorption or scattering of radiation energy, it ionizes the atoms of the material by making them lose a number of orbital electrons of the atom to leave it in an ionized state as a result of the loss of these electrons. higher orbits to leave the atom in an excited state, or if radiation is transformed from one form to another Others, such as photons from the electron-channel and positron process. But in general, charged particles lose most of their energy through ionization, while neutrons and photons lose their energy through scattering and absorption [125].

As for electromagnetic rays, when they fall on the surface of the material, the process of absorbing the photons of these rays by deleting these photons from the beam individually and through one incident in which the photon is either completely absorbed, or scattered outside the ray beam, which leads to the beam decreasing exponentially with increases the thickness

of the absorbent material and the electromagnetic radiation behaves during the interactions as if it were light particles (photons) and gives the energy of one photon by the following relationship [126].

$$E = h\upsilon \quad (2\text{-}11)$$

E; Photon energy, $h = 6.63 \times 10^{-34}\, J.s$; plank constant, and ν; photon frequency.

There are three types of interactions that are important in the field of radiation physics, which photons of electromagnetic rays undergo when passing through materials, these three types are:

2.10.1 Photoelectric Effect

The photoelectric effect is among the most significant interactions of low-energy particles with matter. In this interaction, the entire photon's energy is conveyed to an atomic electron, resulting in both simplicity of production and reduced cost. the electron to be extracted from its inner shell and usually from the shell (K), Figure (2-8) and that the probability of extracting an electron from the shell (K) is (80%), and the probability of extracting it from the shell (L) is (20%), provided that the energy of the photon incident (E) on the atom, is greater than the energy of the binding of the electron to the shell, which is then called the photoelectron, and its kinetic energy is estimated as the initial incident photon energy, minus the binding energy of the electron in the shell (K), meaning that [127].

$$E_{pe} = E - \phi_k \quad (2\text{-}12)$$

E_{pe}: the kinetic energy of the photoelectron, E: the energy of the photon falling on the atom, and ϕ_k: electron-shell binding energy (k).

The result of this interaction is the ionization of the atom, which returns to a stable state by rearranging its electrons and the accompanying emission

of characteristic rays. Both the liberated electron and the characteristic rays cause more interactions with the atoms of the neighboring material before their energies are fully absorbed, and thus a gap occurs in the space of the photoelectron extracted from the shell and this is the principle of fluorescence [128].

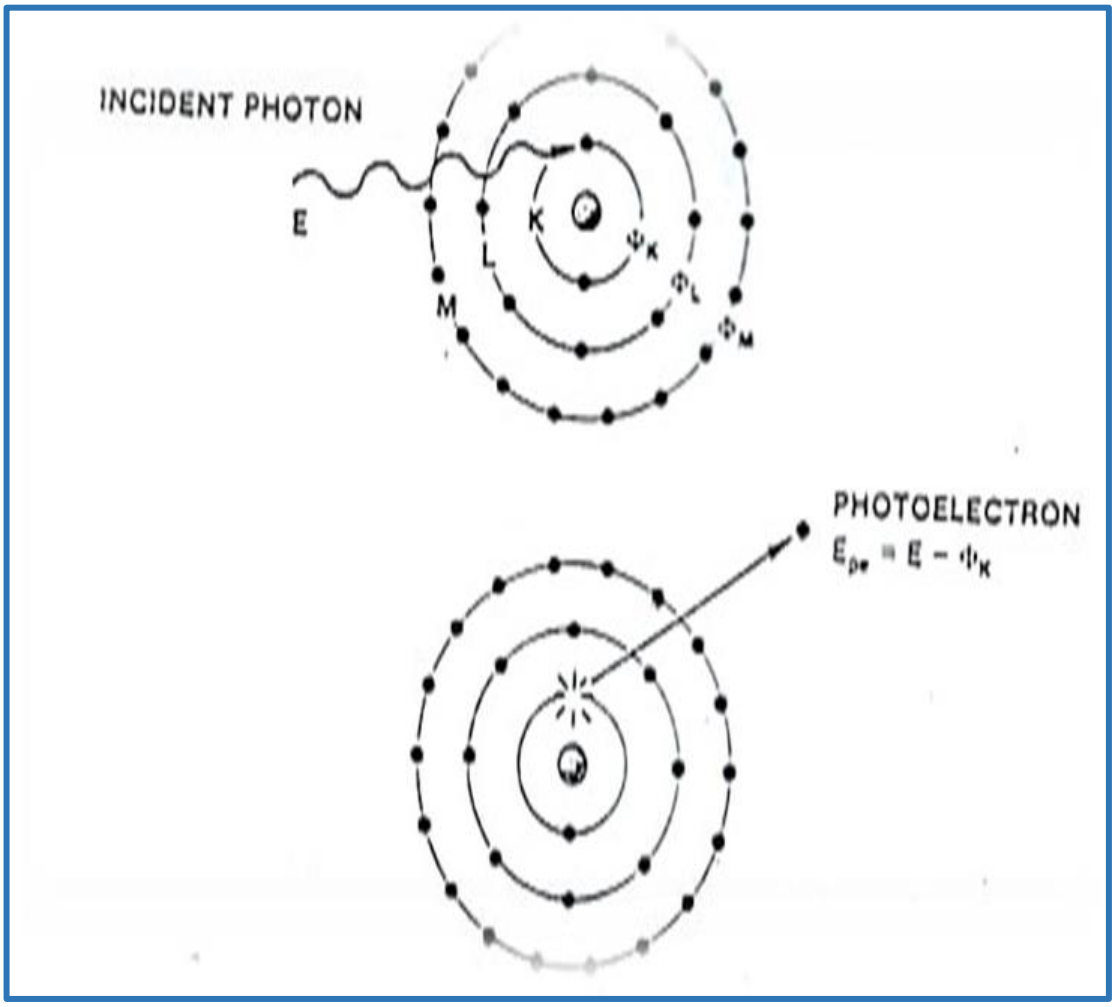

Fig. (2-8): Photoelectric reaction [114].

2.10.2 Compton Effect

When a photon collides with a free or loosely bound electron in the atom, a portion of the photon's energy is transferred to that electron, while the photon is emitted as a result of this collision in a new direction (scattering), but with less energy and a greater wavelength, so the result of this interaction is the liberation of an electron with kinetic energy to do more Interactions within the substance [114]. The scattered photon repeats the previous

interaction inside the material, as well as the distinctive rays emitted due to the vacuum left by the electron, and the subsequent rearrangement of the electrons. More interactions are required to absorb it if (λ), the wavelength, the incident radiation ($\tilde{\lambda}$) the wavelength of the radiation scattered through the angle (ψ), the change in the wavelength of the rays is given by the following equation [129].

$$\lambda' - \lambda = \frac{h}{m_0 c}(1 - cos\phi) \qquad (2\text{-}13)$$

Since h is a Planck constant and which is equal to (6.63 x 10^{-34}) J.s and m_0 is an electronic static mass, c is a release of light is called the magnitude $\frac{h}{m_0 c} = 0.04\ A^0$In the above equation, the Compton wavelength, as thisshows Compton scattering of the ray photon [130] .

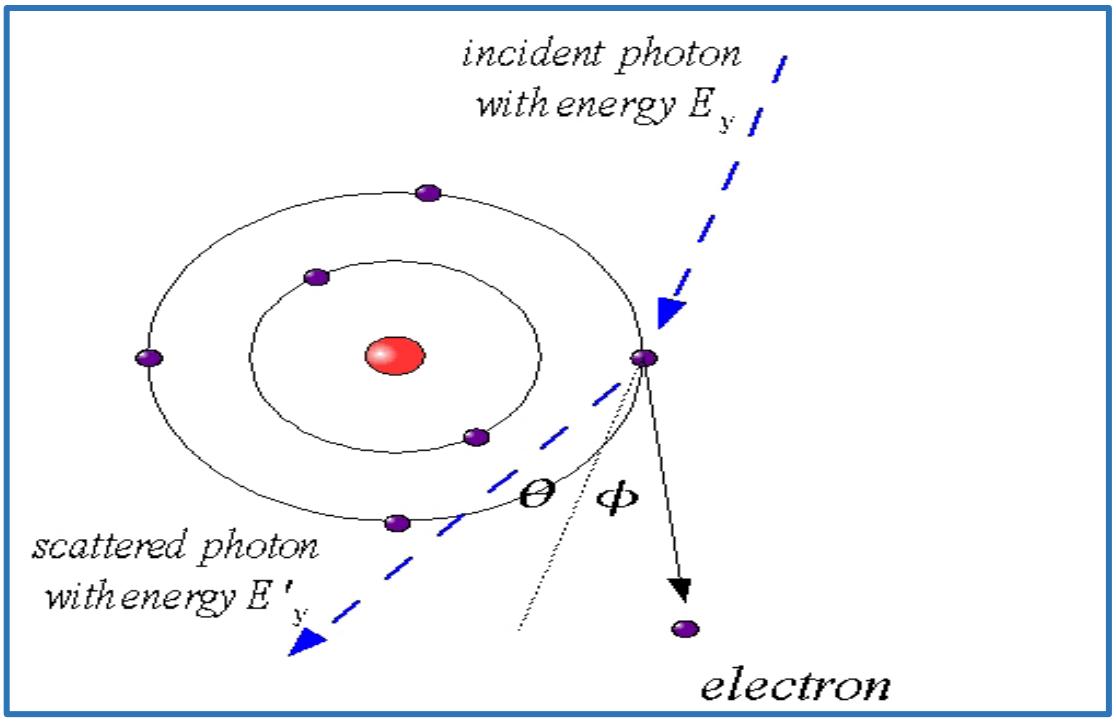

Fig. (2-9) Compton scattering phenomenon [113].

2.10.3 Pair Production Effect

Figure (2-9) shows the kinetics of the pair production reaction occurring in the nuclear domain of an atom. In this reaction, the photon gives all its energy עh to produce an electron-positron pair. Therefore, the energy conservation

equation, if we neglect the slight rebound of the nucleus, can be written as follows [131] .

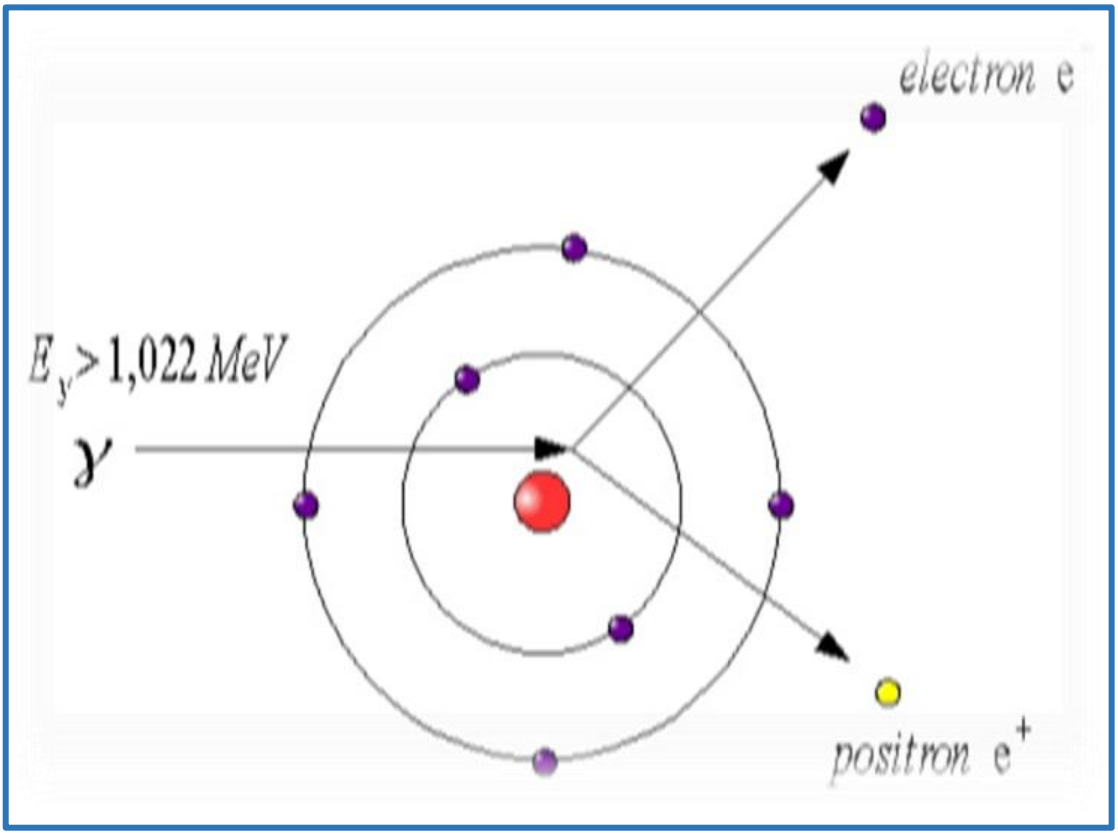

Fig. (2-10): Electron-positron pair production process [127].

The average energy of one particle may be determined using the following formula, where the electron's rest energy, m_0c^2, has been substituted with its value of $0.511\ MeV$. This means that the kinetic energy received by the electron and the positron may not be equal [132].

$$T = \frac{h\nu - 1.022\ MeV}{2} \qquad (2\text{-}14)$$

If the incident photon has more than $2m_0c^2$ of energy, the pair will have kinetic energy balanced as relative kinetic energy. When the incident photon has a power greater than $2m_0c^2$, the (electron-positron) pair will strongly radiate in directions that form an angle (θ) in keeping with the photon's initial direction of travel, then (θ) [133].

$$\theta = \frac{m_0C}{E} = \frac{m_0c^2}{h\nu} \qquad (2\text{-}15)$$

2.11 Radiation Transmission in Matter

The following equation represents a comparison between the intensity of the radiation that has been incident and that which has been transmitted [134].

$$R = \frac{I}{I_0} \qquad (2\text{-}16)$$

where I: Transmission intensity, I_o: Incident intensity, and R: Penetration rate.

The penetration of rays through the substance depends on:

1- The upper limit of the energy of the rays themselves.
2- Thickness of the intermediate material (intercept).
3- The nature of the composition of the transverse (intermediate) material, whether it is fabric, iron, aluminum, lead, or copper.

These energies do not all pass through the thickness of the material that has been placed in their route; rather, they reduce a portion of these rays to the thickness of this material, and the remaining portion penetrates to the detector. Rays are emitted when energies are released; nevertheless, these energies do not all pass through the thickness of the material that has been placed in their path. The amount by which the energy of a beam of radiation is reduced by an intercepting medium is referred to as radiation absorption, mitigation, or reduction of the beam by the intercepting medium. The attenuation of the energy of a beam of radiation is a universal number for each substance and is the same number for any radiation source located anywhere on earth. This number depends on the quality of the material and does not depend on the quality of the detector [135] .

2.12 Attenuation

During the passage of a beam of photons of rays through an intercepting medium (attenuated material), each photon in this beam will be in front of each, either not interacting at all with the medium or through an interaction by means of absorption and scattering interactions [136]. The result of removing the interacting photons from the beam will have an attenuation. And the attenuation of the beam may be in the form of attenuation of its intensity (intensity attenuation) or attenuation of its energy (energy attenuation), as it (the intensity or energy) as its distance from the source in this medium increases [136].

After traversing a space of X through an intercepted medium, a photon in a beam with intensity Io has a certain chance of interacting with anything and being knocked out of the shaft. As a result, we can express the likelihood of losing a photon from the beam per unit of travel as follows [137].

$$\mu = \lim \frac{P}{\Delta X} \qquad (2\text{-}17)$$

Since (μ) represents the linear absorption coefficient, which is a proportionality constant and it depends on:

1- The energy of the incident photon.

2- The type of interaction that the photon undergoes.

3- Composition and density of the intercepting medium.

And (P) represents the probability and is given in the following equation [138].

$$P = \frac{(nAdx)\sigma}{A} = n\sigma dx \qquad (2\text{-}18)$$

When we substitute the value of (P) into equation (2-17), find that the reaction potential per unit path length (μ) is proportional to the atomic density.

$$\mu = \sigma n \quad (2\text{-}19)$$

Since (σ) represents the total cross-section of the photon removal from the beam by the interactions of absorption (photoelectric effect, pair production) and scattering (Compton effect) [134].

$$\sigma = \sigma_{ph} + Z\,\sigma_c + \sigma_{p.p}\ (cm^2/atom) \quad (2\text{-}20)$$

The intensity of an outgoing beam of rays is reduced relative to the power of the beam incident on the surface of a material when the beam passes through the material; the degree to which the outgoing beam's intensity is reduced depends on the change in thickness (dx) of the material and the power of the incident beam I.

$$-dI = ln\sigma\ dx$$

$$-dI = ln\mu I\ dx \quad (2\text{-}21)$$

By integrating this equation, we get the intensity of the photon beam transmitted from the intercepted medium (with the same initial energy) without interacting (where $I_0 > I$)

As we notice from equation (2-21) that the window beam has experienced an exponential decrease in its intensity with the length of the distance (χ) it traveled in the middle of (μ).

The expression is [$exp(-\mu\chi)$]. represents the likelihood of a photon making it to a certain location (χ) within the attenuated medium without interaction and that it may interact only after crossing the distance (χ) directly [139].

$$I = I_0\ exp(-\mu\chi) \quad (2\text{-}22)$$

The half thickness $\chi_{1/2}$ is required to cut the incident beam intensity in half [140] .

When you are $\chi = \chi_{1/2}$, then $I = I_0/2$, and by substituting [135].

$$\frac{I_0}{2} = I_0 \, exp(-\mu\chi) \quad (2\text{-}23)$$

The process of absorption of rays by the material as previously described in the interaction of light with the material. Which is divided into two parts:

1- Compton effect.

2- The real absorption is of two types:

a- photoelectric effect.

b- Electron-positron pair production [141].

However, the photoelectric effect does not occur until the energy of the incoming photon is larger than the work function of the material, making the involvement of scattering crucial at low energies when no particular condition is necessary for this phenomenon. The photon's energy ($1.02\ MeV$) must be higher for fluorescence to occur than the product. of the static energy of the positron electron and tron. It is clear from the following:

1- If the absorption is dominant in the photoelectric phenomenon, and this is what happens in the low energy of the photon, then the bones absorb six times what the tissues absorb into the body.

2- If absorption by Compton is dominant, then one gram of bone absorbs the same amount of tissue.

3- If the absorption is by the third type, then a gram of bone absorbs twice what the tissues absorb.

Linear absorption coefficient as a function of photon energy. It is possible to write the mass absorption coefficient according to the absorption processes, especially dispersion and fluorescence as follows [142].

$$\mu = \delta + \tau \quad (2\text{-}24)$$

$$\mu/\rho = \delta/\rho + \tau/\rho \quad (2\text{-}25)$$

δ : coefficient of dispersion, τ : fluorine transformation, and μ/ρ: mass absorption coefficient.

The mass absorption coefficient is a characteristic of a substance and is the fraction of energy that displaces one gram of a substance from a beam whose section is a given unit of area. All materials are measured, it is necessary to know the mass absorption coefficient of a substance consisting of several elements, regardless of the nature of this substance as a chemical composite, mechanical blend, or solution, as well as its presence in a solid, liquid or gaseous state. The mass absorption coefficient is the average of the mass absorption coefficients of the individual substances that comprise the whole [143].

2.12.1 Linear Absorption Coefficient

Transmittance is a property that describes how well light, sound, or particles go through a given material. A significant absorption coefficient indicates that the penetrating ray is weakened (attenuated) as it passes through the material. In contrast, a small absorption coefficient suggests the substance is transparent to the penetrating light [144] . The absorption coefficient has a unit of 1/centimeter and is calculated using the inverse square root of the length. The linear attenuation coefficient is another name for the absorption coefficient. The incident beam's frequency has a role. Beer-Lambert law describes the correlation between incident ray transmitted intensity and ray incident intensity [145].

$$I = I_0 \exp(-\mu\chi) \tag{2-26}$$

Where: χ is the material's distance of influence and is the linear absorption coefficient The negative sign means the discrepancy in the number of photons that penetrate the material as the penetration distance into the material increases.

2.12.2 Mass Absorption Coefficientt

It is the process of dividing coefficient of linear absorption (μ) to the density of substance (ρ) and it is calculated from the following relationship:

$$\mu_m = \frac{\mu}{\rho} \quad (2\text{-}27)$$

where μ_m is the mass absorption coefficient, μ; Linear absorption coefficient, and ρ; density of matter.

2.12.3 Half Thickness

It means the thickness of the material that absorbs (attenuates) the intensity of the incident radiation by half of its original value.

2.12.4 Attenuation Function

The attenuation function is set by the mathematical link between the incoming radiation type and the attenuation pattern experienced by the incident particle (photon, charged or uncharged particle). Most situations can be handled by one of three attenuation functions [146].

1- Differential Attenuation

This happens in very thin media of thickness (dx), where the likelihood of a photon interacting with the medium and being absorbed is extremely low ($\mu\, dx << 1$) [121].

$$I = I_0\,(1 - \mu\, dx) \quad (2\text{-}28)$$

2- Gaussian Attenuation

This term describes the attenuation of charged particles in matter and follows the Gaussian distribution [147].

3- Exponential Attenuation

The following characteristics distinguish this form of attenuation:

- The photons' energy remains unchanged before and after travelling through the attenuating medium .
- Along the path of particles descending through an attenuated medium, the beam's intensity decreases exponentially .
- Each photon removed from the beam interacts with the elements of the attenuating medium individually.

See Figure (2-10) showing the exponential decrease in the beam's intensity is about its path length [148] .

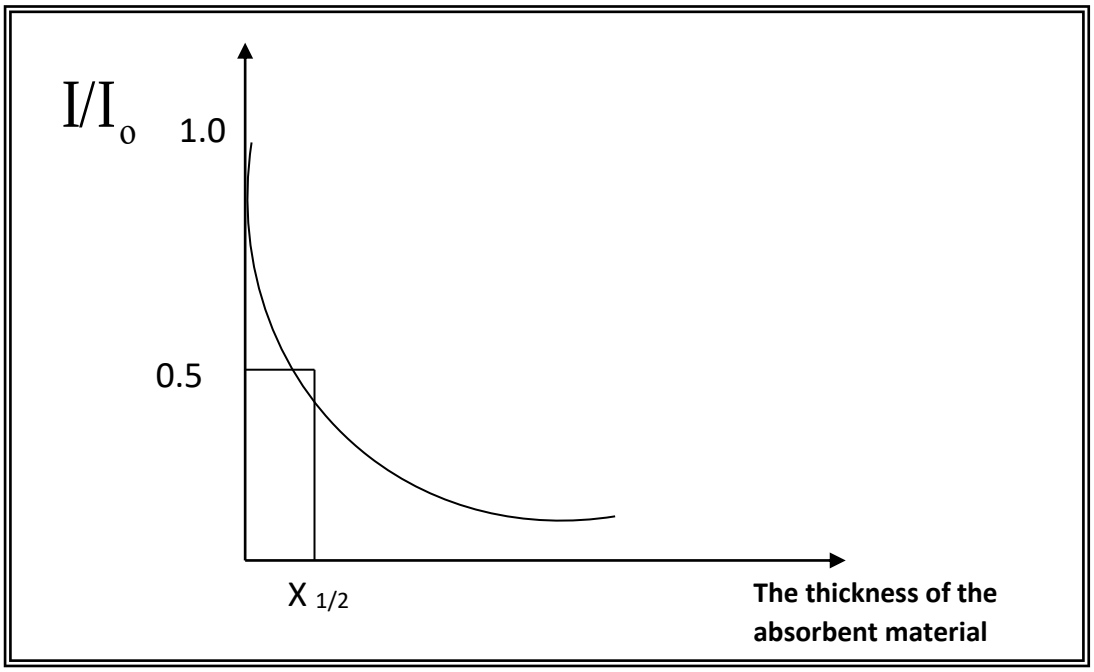

Fig. (2-11): The relationship of intensity with path length according to the attenuation of rays [144].

2.12.5 Attenuation Coefficients

Because (μ) represents the probability of removing one photon from the beam per unit path during its interaction with the atoms of the attenuated medium as a result of absorption and scattering interactions, the amount of attenuation that occurs in the incident beam as it penetrates the target material is a function of the interaction cross-section and the intensity of the incident beam. The total attenuation coefficient (μ) equals the aggregate of the partial

absorption coefficients for (the Compton effect - photoelectric effect and pair production), as shown in the following equation [149]:

$$\mu = \mu_{ph} + \mu_c + \mu_{p.p} \quad (2\text{-}29)$$

where (μ_{ph}) represents the probability of photon removal and absorption in the attenuated medium as a result of the photoelectric effect and is given by the following relationship:

$$\mu_{ph} = n\sigma_a \quad (2\text{-}30)$$

Since (σ_a) is the cross-section of the photoelectric effect. (μ_c) represents the total Compton scattering potential and includes (the scattering potential ($\mu_{c.s}$ and absorption potential ($\mu_{c.a}$) and is given by the relationship:

$$\mu_c = \mu_{c.s} + \mu_{ca} = nZ\sigma_c \quad (2\text{-}31)$$

Since the scattering and absorption cross-section is equal to the Compton effect cross-section (σ_c), the number of atoms in one cubic centimeter (Z) of the absorbent material is denoted by the symbol (η), which is the atomic number of the substance in question

Where ($\mu_{p.p}$) is a probability of photon removal and absorption as a result of pair production n, and it is calculated mathematically through the following relationship:

$$\mu_{p.p} = n\sigma_{p.p} \quad (2\text{-}32)$$

While it is possible to calculate the cross-section of the production of pairs ($\mu_{p.p}$) in a numerical way for some materials using the following equation:

$$\sigma_{p.p} = 5.93\ Z^2 \times 10^{-28}\ (m^2) \quad (2\text{-}33)$$

It is clear from the previous relationship that the cross-section of the production of pairs is proportional to the square of the atomic number

(Z) of the absorbent material, and this confirms the preference of heavy elements in the work of protective barriers from X-rays. According to the foregoing, the attenuation coefficient (μ) generally includes the absorption and scattering interactions [150].

• The attenuation coefficient is expressed as a function of the material's thickness (x) or the route length traveled by the photons (cm) in units of length cm^{-1} and is referred to as the total linear attenuation coefficient (μ) [151].

• Depends on the incoming photon's energy, the attenuated medium's atomic number (z), and the medium's density (ρ).

• When the thickness of the attenuated medium (x) is in units of mass per unit area ((gm/cm^2), the attenuation coefficient resulting from equation (2-29) will be in (cm^2/gm) units and is called the total mass attenuation coefficient (μ_m) (Total mass Attenuation Coefficient) and its relationship to the linear attenuation coefficient is[151].

$$\mu_m = \frac{\mu_L}{\rho} = \frac{1}{\rho x} \ln\left(\frac{I_0}{I}\right) \qquad (2\text{-}34)$$

Where (ρ) is a density of the intercepted medium, The mass attenuation coefficient is a function of the photon's energy and the atomic number (Z) of the medium through which it passes [152]. We note from equation (2-29) and then equations (30), (31) and (32) that the total attenuation coefficient (whether as linear or mass) depends on the cross-section of each interaction contributes to the amount of attenuation, and also the attenuation coefficients are centimeters depending on the above is the following.

1- The photoelectric attenuation coefficient (μ_{ph}) prevails in low photon energies and for materials with large atomic numbers.

2- The effect of Compton attenuation coefficient (μ_c) prevails in the medium photon energies, and for materials with few atomic numbers.

3- The production of pairs ($\mu_{p.p}$) is dominant for high photon energies, and for materials with large atomic numbers.

As for the mass attenuation coefficient ($\mu_{m.c}$) for blends and composites, it is given according to the following relationship [153].

$$\mu_{m.c} = \sum_i w_i \left(\frac{\mu}{\rho}\right)_i \quad (2\text{-}35)$$

Since (w_i) represents the weight ratio of the element to the composite, the mass attenuation coefficient for each element of the composite or blend separately.

2.13 Geiger Counter

The Geiger-Muller counter is a USA-made device that detects various forms of ionizing radiation, including gamma rays, X-rays, and fast electrons. The portable sensitivity of this cylindrical shaped detector makes it ideal for use anywhere. About 15cm long, connected to a small radio-like electronic device by means of a cable, lightweight and convenient to carry. During the measurement, the detector is placed close to the sample radiation source; An internal indicator then displays the amount of radiation detected, sometimes accompanied by a reverberating noise. It is possible to estimate the device's radiation output by listening to its sound frequencies. Whether it is strong radiation (the sound frequency is high) or little radiation (the sound frequency is slow), or the instrument may be equipped with a digital meter for accurate measurement. Geologists can mainly use it to explore nuclear ores, and uranium and thorium have been discovered in rocks in some areas. Every nuclear research facility has this device to sound an alarm if the radiation level in the facility rises suddenly and unexpectedly, giving the personnel enough time to evacuate, locate the source of the radioactive spike, and neutralize it [154].

Chapter Three

Materials and Experimental Technique

Chapter Three: Materials and experimental techniques

3.1 Introduction

This chapter focuses on the development of a rubber batch with special properties suitable for effective nuclear radiation attenuation. The possibility of developing a protective suit using this layered rubber material was considered. Multiple tests must be performed on the proposed batches, which are prepared under different preparation conditions. The primary variable in these tests is the ratios of ingredients, with the goal of achieving an appropriate batch for the intended applications. Mechanical tests, including tensile strength, hardness, modulus of elasticity and elongation, will be performed to evaluate the suitability of the batches.

As well as the radiation attenuation properties and two radiation sources (Cs^{137}, Co^{60}) for the rubber composites, and then conforming to international standards. The above were shown in Figure (3-1).

3.2 Specification of Mechanical Properties

Table (3-1): Contains the specifications of the mechanical properties of the rubber composite.

Mechanical properties of the rubber composites	American international Standards
Tensile	ASTM-D 412-88
Hardness	ASTM-D 1415
Elongation	ASTM-D 412-88
Modulus of Elasticity	ASTM-D 412-88
Density	ASTM-D 1817-66

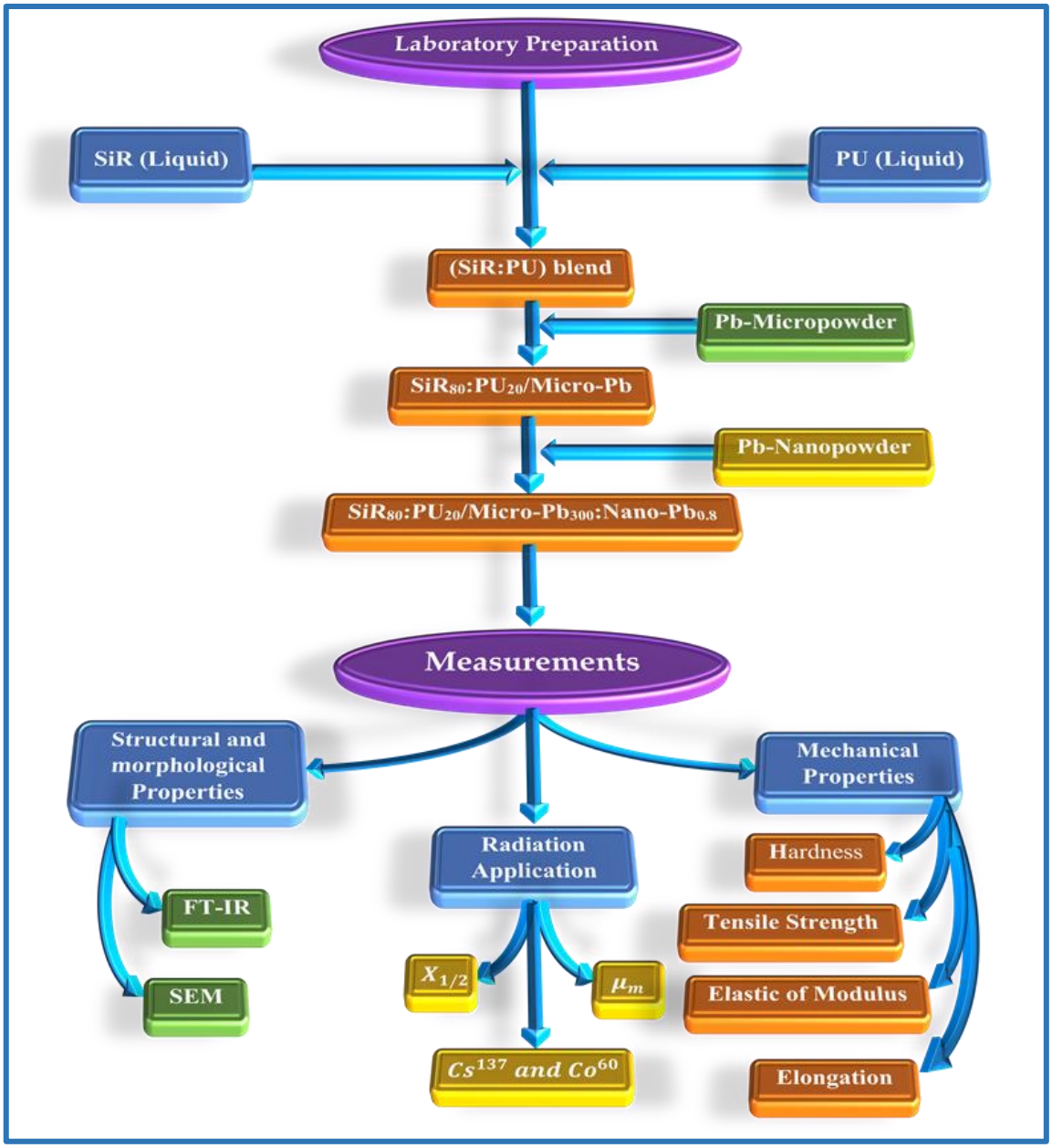

Fig. (3-1): Flow chart of experimental present work.

3.3 Materials Used in Rubber Batches

1- Silicon rubber (SiR) with hardener(A) In China.

2- Polyurethane (PU) with hardener (A) and (B) In Iraq.

3- Hexane in India.

4- Micro lead(micro-Pb) Size 249.307μ_m in India.

5- Nano lead (nano-Pb) Size 86.483 n_m in India.

3.4 (SiR:PU) Blends

In this batch, silicone rubber (SiR) in different proportions was prepared with polyurethane (PU) in different proportions also without additives. Table (3-2) shows the components of the base batch without additives.

Table (3-2): Represents the components of the basic batch (SiR:PU) without additives (Group A)

No. of Sample	Silicon Rubber (pphr)		Polyurethane (pphr)	
	A	B	A	B
S1	100	1	0	0
S2	90	0.9	5	5
S3	80	0.8	10	10
S4	70	0.7	15	15
S5	60	0.6	20	20
S6	50	0.5	25	25
S7	40	0.4	30	30
S8	20	0.2	40	40
S9	0	0	50	50

And PU Table (3-3) represents group (B) of rubber batches rubber composites with the addition of Micro-lead. Table (3-4) representing group (C) of rubber batches or (SiR:PU) composites with Micro-lead and Nano-lead. The sample with components (SiR80:PU20) was chosen because it is suitable for mechanical properties from group (A).

Table (3-3): Components of group (B) for samples with the addition of micro lead in different ratios (Group B)

No. of Sample	SiR_{80}:PU_{20} (pphr)	Micro-Pb (pphr)
S1	100	0
S2	100	20
S3	100	40
S4	100	60
S5	100	80
S6	100	100
S7	100	150
S8	100	200
S9	100	250
S10	100	300

The concentration of sample (10) is (20% + 5% + 75%).

Table (3-4): Components of group (C) for samples with the addition of nano lead in different ratios Group (C)

No. of Sample	(SiR_{80}:PU_{20}) (pphr)	(Micro-Pb) (pphr)	(Nano-Pb) (pphr)
S1	100	300	0
S2	100	300	0.2
S3	100	300	0.4
S4	100	300	0.6
S5	100	300	0.8

The concentration of sample (5) is (24.9% + 74.8% + 0.19%).

3.5. Preparation (SiR:PU) Blends

The batch is created by weight the materials using a sensitive electronic scale, which is a commonly used instrument in scientific investigations. It is important to ensure that the weight of the needed amounts is free from any external contaminants. It is also advisable to have consistent terminology. To ensure the accuracy and reliability of the experiment, it is essential to maintain a state of equilibrium in order to minimize the occurrence of any potential errors over the extended duration of the preparation phase. This particular sort of equipment has the capability to accurately calculate weights with a high level of precision, achieving an accuracy of ±0.0001 grams. The precision of the balance and the duration necessary for effective homogenization. For every individual material and across all categories of batches. The rubber batch components are homogenized by the use of a German-made stirrer (HT-120DX), operating at a speed of 50-1000 revolutions per minute. The kneading and mixing procedures in this Blender were conducted in accordance with the ASTM D15 standard, which specifies a temperature range of (50 ± 5) degrees Celsius and a prescribed sequence for adding ingredients to the Blender. The research was conducted at the University of Babylon, namely at the College of Education for Pure Sciences, Iraq.

The process of mixing and homogenizing the rubber batches was carried out according to the following steps:

1- All materials for each sample are weighed by a sensitive electronic scale.

2- Mixing (SiR: PU) where mixing is done (5 minutes for homogenization).

3- Mixing silicone hardener (A) with polyurethane hardener type (A) and mix for (5 minutes) until homogeneous, then pour the blend into the hardening and tensile molds as the first part of the work.

4-In the same way, micro lead powder, with different weight ratios, is added to paragraphs (2) and (3), and mixing is done until homogeneity as a second part of the work.

5- In the same way, nano-lead powder is added in different weight ratios to paragraphs (2, 3, and 4) and mixing is done until homogeneity as a third part of the work.

6- Samples are left for 24 hours so they can be properly prepared for testing.

3.6 Preparation of Samples to Examine the Mechanical Properties

3.6.1 Preparation of Hardness

These samples are prepared using a mold with dimensions of (200 × 180 × 6.5) mm containing nine equal sized circular holes with a diameter of 40 mm and a thickness of 4 mm as shown in Figure (3-4). The mold is first cleaned with acetone and a cloth, and then filled with the required amount of batch.

Next, the mold is placed at room temperature for 40 minutes to complete the cold vulcanization process. Subsequently, specimens are collected in the shape of round discs, with a thickness of 4 mm and a diameter of 40 mm. As shown in Figure (3-5), It is recommended to provide a 24-hour timeframe for the purpose of allowing sufficient time for chilling prior to completing the assessment. The examination was conducted in the College of Education for Pure Sciences, University of Babylon, Iraq.

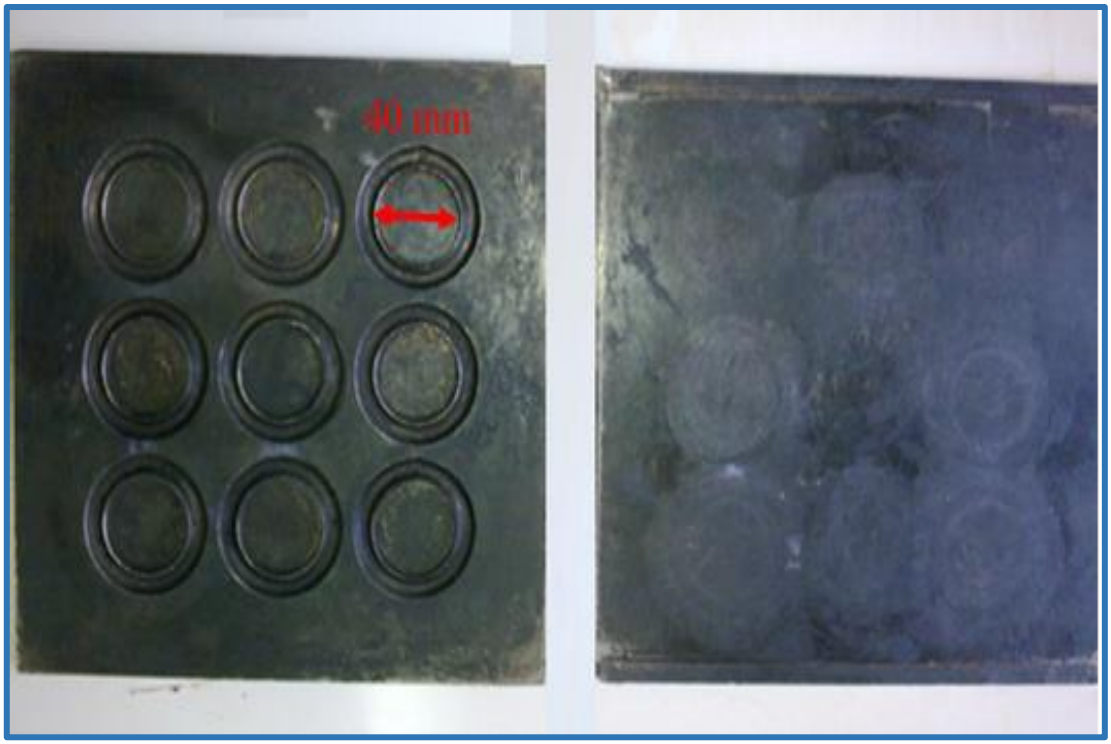

Fig. (3-2): The template for preparing hardness test samples.

Fig. (3-3): Image of Hardness test sample.

3.6.2 Preparation of Tensile Test Samples, Modulus of Elasticity and Elongation

The samples were prepared for these examinations using the template shown in Figure (3-6), which consists of two parts. The first part has dimensions (395×160×2.5) mm and contains two sections, the dimensions of one section are (150×150×2.5) mm, while the second part represents the upper cover. And it has dimensions (395×160×10) mm, the mold is cleaned first and then filled with the required quantity of the batch, after which the cover is placed on the mold for 40min, according to the American Standard ASTM-D412-88, then take out the slice, which has dimensions of (150×150×2) mm, and leave it for 24 hours to be ready for laboratory tests. The slide was cut into four standard test samples and Figure (3-7,b) shows the slide after cutting the samples, where the cutting was done by the manual cutter shown in Figure (3-7,a). The sample dimensions are 115 mm long, 22.5 mm wide, the Benchmark is 35 mm long, 6 mm wide, and the thickness is 2 mm. Figure (3-7,c) shows the dimensions of the tensile sample. The exam was taken in the College of Materials Engineering, Polymer Department, University of Babylon.

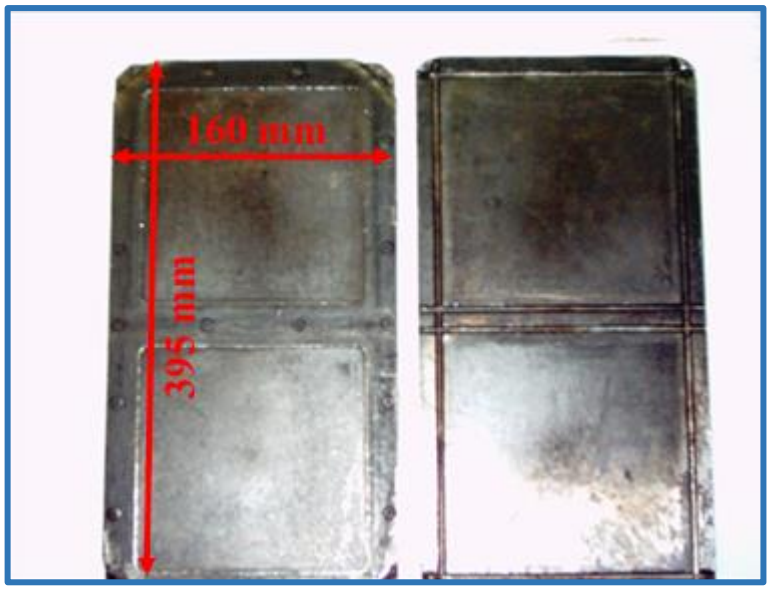

Fig. (3-4): Mold for forming samples of tensile properties tests.

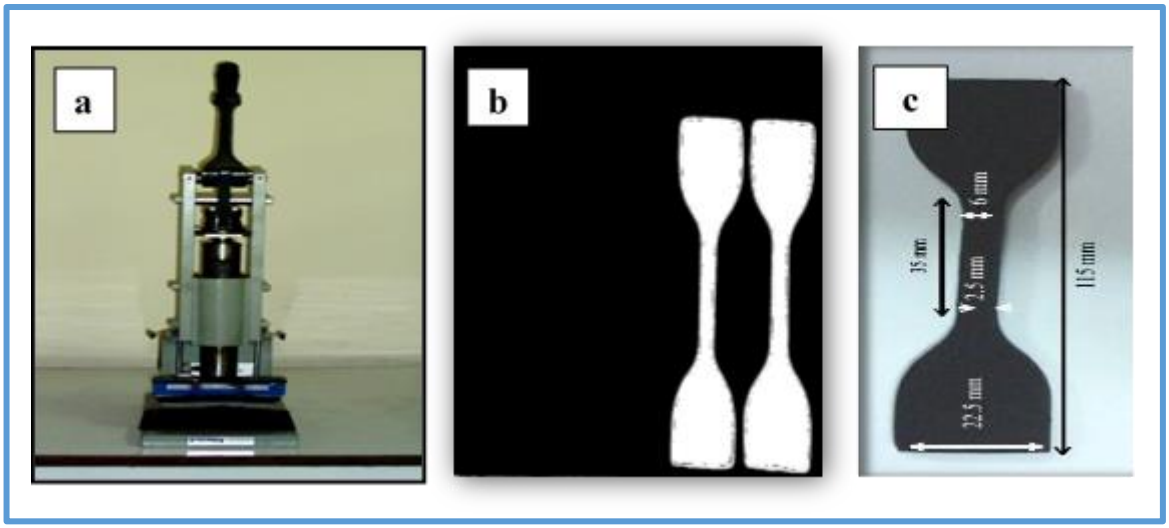

Fig. (3-5): a- manual cutter b- Slide after cutting samples c- Dimensions of the tensile sample.

3.6.3 Specific Gravity

The density is checked in the Densitometer device shown in Figure (3-8) according to the principle of Archimedes' rule, by placing rubber models in the form of vulcanized discs with a thickness of (4) mm and a diameter of (40) mm on a stand that moves automatically as it pulls out one of the models and weighs in Air first, then the model is weighed in a small basin containing water, and after a few seconds the result appears on the data recorder printer paper attached to the main device [155].

The forms used for this test are prepared by taking the weight of (12) grams of the laboratory dough to be checked for its density, after which it is shaped by placing it in a special rectangular mold that contains circular molds with diameters of (40 mm) and a depth of (4 mm) for a period of (40 minutes). This test is used to know the material losses during the batching process, as it is a measure of the weight of the used batch. The exam was taken in the College of Materials Engineering, University of Babylon, Iraq.

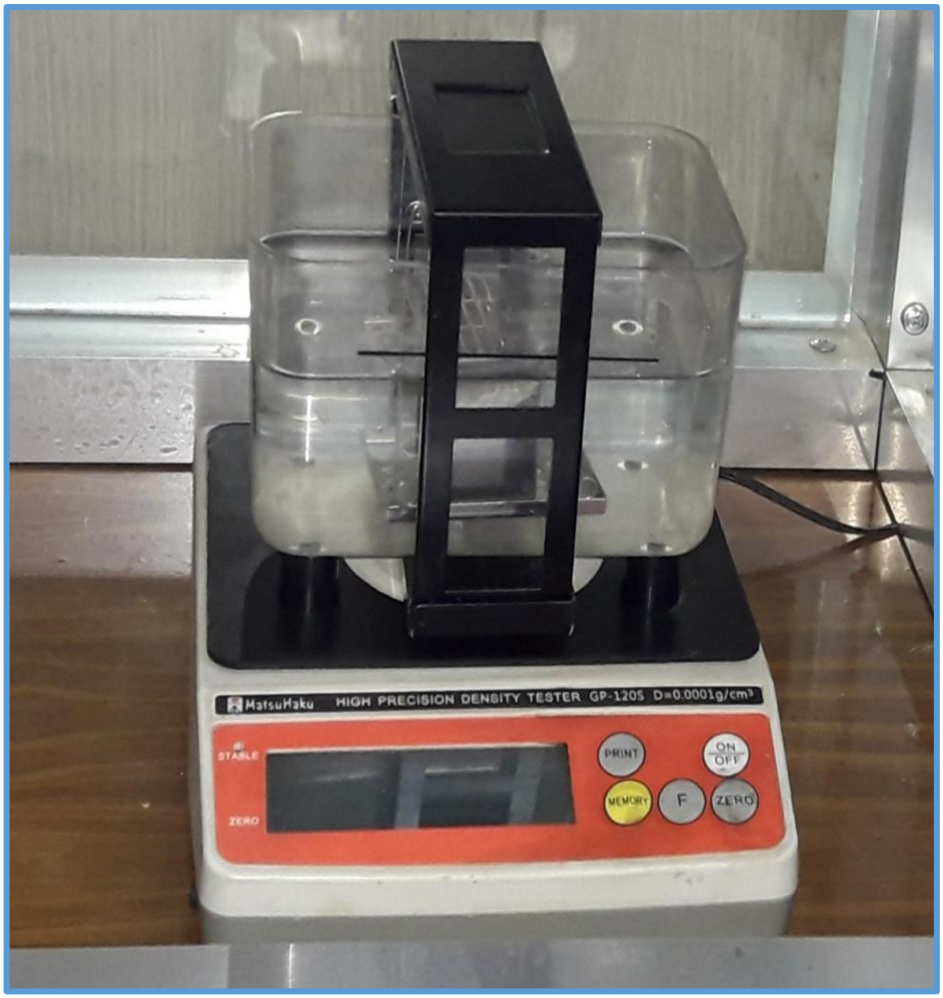

Fig. (3-6): Densitometer device for checking density.

3.7 Test Equipment and Characterizations

3.7.1 FTIR Spectrometer

Fourier Transform Infrared Spectroscopy (FTIR) was used to get the FTIR spectra of composites comprising of (SiR_{80}:PU_{20}/micro-Pb_{300}) and (SiR_{80}:PU_{20}/micro-Pb_{300}:nano-$Pb_{0.8}$). The FTIR measurements were conducted using a Bruker vertex-70 spectrometer, manufactured by the Bruker firm in Germany. The experiments were carried out at the University of Babylon, specifically at the College of Education for pure sciences. Figure (3-7) displays Fourier transform infrared spectrometer is used to measure wavenumbers within the range of 600 to 4000 cm^{-1}.

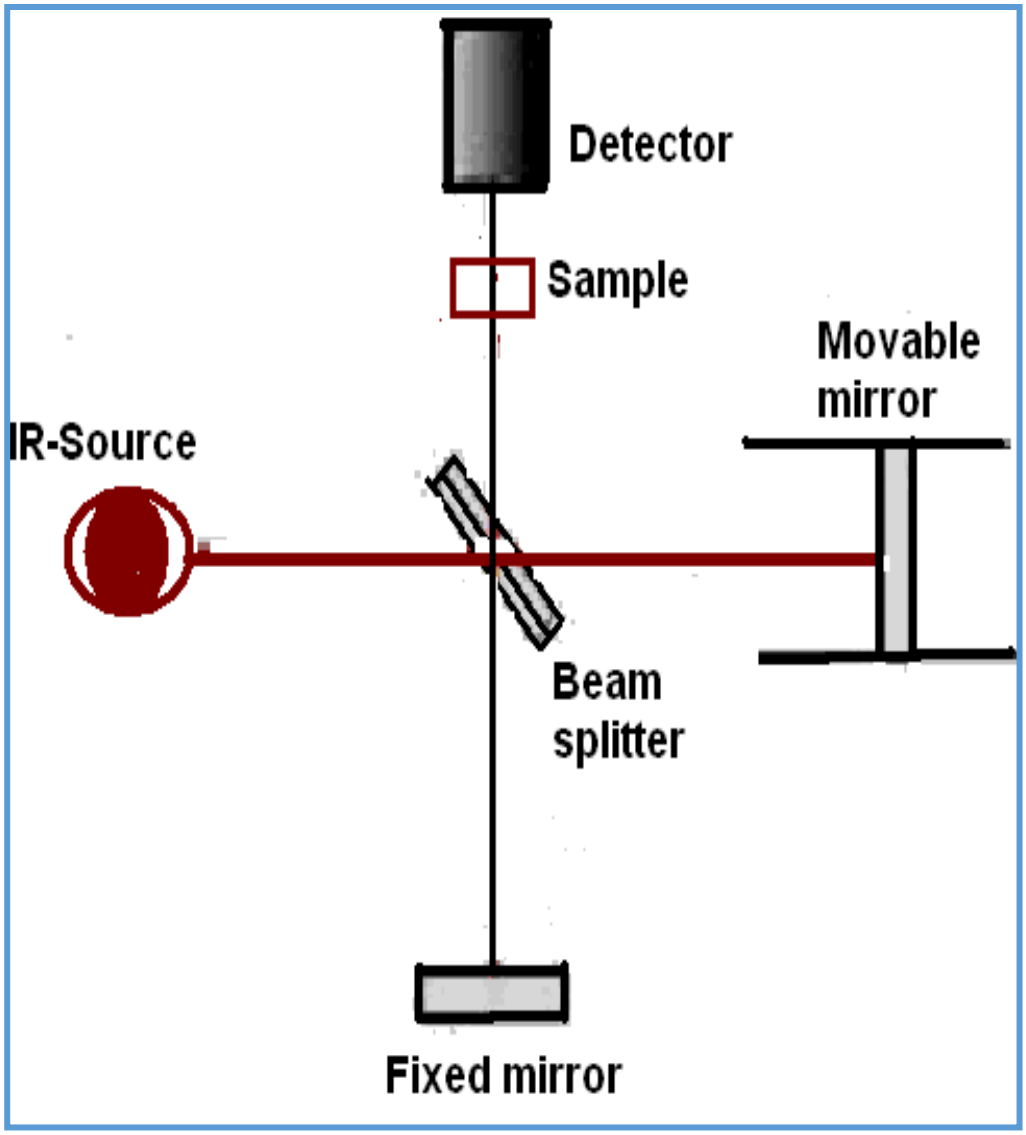

Fig. (3-7): Schematic representation of FTIR spectrometer.

3.7.2 Scanning Electron Microscope

The surface morphology of two composites, SiR_{80}:PU_{20}/micro-Pb_{300} and SiR_{80}:PU_{20}/micro-Pb_{300}:nano-$Pb_{0.8}$, with different concentrations of micro-Pb and micro-Pb/nano-Pb, respectively, was analyzed using a scanning electron microscope (SEM) of German origin (Company, type vertex-5600 LV SEM). The analysis was conducted at the University of Babylon, specifically in the College of Materials Engineering, Department of Polymer Engineering and Petrochemical Industries, Iraq. The results are presented in (Figure 3-8).

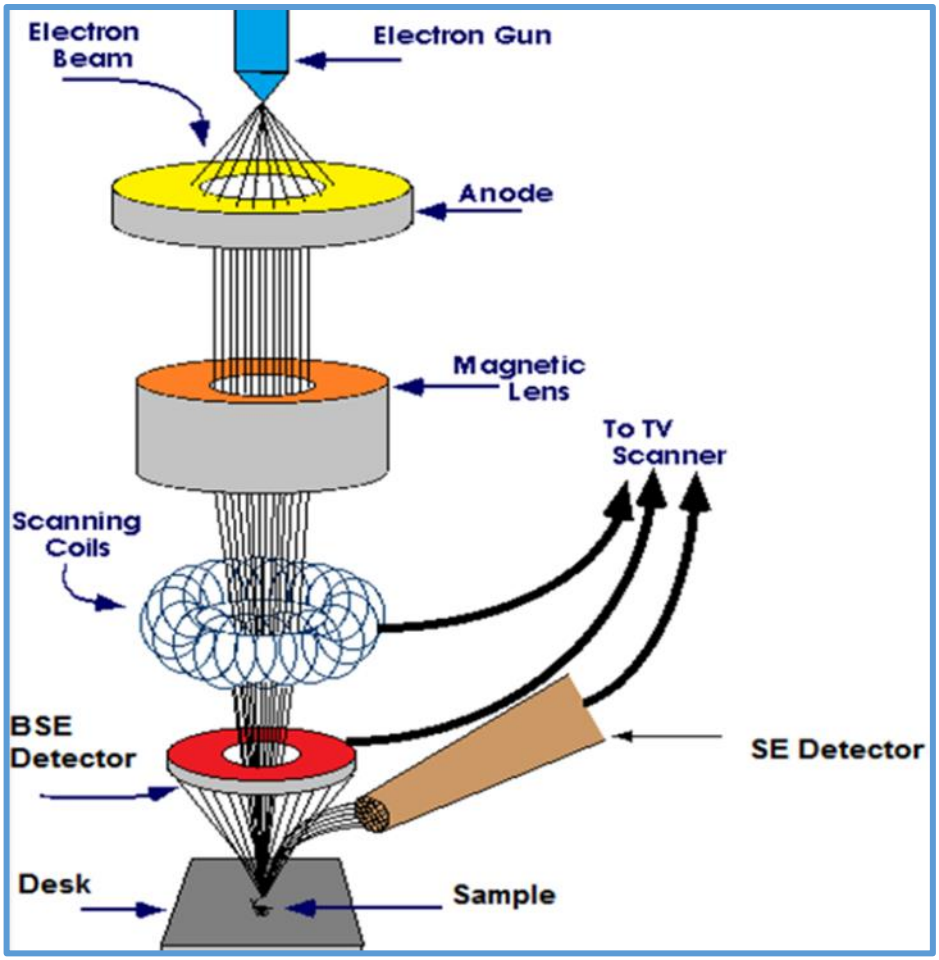

Fig. (3.8): A graphical representation of how the SEM.

3.7.3 Monsanto T10 Tensometer Equipment

In accordance with ASTM D-412-88, a tensile strength at break (Mpa), modulus of elasticity at 100%, 200%, and 300% elongation (Mpa), are all tests that may be run on a Monsanto T10 Tensometer. The thickness and width of the sample were measured to within 2 mm before analysis. Figure (3-9) depicts a tensile test, which you should do and then store in the device's memory so that you can readily get the stretch and stress you require. A computer and plotter are used to operate this apparatus. In addition, the plotter generates a (stress-strain) curve by forcing one jaw of the sample container to move at a high rate of speed (500 mm/min) while the other jaw remains stationary. The examination was held at the University of Babylon in Iraq, in the Department of Materials Engineering.

Fig. (3-9): Image of Tensile test device.

3.7.4 Hardness Test Equipment

The Shore A hardness instrument in Figure (3-10) tests hardness. The strain caused by a model-pressing spring influences rubber hardness. The test follows ASTMD-1415. The Brunel method predicts Figure (3-3) for the 4-millimetre-thick model. The model is placed at the bottom of the device and the fulcrum is used to manually examine the device. The indicator then displays the relevant reading (Shore A) and the process is repeated. The average is obtained after four examinations of various model surfaces. University of Babylon, Iraq, College of Education for Pure Sciences hosted the test.

Fig. (3-10): Hardness Equipment (Shore A).

3.8 Preparation of Samples for Radiation Testing

Figure (3-11) depicts the rubber samples being cut to the appropriate dimensions (16mm ×25mm× 2mm) in preparation for placement inside the room of the American-made Geiger counter device, where they will undergo radiation analysis using the Geiger counter device depicted in Figure (3-12). The radiation characteristics of the samples were analyzed at the University of Babylon's College of Education for Pure Sciences.

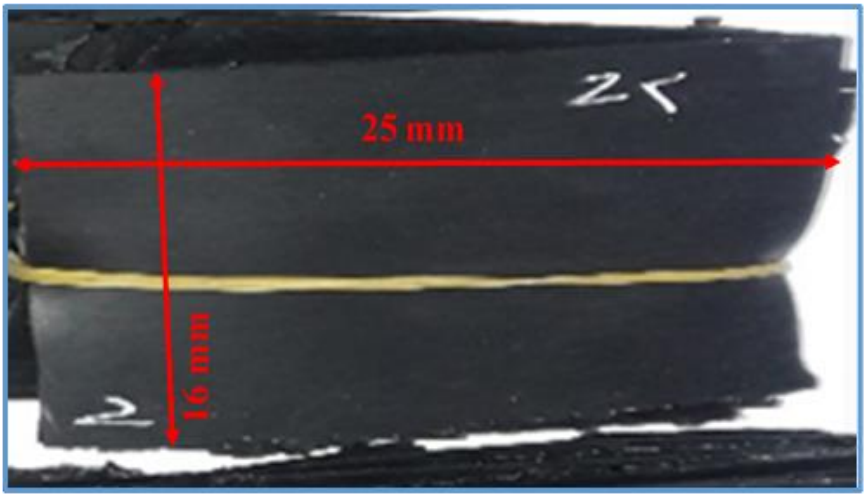

Fig. (3-11): Represents the rubber samples for examining radiation sources

Fig. (3-12): Geiger counter.

3.8.1 Radioactive Sources

Two sources of radiation were used, each of the cesium source (Cs^{137}) and the cobalt source (Co^{60}), and the number of radiations was detected by the aforementioned Geiger counter, where the back reading of the device (N_b) was taken for cesium (43) and cobalt (23) without the radiation source and (N_0) obtained, in the presence of the radioactive source for each source and mean values (N_{av}) were obtained for all rubber samples, and then the following relationship was used.

$$N = N_{av} - N_b \qquad (3\text{-}1)$$

N_{av} average values, and N_b background reading.

3.8.1.1 Cesium Source (Cs^{137})

It has the symbol (Cs^{137}) in the periodic table. Its half-life is ($t_{1/2}$) (30.07 years) and the activity is (5μci).It emits Beta/Gamma radiation)) Year of manufacture (December/12/2008) It is from rare sources, its color is golden to silver. It belongs to the group of metals. Cesium is the most energetic of the metals. The work was done to examine the samples for radiation properties in the College of Education for Pure Sciences, University of Babylon, Iraq.

3.8.1.2 Cobalt Source (Co^{60})

Co^{60} is a periodic table chemical with a half-life of $t_{1/2}$. With a lifespan of (5.37) years, its efficacy is 1μci. The November/11/2008-made metallic gray device emits gamma radiation. When the loading percentage of the additive increases, the half thickness decreases due to the increase in radiation absorbed by the material and the interaction between them, which increases linear and mass absorption. The probability of interaction depends mainly on the number of particles in the radiation path. The College of Education for Pure Sciences, University of Babylon, Iraq, examined the samples for radiation characteristics.

3.9 Examination of Group Samples (B) and (C) by Geiger Counter

The examination of samples for group (B) in the presence of micro-lead and group (C) in the presence of nano-lead was carried out by American-made Geiger counter [156].Taking into account the following points:

1- Ensure that the zirconium filter is placed in the appropriate position in the radiation path to obtain a wavelength of (0.71 encestroms).
2- Calculate the effect of the background radiation for a period of (100) seconds. Anode voltage (600) volts.
3- Calculate the number of pulses in (100) seconds without putting the absorbent material to find (I_0).
4- Find the change in the pulse rate (I) with the change in the thickness of the new polymer slices.
5- Calculate the linear absorption coefficient (μ) and the mass (μ_m) for the new superimposed, the thickness of the half ($X_{1/2}$), and the absorbance.

Chapter Four

Results and Discussion

Chapter Four: Results and Discussion

4.1 Introduction

This chapter includes practical results obtained from measurements and tests conducted on rubber models or batches consisting of silicon rubber and polyurethane with different weight ratios.

The rubber batches were examined for mechanical characteristics of hardness, Tensile strength, elongation, and elastic modulus. These results are characteristic of FTIR and SEM examinations, mechanical properties, radiation properties, and how to discuss them in many applications, especially their use in radiation shielding to attenuate radiation within the range that contains radiation due to the risks and health damages caused by these radiations to humans.

4.2 The Mechanical Properties of the Rubber Blend

4.2.1 The Hardness of the Rubber Blend

From Figure (4-1), The measured hardness values of quantities of rubber with a progressive and irregular increase in additive (PU) concentration. The presence of certain interactions between the rubber molecules and additives within the prepared sample, which is responsible for its resistance to external forces, increases the surface hardness of the prepared material, which is consistent with previous research [160]. The decrease in density observed in samples 3 and 5 can be attributed to the interconnection of rubber strands and the relatively low concentration of polyurethane within them. Specifically, the addition of polyurethane resulted in a gradual and incremental increase in hardness.

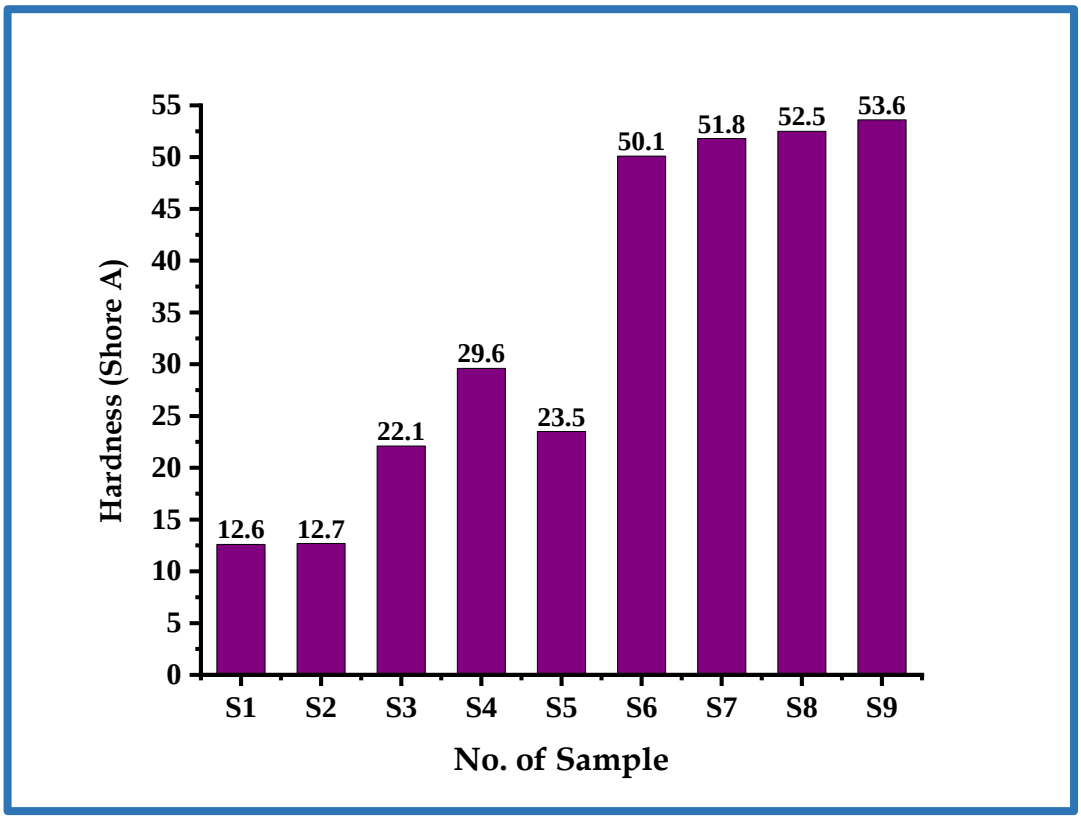

Fig. (4-1): Plot of change in the hardness of different blends samples group A.

4.2.2 Tensile Strength, Modulus of Elastic and Elongation of the Rubber blend

Figures (4-2), (4-3) and (4-4) show the effect of polyurethane (PU) additive with loading rates (0, 10, 20, 30, 40, 50, 60, 80, 100) pphr on some mechanical properties respectively, tensile strength, elongation and modulus of elasticity of the rubber blends consisting of silicon rubber and polyurethane (SiR_{80}:PU_{20}) and the result of comparison between the results of mechanical tests represented respectively (tensile strength, elongation and modulus of elasticity).

From the Figures (4-2) and (4-3) that the decline in the tensile strength and elongation chart is explained on the basis of the material reaching the yield point, where the material continues to resist until its resistance collapses as a result of the lack of distance between the rubber chains, as it is at a certain percentage that it cannot bear the added material, which leads to the occurrence

of cracks and pores in the batch inflatables. This is consistent with previous research [161].

The Figure (4-4) demonstrates a marginal rise in the modulus of elasticity as the loading percentage of polyurethane increases. This can be attributed to the enhanced physical adhesion and cohesion force between the filler and rubber. The observed improvement in certain properties is a consequence of the powder material (PU) present, which facilitates an increased surface area for diffusion. Consequently, a greater number of bonds are formed with the rubber chains, aligning with previous research findings [162]. The decrease in the sample (9) due to the increase in the polyurethane additive as for the increase in the modulus of elasticity, it may indicate a strong decrease in the elongation shown in Figure (4-3). As a result of its inverse proportion to the property of the modulus of elasticity, it caused a clear increase in the modulus of elasticity. Sample (3) with composite compounds (SiR_{80}:PU_{20}) was adopted. As more convenient and to achieve mechanical properties.

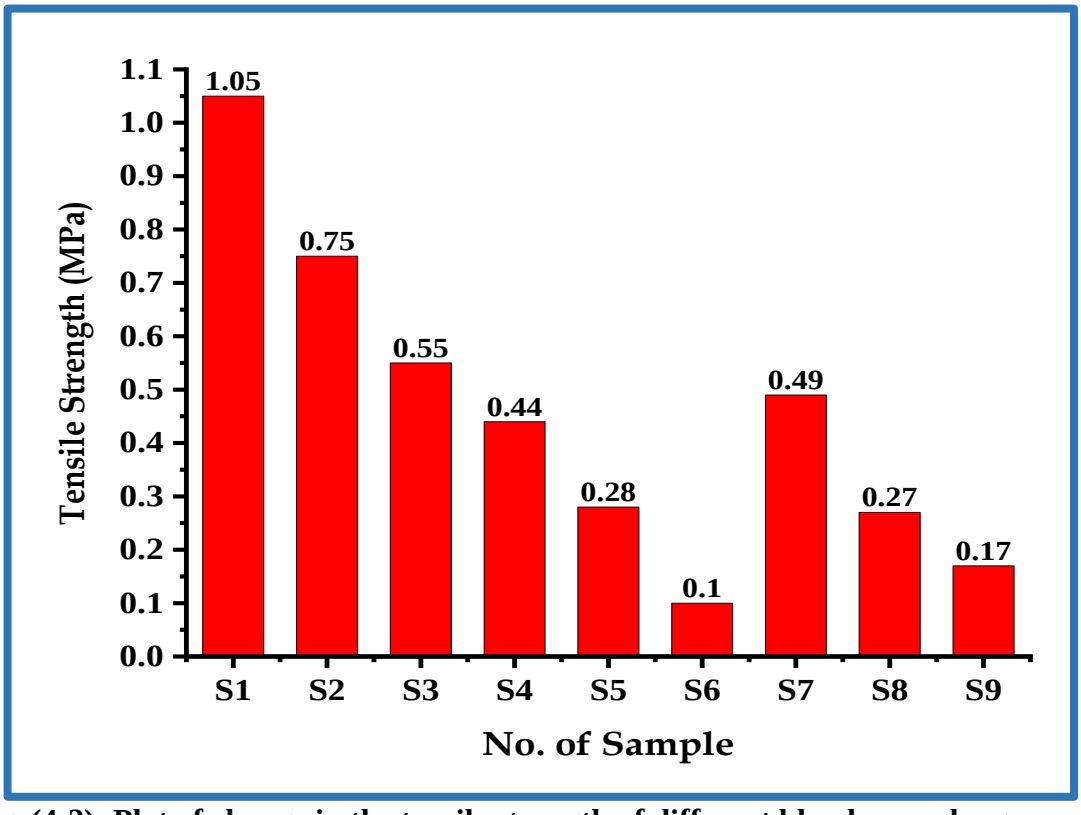

Fig. (4-2): Plot of change in the tensile strength of different blends samples group A.

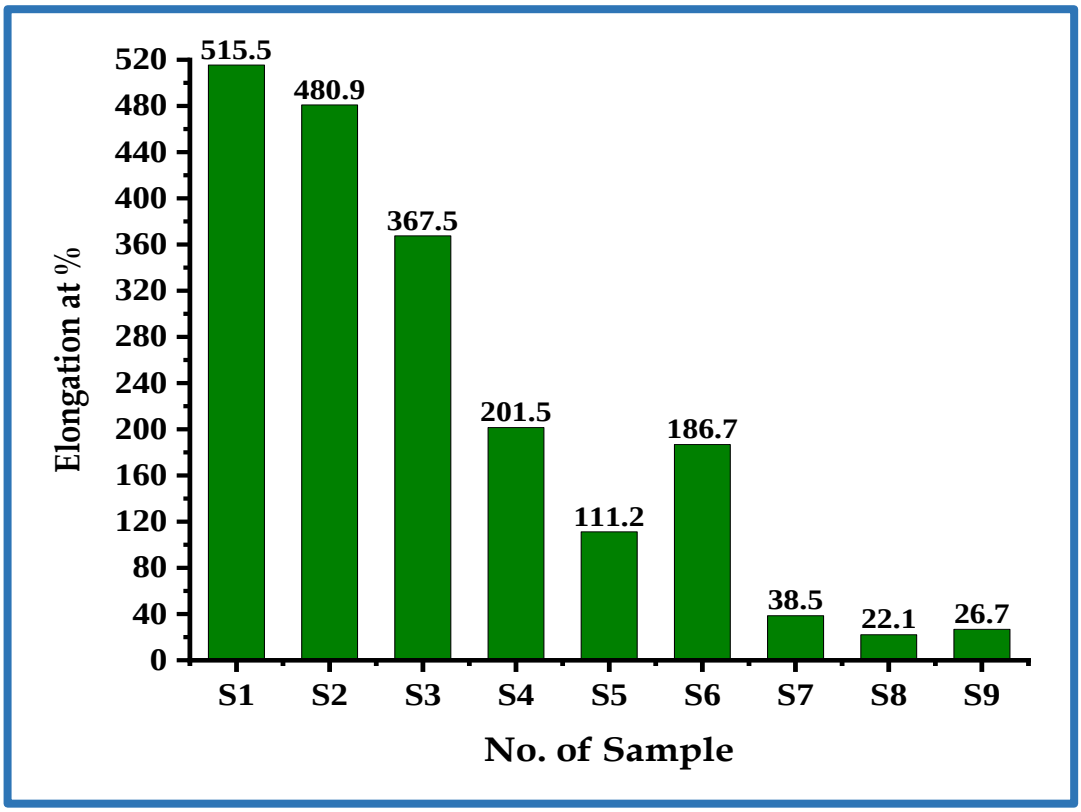

Fig. (4-3): Represents change in the elongation of different blends samples group A.

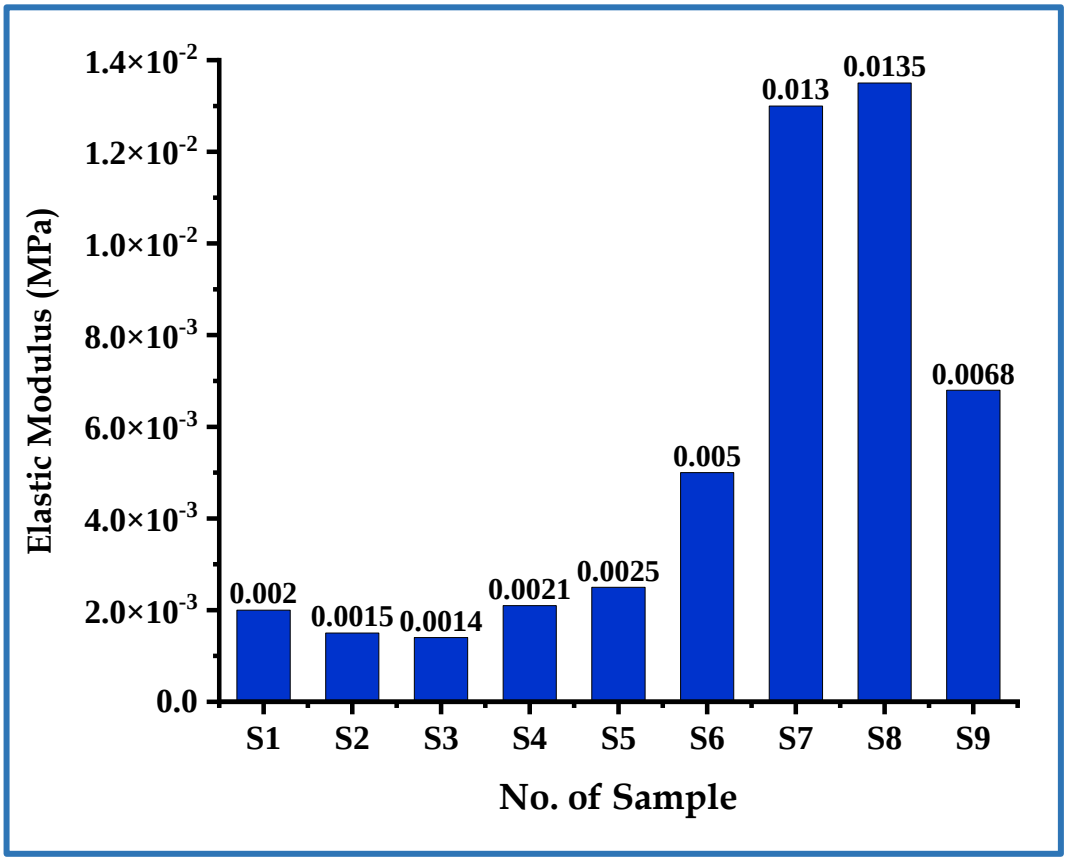

Fig. (4-4): Represents change in the modulus of elasticity of different blends samples group A.

4.3 The Structural Properties of the (SiR_{80}:PU_{20}/micro-pb) Composites

4.3.1 FTIR Spectrum

Fourier transform infrared (FTIR) spectrum of (SiR_{80}:PU_{20}/micro-Pb_{300}) rubber composite and hexane were recorded at room temperature in the trem (600-4000 cm^{-1}) as shown in Figure (4-5), where it was observed that there are no apparent changes in the radiation spectrum. Infrared for the rubber composite, even when the loading ratios changed, but the presence of hexane closed the gaps in the rubber composite, and the distribution of lead was evenly distributed. The spectra displayed the distinctive bonds of vibrations. It extends from the functional groups that were formed in the composites from these spectra of the stretching vibration of aliphatic extends to the region belong (c=c) stretching. The two peaks at the two areas (698-1009) cm^{-1} are the bending vibration [158].

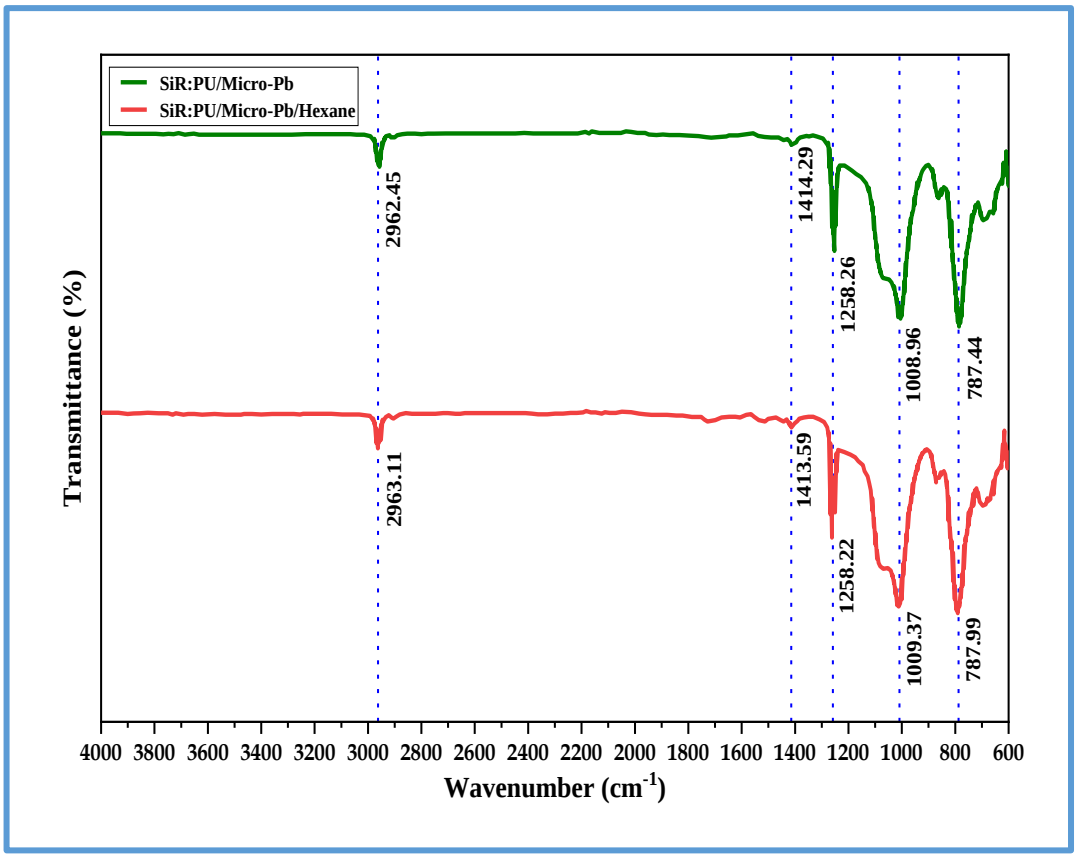

Fig. (4-5): FTIR spectra of (SIR_{80}:PU_{20}/Micro-Pb_{300}) of the sample with and without hexane.

Table (4.1): FT-IR Transmittance bands positions and their assignments of (SiR_{80}:PU_{20}/Micro-Pb_{300}) Composites

Vibration frequency (cm^{-1})	Band assignment of Composite
2962.45	O–H Stretching
1258.26	C-O-C Stretching
1008.96	C-O Stretching
787.44	=C-H out-of-plane bending

4.3.2 SEM of the (SIR_{80}:PU_{20}/Micro-Pb_{300}) Composites

Figure (4-6) displays of (SiR_{80}:PU_{20}/microPb_{300}) composites was examined by a scanning electron microscope before mixing hexane, representing an image (A) with lumps and heterogeneity, the micro-lead undistributed, and there are gaps. As for image (B), after mixing the hexane, we notice clearly that the micro-lead was distributed evenly and has no lumps; the two images are similar and have the same ingredients and quantities [159]. Represents image (A) of the sample without hexane and image (B) when hexane is added, are Figure (4-7) represents the distribution function, the Figures (A and A1), the diameter and the surface area of the micro-lead without adding hexane, while the Figures (B and B1), represents the diameter and surface area of micro-lead when adding hexane and this indicates that the micro-lead homogeneous distribution on the sample. The distribution function (Gaussian) was calculated using the image processing program (ImageJ), where the results of the distribution function showed that the average diameter of fine lead microparticles in the absence of hexane was 82.32 μm, with an average area of 1120.38 μm^2, but in the presence of hexane, the average diameter was 131.37 μm, with an average area of 1849.31 μm^2, and this means that lead was

distributed homogeneously and this improvement is attributed to the interconnection of the bonds between the polymeric chains.

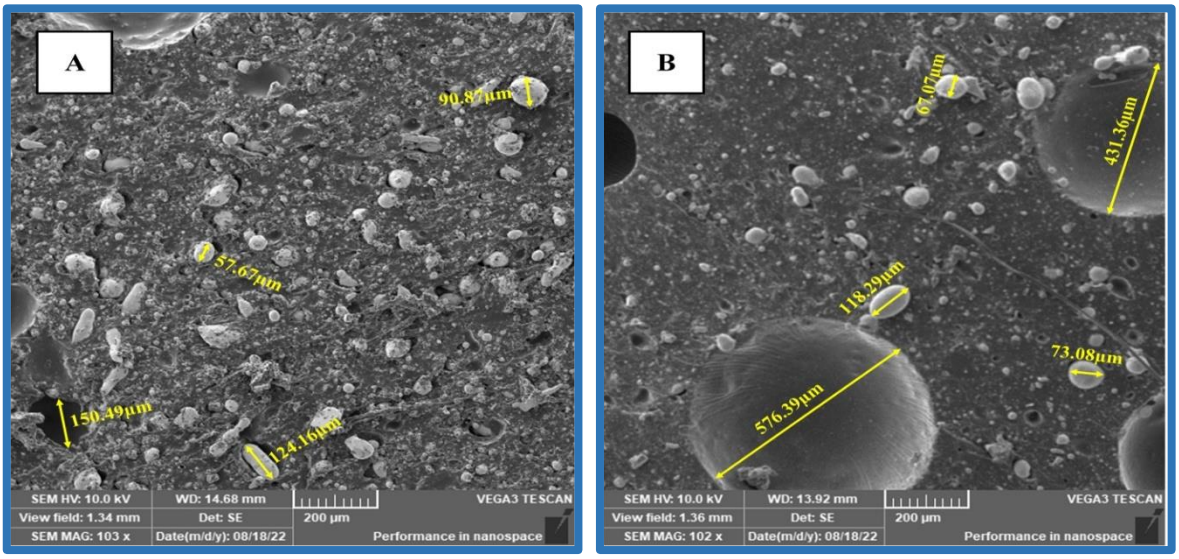

Fig. (4-6): SEM images for (SiR_{80}:PU_{20}/microPb_{300}) of (A) of the sample without hexane and the image (B) when hexane is added.

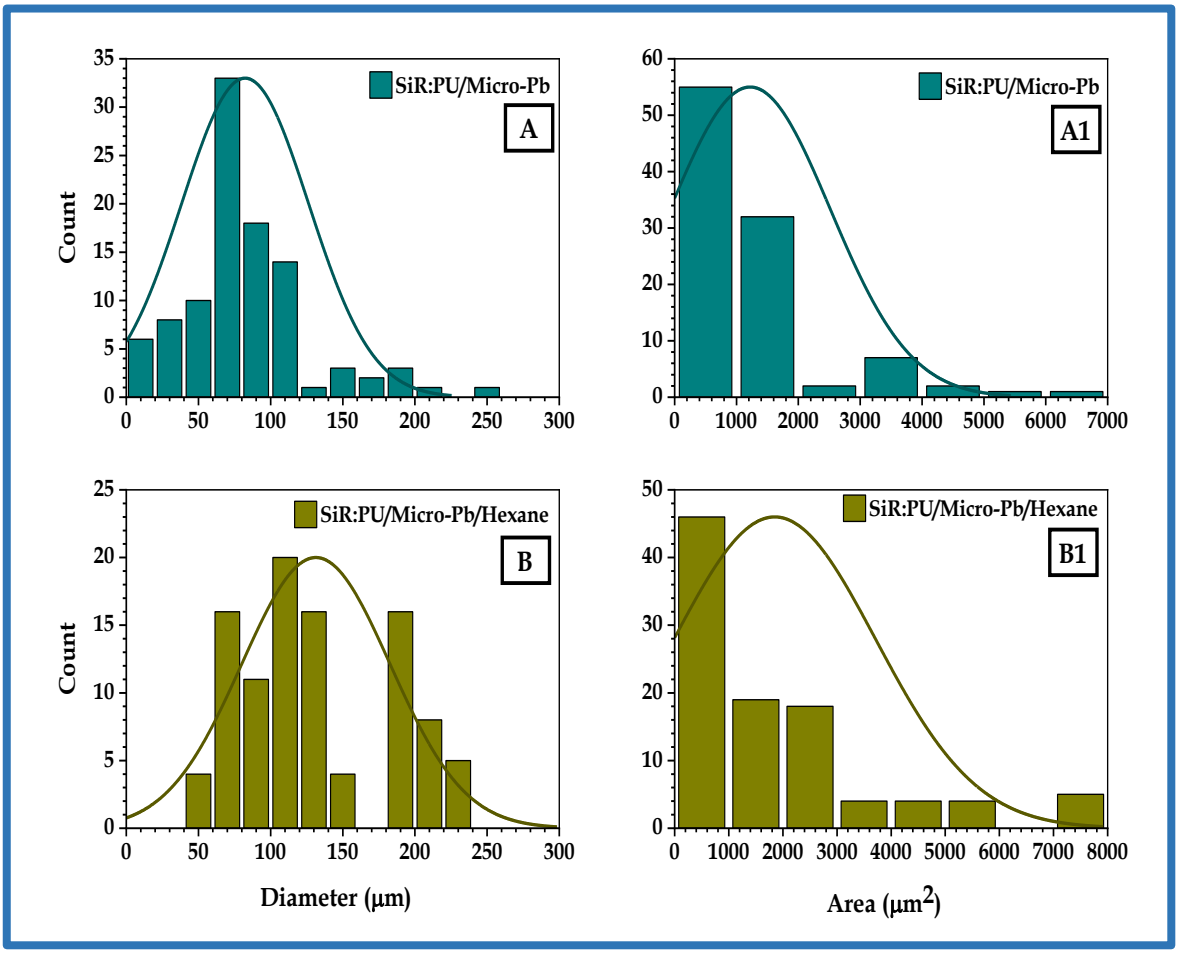

Fig. (4-7): Represents the distributive function (A and A1) represent the diameter and volume area of micro-lead without adding hexane. (B and B1) represents the diameter and volume area of micro-lead with hexane.

4.4 The Mechanical Properties of the (SiR_{80}:PU_{20}/Micro-Pb) Composites

4.4.1 Hardness of the (SiR_{80}:PU_{20}/ Micro-Pb) Composites

Based on Figure (4-8), it is evident that the surface hardness values obtained for the rubber batches exhibit a progressive and uneven rise as the concentration of the additive (Micro-Pb) increases. The cause of this phenomenon can be attributed to the interference that arises between the supporting material and the underlying material. This interference leads to an increase in hardness and the filling of voids within the basic material, specifically the rubber blend. The occurrence of cross-linking between the rubber chains and the additive present in the prepared blend plays a crucial role in enhancing the material's ability to withstand external forces. As a result, the surface hardness of the prepared material is heightened, aligning with findings from prior investigations [160].

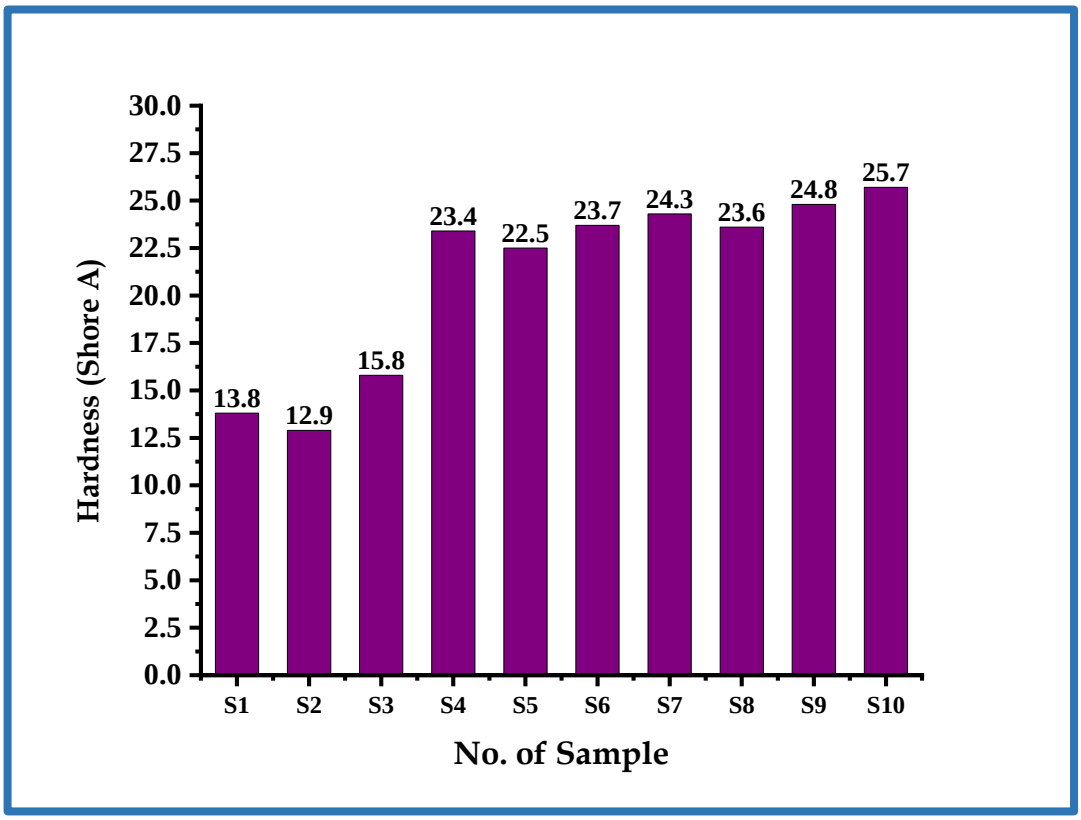

Fig. (4-8): behaviour of hardness for different loading ratio of micro-Pb group B

4.4.2 The Tensile Strength, the Elastic Modulus, and the Elongation of the (SiR_{80}:PU_{20}/Micro-Pb) Composites

Figures (4-9), (4-10), and (4-11) depict the changes in tensile, modulus of elasticity, and elongation of the composites composed of (SiR_{80}:PU_{20}) for rubber batches caused by adding micro lead powder at loading ratios of (0, 20, 40, 60, 80, 100, 150, 200, 250, and 300) pphr. Mechanical tests (tensile strength, modulus of elasticity, and elongation) and radiation characteristics of batch models were compared, and the sample (10) with components (SiR_{80}:PU_{20}/Pb-micro$_{300}$) was found to be optimal. From Figure (4-9) there is a clear increase in the tensile strength due to the added material of micro lead, which led to the interconnection of the polymer chains. The tensile strength increases as the loading percentage increases. Figure (4-10) represents the modulus of elasticity, where the clear increase is due to the increase in the loading percentage of the material. Micro lead and also because of the cohesion of the bonds between the polymer chains. From Figure (4-11), Which represents elongation, and the decrease that occurs is its inverse proportion to the tensile strength and modulus of elasticity, as the material reaches the point of yielding and the material continues to resist until it collapses with an increase in the percentage of partial lead powder loading. This is due to the lack of space between the rubber chains. The micro-lead powder has a small granular size that increases the surface area for diffusion and, thus, the formation of a larger amount of crosslinking with the rubber chains, and this is consistent with previous research [161]. It is also noted from the figures that the decline in the tension and elongation diagram is explained depending on the material to the point of yielding, where the material continues to resist until its resistance collapses as a result of the lack of space between the rubber chains, as they are at a certain percentage that cannot withstand the added material, which leads to the occurrence of cracks and toxins in the sample and this is consistent with previous research [162].

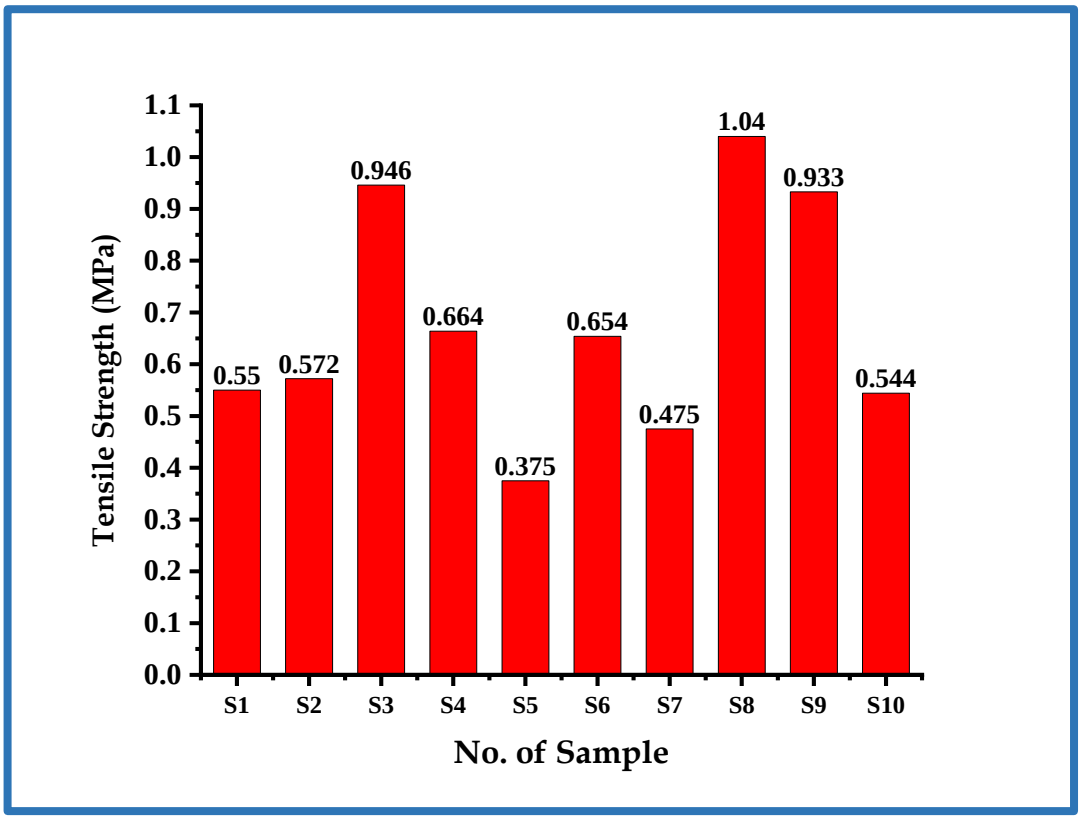

Fig. (4-9): Plot of change tensile strength for different loading ratio of micro-Pb group B

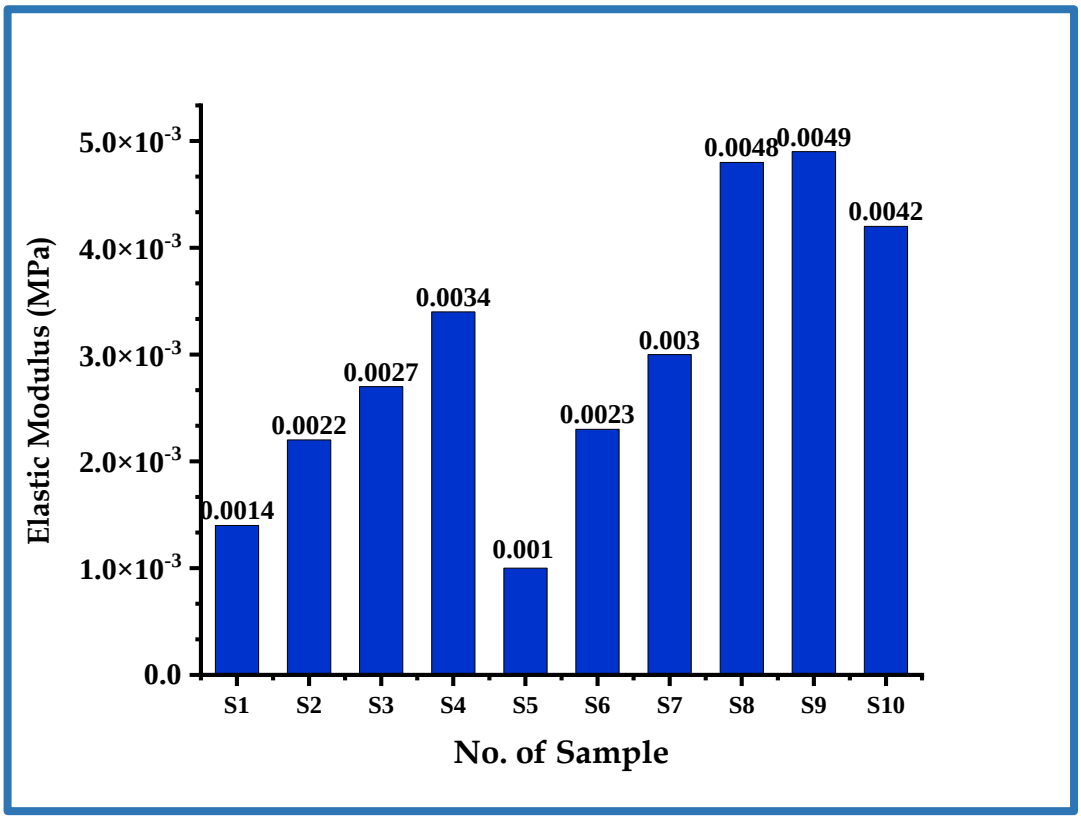

Fig. (4-10): Plot of change the elastic modulus for different loading ratio of micro-Pb group B

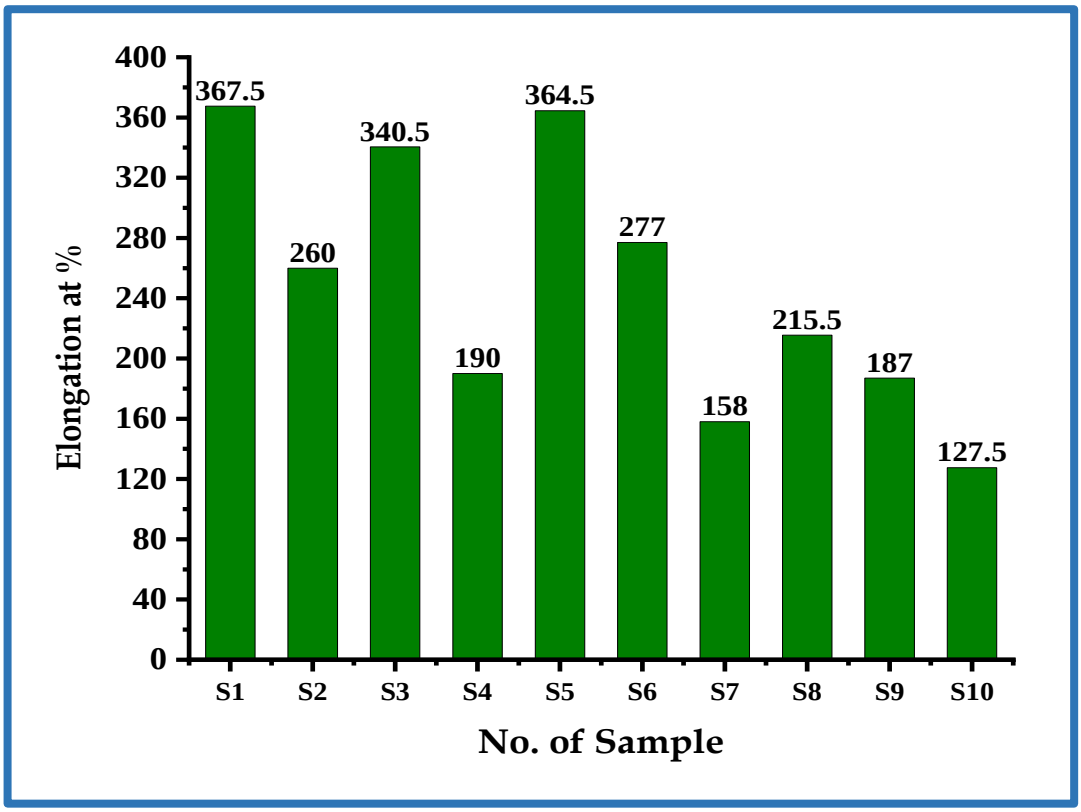

Fig. (4-11): Plot of change the elongation for different loading ratio of micro-Pb group B

4.4.3 Specific Gravity of the (SiR_{80}:PU_{20}/Micro-Pb) Composites

Figure (4-12) demonstrates that there is a linear correlation between the increase in the loading rate of polyurethane from the rubber overlays and the rise in the density value. This is because there has been an increase in the mass of the uniform material per unit volume. Due to the fact that this material overlaps with the molecules of the polymeric chains found in the ordinary substance, its concentration rises even further with the addition of micro lead powder This information suggests that as more polyurethane is added through rubber overlays, it leads to an increase in density due to the additional mass per unit volume. The interaction between this material and the existing polymeric chains in the substance further contributes to the rise in density, especially when micro lead powder is introduced, consistent with prior research findings [163].

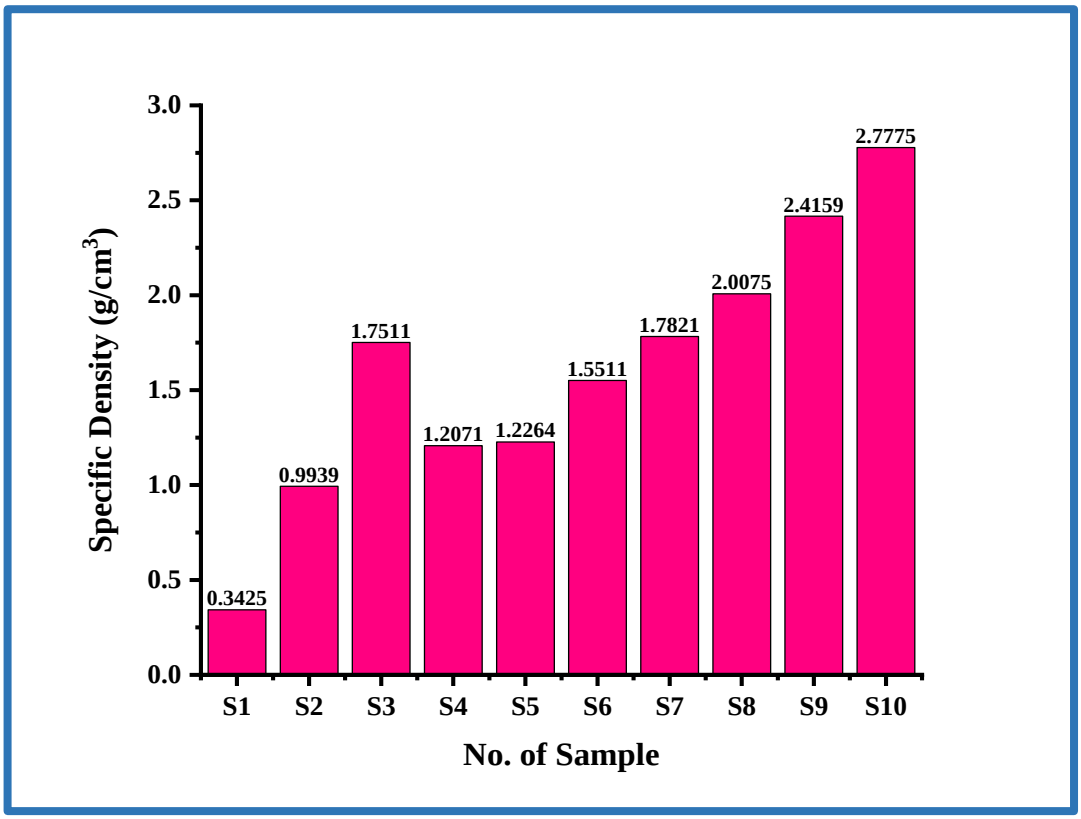

Fig. (4-12): behaviour of change the specific gravity for different loading ratio of micro-Pb group B.

4.5 The Properties of Radiation of the (SIR_{80}:PU_{20}/Micro-Pb) Composites

4.5.1 Calculation of Half Thickness ($X_{1/2}$), the Linear Absorption Coefficient (μ), and the Mass Absorption Coefficient (μ_m) When Using a Cs^{137} Source.

The values of the thickness of the half are determined practically through Figure (4-13), which shows the graphic relationship between the thickness and the transmitting radiation (N) when using the Cs^{137} radioactive source and for different loading percentages of (micro-Pb). And through the equations (2-26) and (2-27) referred to in the second chapter, where a decrease was observed in the value of the half thickness $X_{1/2}$, an increase in the linear absorption coefficient, and a slight decreased in the mass absorption coefficient due to the increased in the density of the material with the increase in the loading rates. This is due to the efficiency of the prepared composite

in absorbing and attenuating the used rays, and this efficiency increases with increasing the loading percentage of the micro lead powder, see Table (4-1).

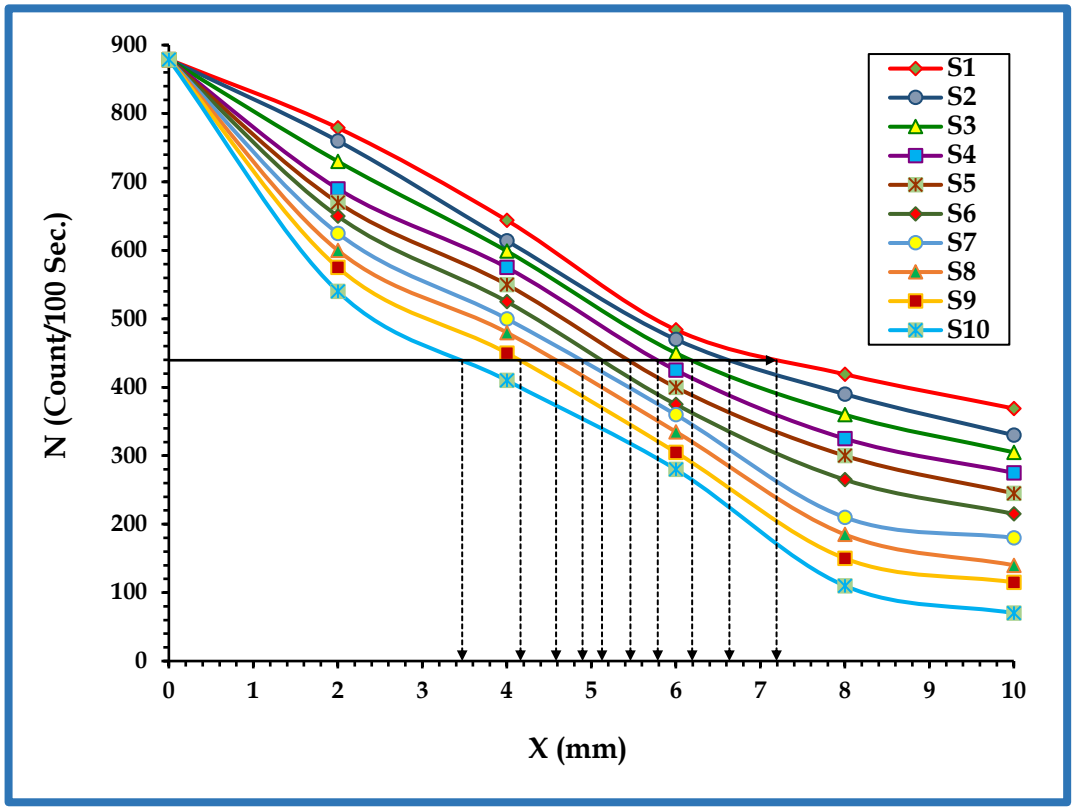

Fig. (4-13): Inter-relationship between the thickness and the number of transmitting radiations (N) when using the (Cs^{137}) source for different loading percentages of micro-lead.

Table (4-2): Linear and mass absorption coefficient and half thickness of cesium source Cs^{137} for different loading ratios of micro-Pb powder for rubber samples.

No. of Batch	Micro-Lead (pphr)	$X_{1/2}$ (mm)	μ (cm)	ρ (gm/cm^3)	μ_m (cm^2/gm)
A	0	7.192	0.964	0.3425	2.814
B	20	6.634	1.045	0.9939	1.051
C	40	6.193	1.119	1.7511	0.639
D	60	5.786	1.198	1.2071	0.992
E	80	5.463	1.269	1.2264	1.035
F	100	5.127	1.352	1.5511	0.872
G	150	4.896	1.416	1.7821	0.794
H	200	4.583	1.512	2.0075	0.753
I	250	4.162	1.665	2.4159	0.689
J	300	3.472	1.996	2.7775	0.719

4.5.2 Calculation of Half Thickness ($X_{1/2}$), the Linear Absorption Coefficient (μ), and the Mass Absorption Coefficient (μ_m) When Using a Co^{60} source.

A second source of electromagnetic radiation was used, which is the source of Co^{60}, where the superimposed rubber models were examined, and noticed a decrease in the half thickness of the when increasing the loading ratio of the added material, and this causes an increase in the radiation absorbed by the material, as well as due to an increase in interaction between them, which leads to an increase in linear and mass absorption, and the possibility of interaction depends mainly on the number of particles present in the radiation path. Figure (4-14) and Table (4-2) show the results obtained for the Co^{60} cobalt source.

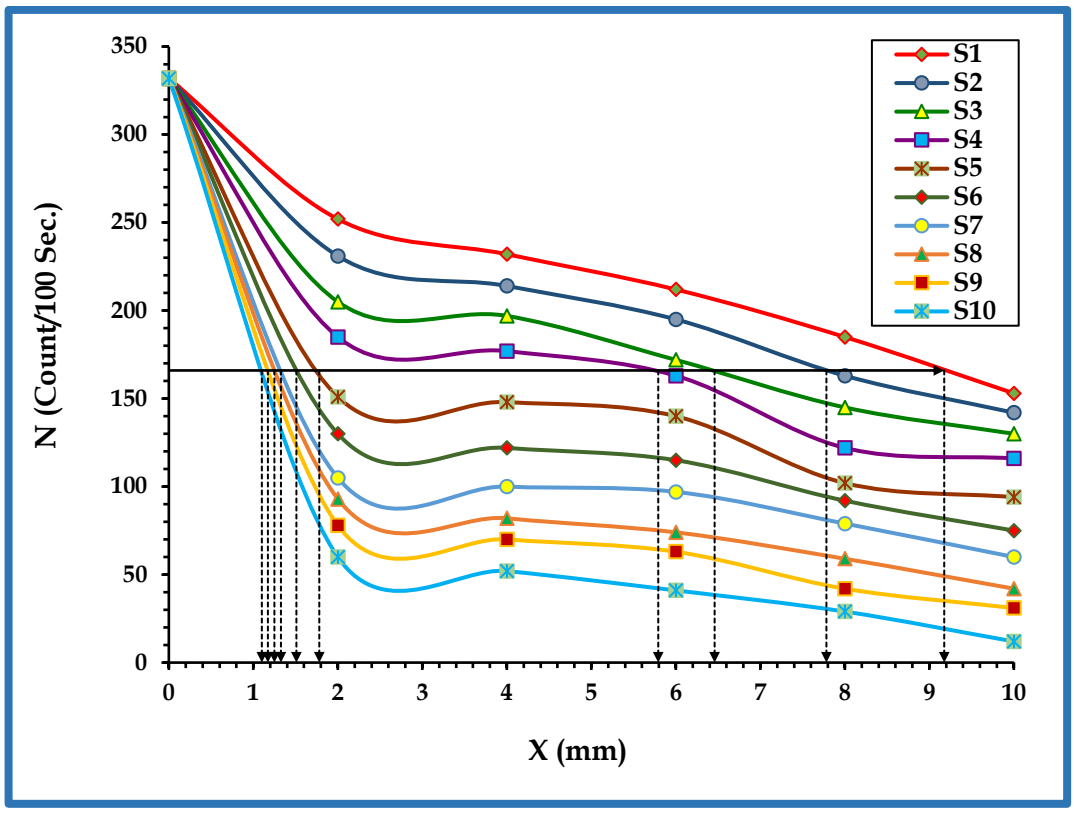

Fig. (4-14): Inter-relationship between the thickness and the number of transmitting radiations (N) when using the (Co^{60}) source for different loading percentages of micro-lead.

Table (4-3): Linear and mass absorption coefficient and half thickness of cobalt source Co^{60} for different loading ratios of micro-Pb powder for rubber samples.

No. of Batch	Micro-Lead (pphr)	$X_{1/2}$ (mm)	μ (cm)	ρ (gm/cm^3)	μ_m (cm^2/gm)
A	0	9.177	0.755	0.3425	2.205
B	20	7.782	0.891	0.9939	0.896
C	40	6.459	1.073	2.9511	0.364
D	60	5.792	1.197	1.2071	0.991
E	80	1.781	3.893	1.2264	3.174
F	100	1.510	4.591	1.5511	2.960
G	150	1.327	5.225	1.7821	2.932
H	200	1.249	5.548	2.0075	2.764
I	250	1.172	5.912	2.4159	2.447
J	300	1.101	6.296	2.7775	2.267

4.6 Structural Properties of (SiR_{80}:PU_{20}/Micro-Pb_{300}: Nano-Pb) Nanocomposites

4.6.1 FTIR of the (SiR_{80}:PU_{20}/Micro-Pb_{300}:Nano-Pb) Nanocomposites

Fourier transform infrared spectroscopy (FT-IR) analysis of Nano-lead based (SiR_{80}:PU_{20}/Micro-Pb_{300}) rubber compounds at different weight ratios of (0, 0.2, 0.4, 0.6, and 0.8) pphr, respectively. Where the first curl is without the addition of hexane, while the second curl is with the addition of hexane at room temperature in the range (600-4000 cm^{-1}), as shown in Figure (4-15), where it was observed that there are no clear changes in the radioactive spectrum of the rubber compound. Even when the loading ratios were changed, the spectra displayed characteristic frequencies of vibrations. In the region (2961.54 cm^{-1}) (O-H) stretching occurs, as well as in the two regions (1258.23 cm^{-1}) and (1009.39 cm^{-1}), respectively, (C-O-C) stretching occurs, while in the region (786.93 cm^{-1}) out of bending (=C-H) as shown in Table (4-4) [164]. while the (CH_3) band extends to the region (1411.76 cm^{-1}) [165, 166].

The distribution of lead throughout the rubber composite was found to be uniform when hexane was present.

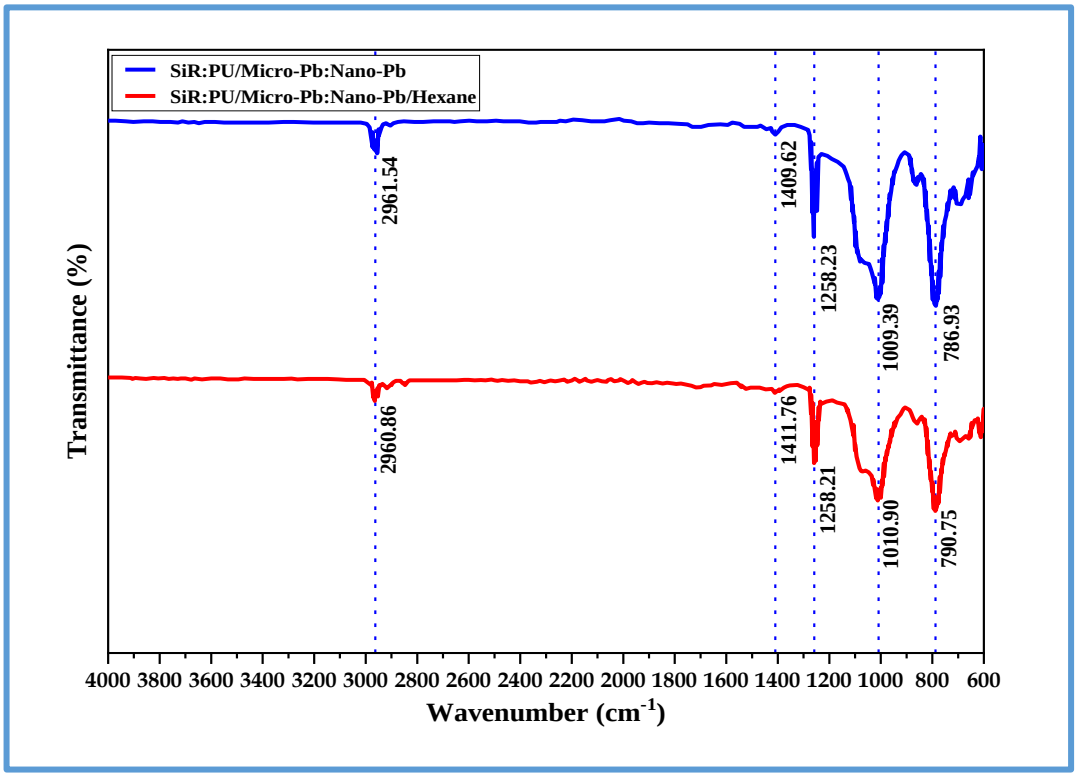

Fig. (4-15): FTIR spectra of (SiR_{80}:PU_{20}/micro-Pb_{300}:nano-$Pb_{0.8}$) of the sample without hexane and within hexane.

Table (4.4): FT-IR Transmittance bands positions and their assignments of (SiR_{80}:PU_{20}/micro-Pb_{300}:nano-$Pb_{0.8}$) Composites

Vibration frequency (cm^{-1})	Band assignment of Composite
2961.54	O–H Stretching
1258.23	C-O-C Stretching
1009.39	C-O Stretching
786.93	=C-H out-of-plane bending

4.6.2 SEM of the (SiR_{80}:PU_{20}/Micro-Pb_{300}:Nano-Pb) Composites

Figure (4-16) (SiR_{80}:PU_{20}-microPb_{300}-nano$Pb_{0.8}$) pphr was examined by a scanning electron microscope before mixing hexane, representing an image (D) with lumps and heterogeneity, the Nano-lead is undistributed, and there are gaps. As for image (C), after mixing the hexane, we notice clearly that the Nano-lead is distributed evenly and has no lumps; the two images are similar and have the same ingredients and quantities [167]. Figure (4-16) represents image (D) of the sample without hexane and image (C) when hexane is added, and Figure (4-17) represents the distributive function the Figures (B and B1), the diameter and the volume area of the nano-lead without adding hexane, while the Figures (A and A1) represents the diameter and the area of the volume of the nano-lead when adding hexane and this indicates that the Nano-lead is distributed evenly on the sample. The distribution function (Gaussian) was calculated using the image processing program (Image J), where the results of the distribution function showed that the average diameter of lead nanoparticles in the absence of hexane was 39.71 μm, with an average area of 682.78 μm^2, but in the presence of hexane, the average diameter was 42.47 μm, with an average area of 903.96 μm^2, and this means that Because of the increased cohesiveness between the polymeric chains and the filling of gaps caused by the loading percentage of hexane added to the rubber compound, the lead was distributed uniformly [168].

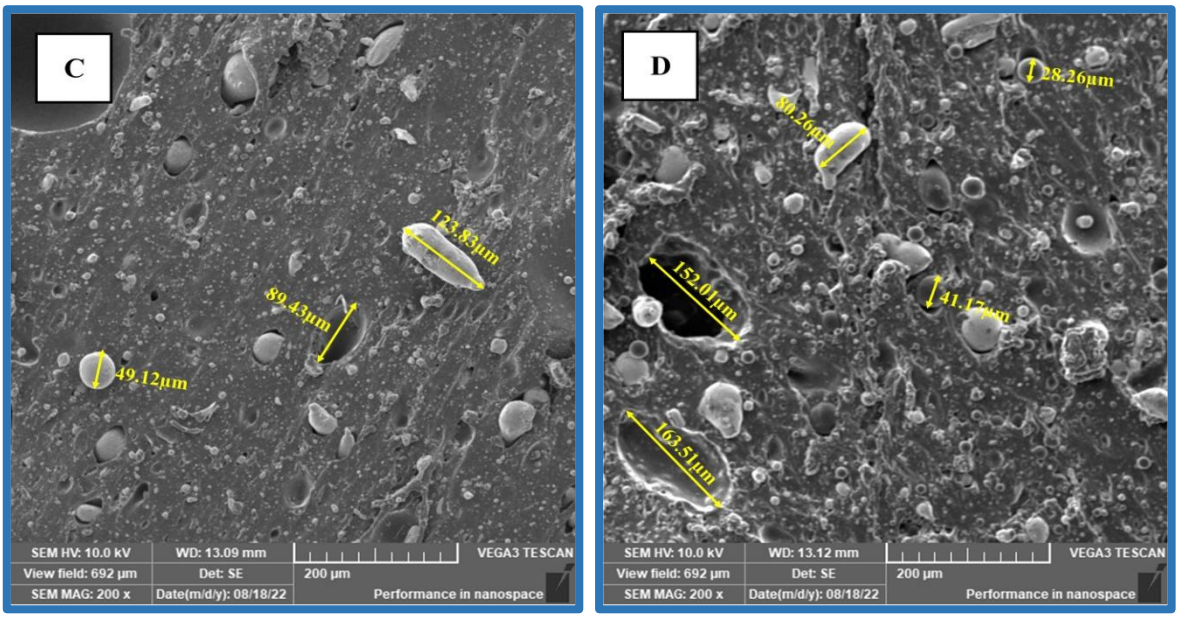

Fig. (4-16): SEM images for (SiR_{80}:PU_{20}/microPb_{300}:nano-$Pb_{0.8}$) of (C) of the sample without hexane and the image (D) when hexane is added.

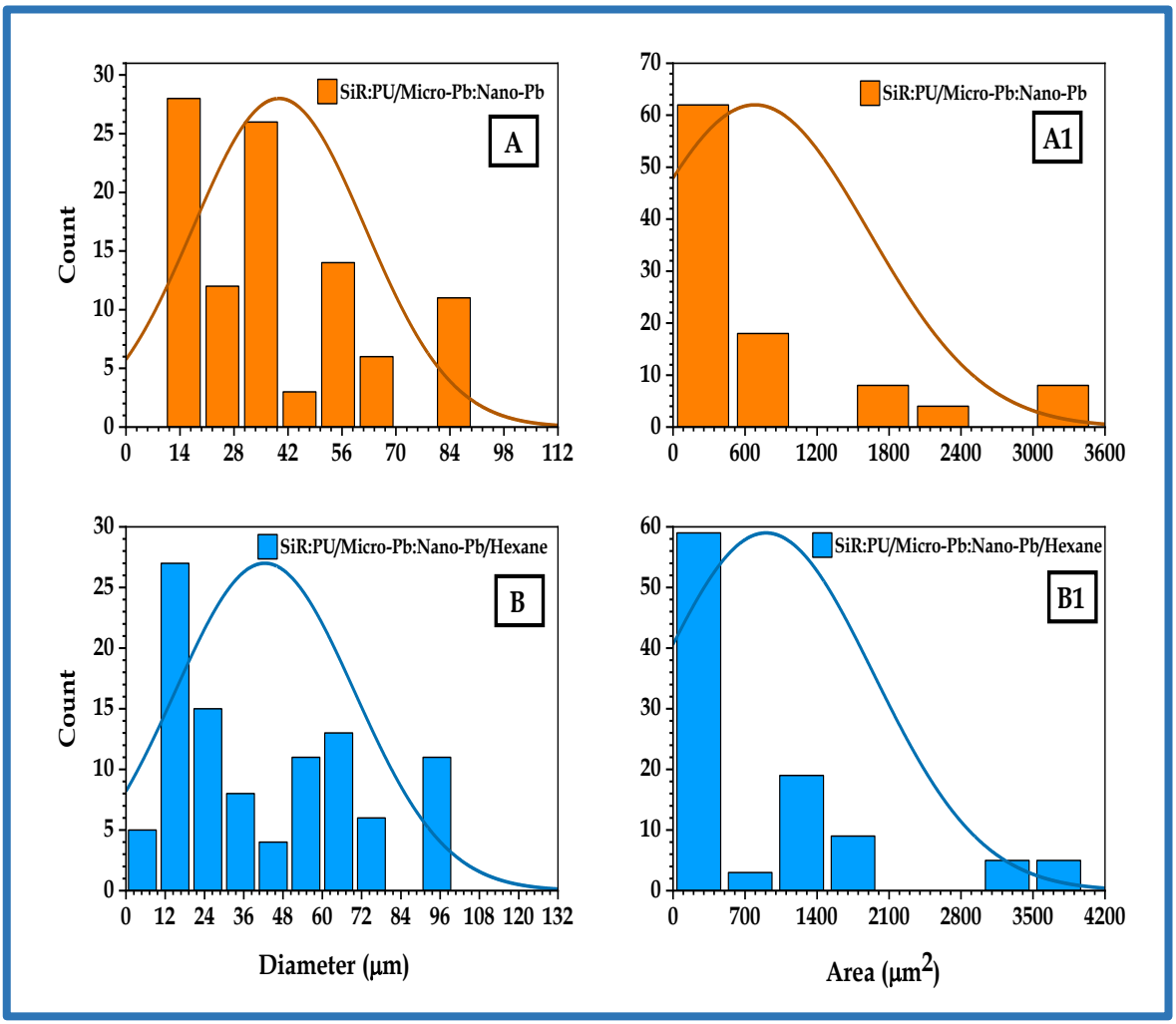

Fig. (4-17): Plot of the distribution function (B and B1) represent the diameter and volume area of Nano-lead without adding hexane. (A and A1) represents the diameter and volume area of nano-lead with hexane.

4.7 Mechanical Properties of (SiR_{80}:PU_{20}/Micro-Pb_{300}: Nano-Pb) Nanocomposites

4.7.1 Hardness of (SiR_{80}:PU_{20}/Micro-Pb_{300}: Nano-Pb) Nanocomposites

Figure (4-18) shows that the measured surface hardness values of rubber batches Expansion is slow and erratic at greater concentrations of the additive (Nano-Pb). This is because the reinforcing material and the basic material interfere with one another, which raises the hardness value. Because it is the cross-linking between rubber chains and the additive within the prepared dough that increases the hardness of the surface of the prepared material and makes it more resistant to the external forces applied to it ,this is consistent with previous studies [169].

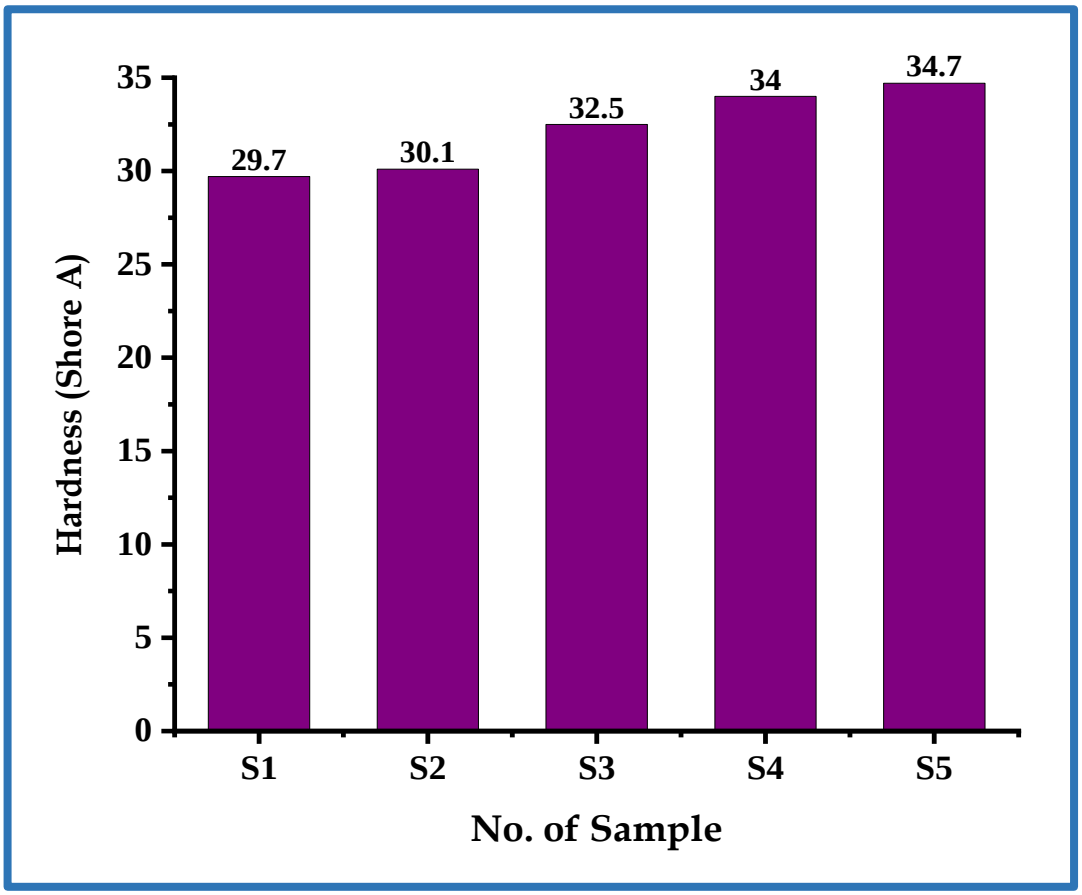

Fig. (4-18): behaviour of change the hardness for different loading of nano-lead

4.7.2 Tensile Strength, Elastic Modulus, and Extension of the (SiR_{80}:PU_{20}/Micro-Pb_{300}:Nano-Pb) Nanocomposites

The addition of lead nano powder to the rubber composite (SiR_{80}:PU_{20}/Micro-Pb_{300}) altered its mechanical characteristics, including its tensile strength, modulus of elasticity, and elongation, as shown in Figures (4-19), (4-20), and (4-21). Included are mechanical test results and a comparison of the effects of different rubber batch components and a discussion of the radiation properties of several model rubber batches. From Figure (4-19), which represents the tensile strength as it gradually increased for the prepared samples with increasing loading of nano-lead due to the cohesion of the rubber filler, from Figure (4-20), which represents the modulus of elasticity and the apparent increase in the prepared samples due to the increase in the loading percentage of nano-lead. And the increase in physical bonds and the cohesion of the filler with rubber, from Figure (4-21), where the decrease in elongation was observed with the increase in the loading percentage of nano-lead Increasing the loading of lead nano powder with a small grain size improves the mechanical properties because it increases the surface area for diffusion, resulting in more crosslinking between the rubber chains. This is consistent with previous research [144]. It is also noted from the figures that the decline in the elongation scheme is explained based on the material reaching the point of submission, where the material continues to resist until its resistance collapses as a result of the lack of distance between the rubber chains, as they are at a certain percentage that cannot withstand the added substance, which leads to cracks and poisons in the sample elasticity and this is consistent with previous research [144]. As for the increase in the modulus of elasticity, it can indicate a robust lessening of the elongation, and because of its inverse proportion to the modulus of the elastic property. The reason for the obvious increase in the hardness, modulus of elasticity and tensile strength is the increase in the loading percentage of the nano-added material.

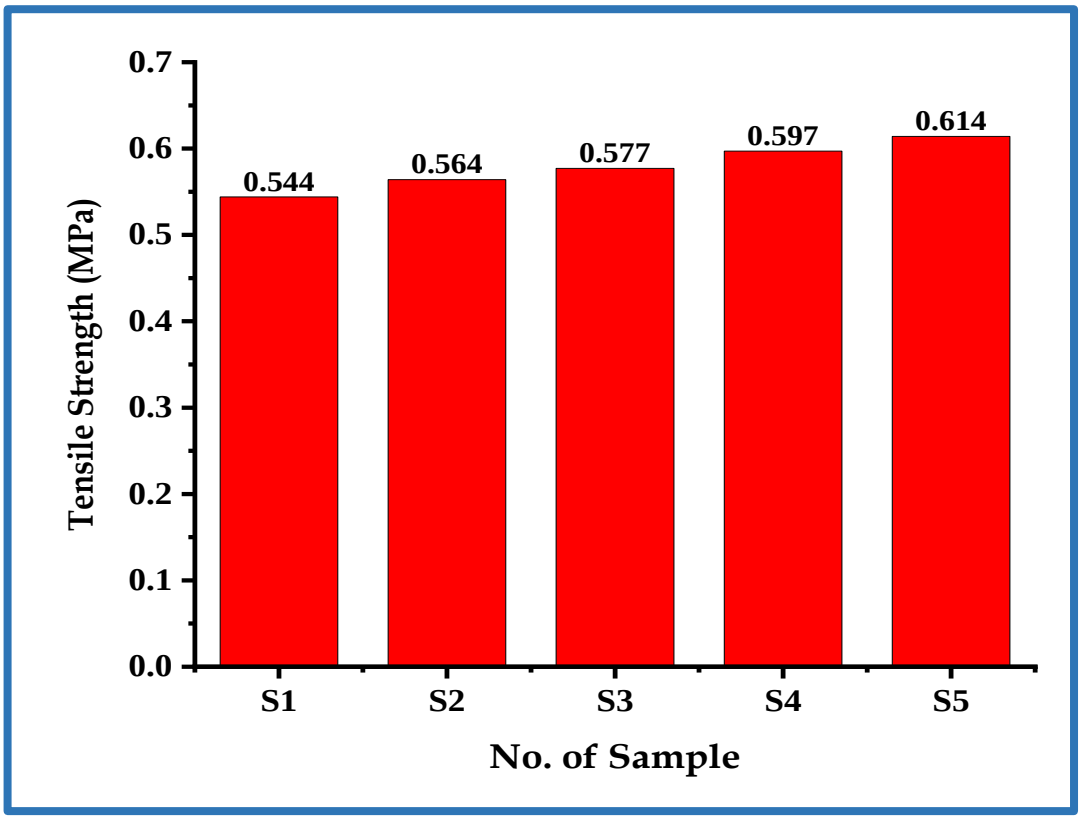

Fig. (4-19): Plot of change the tensile strength for different loading of nano-lead.

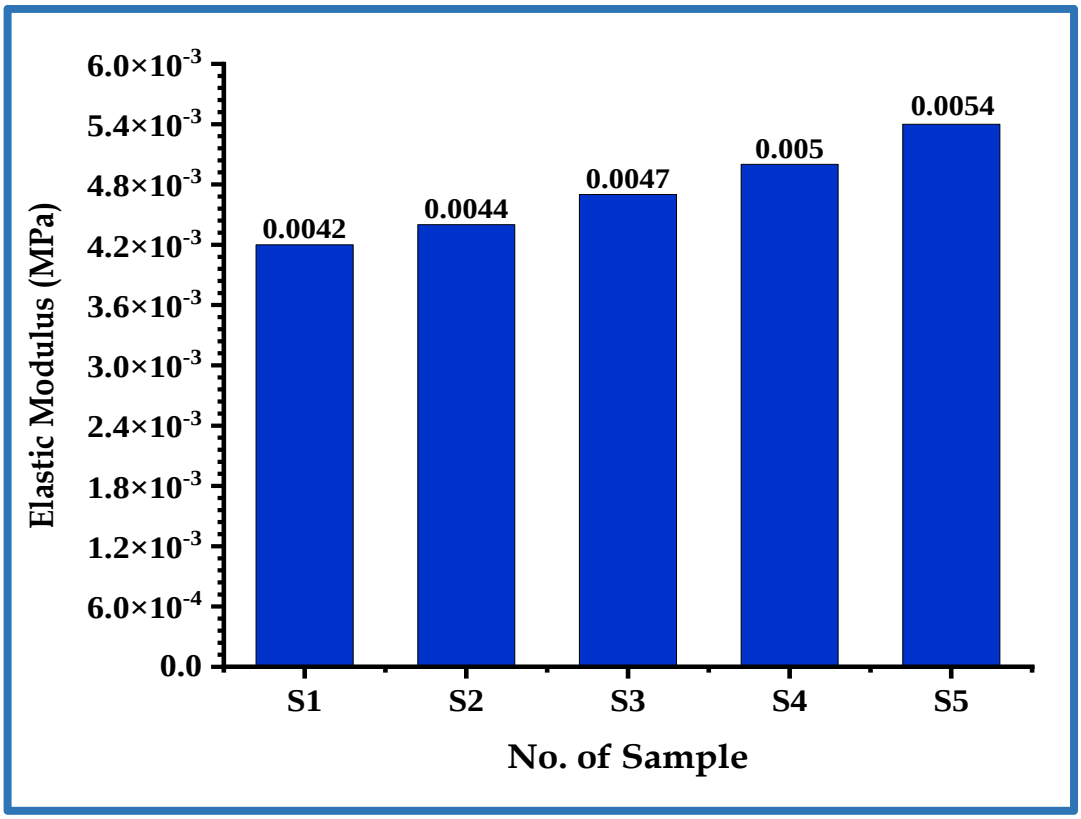

Fig. (4-20): Plot of change the elastic modulus for different loading of nano-lead

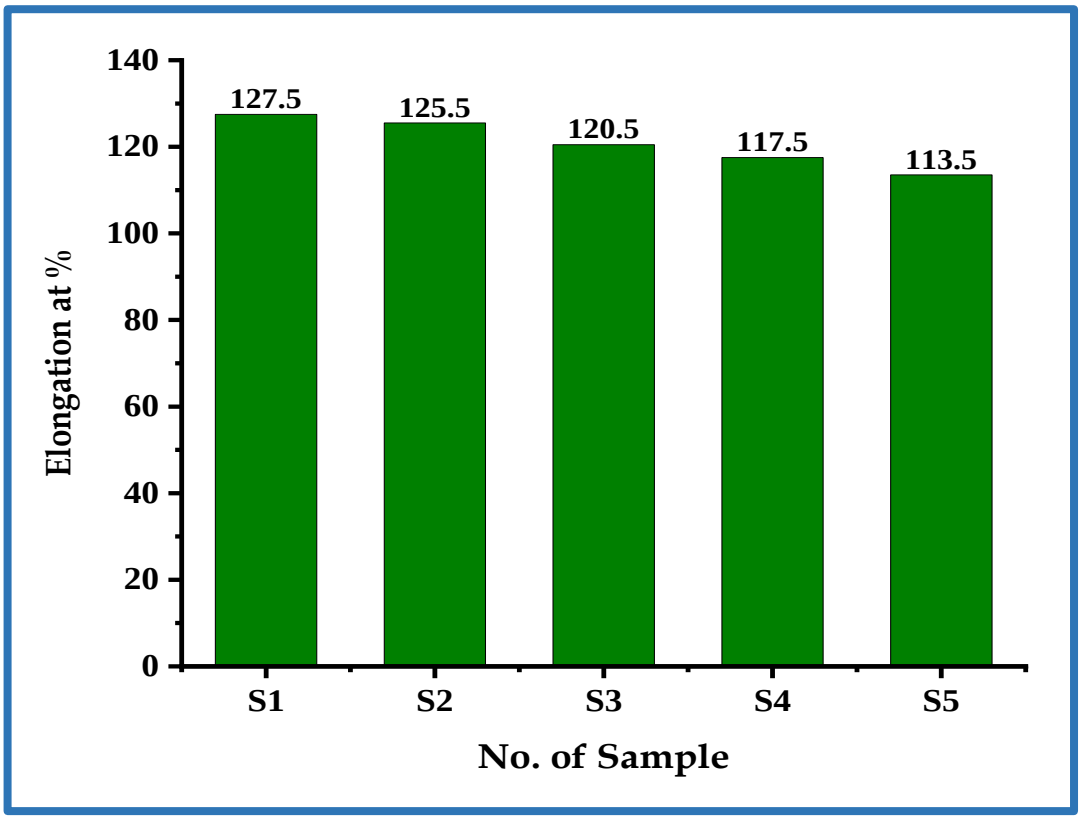

Fig. (4-21): Plot of change the elongation for different loading of nano-lead

4.8 The Radiation Properties of the (SiR_{80}/PU_{20}/Micro-Pb_{300}/Nano-Pb) Nanocomposites

4.8.1 Calculation of Half Thickness $X_{1/2}$, the Linear Absorption Coefficient (μ), and the Mass Absorption Coefficient (μ_m) When Using a Cs^{137} Source.

The values of the half-thickness are practically determined through Figure (4-22), which shows the graphical relationship between thickness and penetrating radiation (N) when using the Cs^{137} radiating source and for different loading ratios of (Pb-Nano). Where it was noticed a decrease in the value of the half thickness $X_{1/2}$ and an increase in both the linear and mass absorption coefficients with the increase in the loading ratios. This is due to the efficiency of the prepared composite in absorbing and attenuating the used rays, and this efficiency increases with the increase in the percentage of loading of the microscopic lead powder [170], see the Table (4-5).

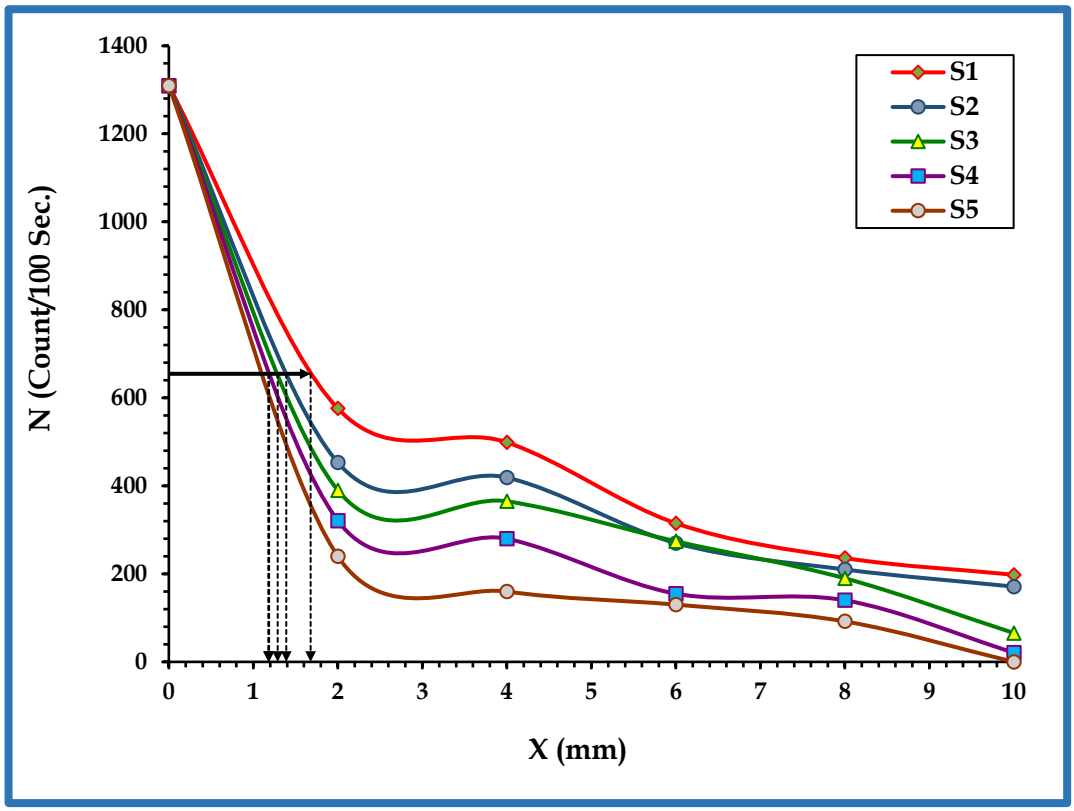

Fig. (4-22): The graphical relationship between thickness and the number of penetrating radiation (N) when using a source (Cs^{137}) for different loading ratios of (nano-Pb).

Table (4-5): Linear and mass absorption coefficient and half thickness of Cs^{137} for different loading ratios of nano-Pb powder for rubber samples

No. of Batch	Nano-Pb (pphr)	$X_{1/2}$ (mm)	μ (cm^{-1})	μ_m (cm^2/gm)
A	0	1.678	4.131	1.487
B	0.2	1.390	4.987	1.622
C	0.4	1.288	5.381	1.723
D	0.6	1.178	5.887	1.877
E	0.8	1.186	5.842	1.861

4.8.2 Calculation of the Half Thickness $X_{1/2}$, the Linear Absorption Coefficient (μ), and the Mass Absorption Coefficient (μ_m) When Using the Cobalt Source Co^{60}

Figure (4-105) displays the variation of the number of penetrating radiation (N) for (SiR_{80}-PU_{20}:Micro-Pb_{300}) composite with different concentrations of Pb nanoparticles. As shown in the figure, the transmission radiation decreases with the increasing of the concentrations of nanoparticles which attributed to the increase of the attenuation radiation. From the figure, the attenuation coefficients increase with the increase of nanoparticles concentrations, this is due to the absorption or reflection of gamma radiation by (SiR_{80}-PU_{20}:Micro-Pb_{300}:Nano-$Pb_{0.8}$) nanocomposites shielding materials. The nanocomposites have highest attenuation coefficients which is due to the high atomic number of Pb nanoparticles [171].

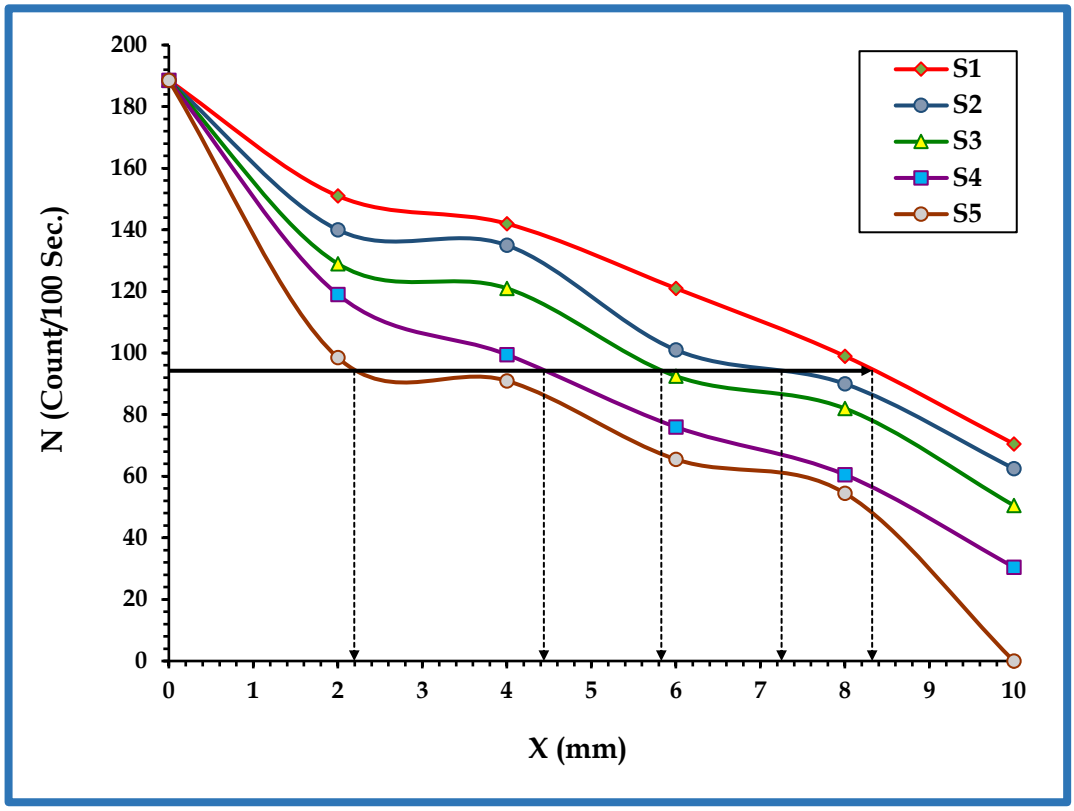

Fig. (4-23): The graphical relationship between thickness and the number of penetrating radiation (N) when using a source (Co^{60}) for different loading ratios of (nano-Pb).

Table (4-6): linear and mass absorption coefficient and half thickness of Co^{60} for different loading ratios of nano-Pb powder for rubber samples.

No. of Batch	Nano-Pb (pphr)	$X_{1/2}$ (mm)	μ (cm^{-1})	μ_m (cm^2/gm)
A	0	1.624	4.269	1.537
B	0.2	1.389	4.991	1.623
C	0.4	1.234	5.616	1.799
D	0.6	1.108	6.253	1.994
E	0.8	0.985	7.040	2.243

Chapter Five

Conclusions and Future Projects

Chapter Five: Conclusions and Future Projects

5.1 Conclusions

According to the results obtained, which showed the effect of adding polyurethane powder and micro and nano lead powder on the mechanical properties and radiation of the prepared overlapping rubber samples, the following conclusions were reached:

1- A composite of (SiR_{80}:PU_{20}) was found to be more suitable for mechanical properties, with a slight decrease in tensile strength and elongation coefficient and a gradual increase in hardness and modulus of elasticity. Micro-lead powder applied to (SiR_{80}:PU_{20}) composites at 300 pphr increased tensile strength, hardness, modulus of elasticity, and decreased elongation coefficient. Nano lead powder applied to the composite (SiR_{80}:PU_{20}/micro-Pb_{300}) at (0.8 pphr) increased tensile strength, hardness modulus, and modulus of elasticity and decreased elongation.

2- Adding hexane to the rubber composite of (SiR_{80}:PU_{20}/micro-Pb_{300}) as well as the composite of (SiR_{80}:PU_{20}/micro-Pb_{300}:nano-$Pb_{0.8}$) to fill the gaps and equal distribute of lead in the samples.

3- The rubber batch samples produced were tested using FTIR, and the rubber compounds were unchanged and gradually showed physical bonding. The rubber batch samples examined by the (SEM) device were examined, as the lead was distributed evenly, and there were no voids on the samples prepared in the presence of hexane.

4- Two cesium and cobalt sources were used to evaluate rubber batch samples for radiation analysis. The study found that the linear absorption coefficient (μ) and mass absorption coefficient (μ_m) are rising, but the half thickness ($X_{1/2}$) decreases with ray attenuation. The lowest thickness and the largest linear and mass absorption coefficients

were obtained at the loading ratio of (300 pphr) and (0.8 pphr) when using the Co^{60} source.

5- The sample selected of (SiR_{80}:PU_{20}/micro-Pb_{300}:nano-$Pb_{0.8}$) nanocomposites can be used in shielding applications as an armor suit to protect against harmful radiation.

5.2 Recommendation and Future Projects

1- Preparation (Rubber blend / nanoparticles) nanocomposites as antimicrobial materials.

2- Using another type of rubber, such as NBR or IIR, with micro or nano-lead powder in the field of producing protective suits used in radiation shielding.

3- Other tests can be examined such as x-ray examination to see the extent of its attenuation and for the same rubber Samples prepared in this research.

4- Preparation of a rubber composites of (NR/SBR) reinforced with lead or lead oxide nanoparticles used for radiation shielding.

5- A study of the mechanical and radiation properties of rubber blends reinforced with titanium oxide.

References

References

1. Wichaita, W., Promlok, D., Sudjaipraparat, N., Sripraphot, S., Suteewong, T., Tangboriboonrat, P.: A concise review on design and control of structured natural rubber latex particles as engineering nanocomposites. Eur. Polym. J. 159, 110740 (2021)

2. Zhu, Q., Wang, Z., Zeng, H., Yang, T., Wang, X.: Effects of graphene on various properties and applications of silicone rubber and silicone resin. Compos. Part A Appl. Sci. Manuf. 142, 106240 (2021)

3. Gürsoy, M.: Vapor deposition polymerization of synthetic rubber thin film in a plasma enhanced chemical vapor deposition reactor. J. Appl. Polym. Sci. 138, 49722 (2021)

4. Chae, S., Xu, Y., Yi, R., Lim, H., Velickovic, D., Li, X., Li, Q., Wang, C., Zhang, J.: A Micrometer-Sized Silicon/Carbon Composite Anode Synthesized by Impregnation of Petroleum Pitch in Nanoporous Silicon. Adv. Mater. 33, 2103095 (2021)

5. Wang, G., Li, A., Zhao, W., Xu, Z., Ma, Y., Zhang, F., Zhang, Y., Zhou, J., He, Q.: A review on fabrication methods and research progress of superhydrophobic silicone rubber materials. Adv. Mater. Interfaces. 8, 2001460 (2021)

6. Chen, J., Liu, J., Peng, Z., Yao, Y., Chen, S.: The microscopic mechanism of size effect in silica-particle reinforced silicone rubber composites. Eng. Fract. Mech. 255, 107945 (2021)

7. Fink, J.K.: Liquid Silicone Rubber: Chemistry, Materials, and Processing. John Wiley & Sons (2019)

8. Maghsoudi, K., Momen, G., Jafari, R., Farzaneh, M.: Rigorous testing to assess the self-cleaning properties of an ultra-water-repellent silicone rubber surface. Surf. Coatings Technol. 374, 557–568 (2019)

9. Mahmoud, D.S., El-Sabbagh, S.H., El-Basheer, T.M., Moustafa, A.M., Barakat, M.A.Y.: Rheometeric, ultrasonic and acoustical shielding properties of Cu-alloy/silicone rubber composites for electronic applications. J. Thermoplast. Compos. Mater. 08927057231162016 (2023)

10. Marucheck, A., Greis, N., Mena, C., Cai, L.: Product safety and security in the global supply chain: Issues, challenges and research opportunities. J. Oper. Manag. 29, 707–720 (2011)

11. Song, P., Wang, G., Zhang, Y.: Preparation and performance of graphene/carbon black silicone rubber composites used for highly sensitive and flexible strain sensors. Sensors Actuators A Phys. 323, 112659 (2021)

12. Ha, D.Y., Kang, J.H., Kim, T., Lee, S.Y., Park, J.-S., Choi, Y., Jung, S.: Improved Elasticity and Conductivity in a Ni@ Ag/Silicone Rubber Composite due to Lowered Percolation Threshold via Magnetic-Field-Induced Alignment. ACS Appl. Electron. Mater. (2022)

13. Grassie, T.: Optimisation of fluid-flow in a flat plate solar water heater., (2001)

14. Chmielewski, A.G., Haji-Saeid, M., Ahmed, S.: Progress in radiation processing of polymers. Nucl. Instruments Methods Phys. Res. Sect. B Beam Interact. with Mater. Atoms. 236, 44–54 (2005)

15. Zhao, Q., An, J., Wang, X., Li, N.: In-situ hydrogen peroxide synthesis with environmental applications in bioelectrochemical systems: a state-of-the-art review. Int. J. Hydrogen Energy. 46, 3204–3219 (2021)

16. Savani, N.G., Naveen, T., Dholakiya, B.Z.: A review on the synthesis of maleic anhydride based polyurethanes from renewable feedstock for different industrial applications. J. Polym. Res. 30, 1–26 (2023)

17. Long, J.C.: The history of rubber—a survey of sources about the history of rubber. Rubber Chem. Technol. 74, 493–508 (2001)

18. Zhang, Y., Xu, M., Song, J., Wang, C., Wang, X., Hamad, B.A.: Study on the corrosion change law and prediction model of cement stone in oil wells with CO2 corrosion in ultra-high-temperature acid gas wells. Constr. Build. Mater. 323, 125879 (2022)

19. Liu, X., Hong, W., Chen, X.: Continuous production of water-borne polyurethanes: A review. Polymers (Basel). 12, 2875 (2020)

20. Zhao, H., Gao, W.-C., Li, Q., Khan, M.R., Hu, G.-H., Liu, Y., Wu, W., Huang, C.-X., Li, R.K.Y.: Recent advances in superhydrophobic polyurethane: Preparations and applications. Adv. Colloid Interface Sci. 102644 (2022)

21. Musino, D., Rivard, C., Landrot, G., Novales, B., Rabilloud, T., Capron, I.: Hydroxyl groups on cellulose nanocrystal surfaces form nucleation points for silver nanoparticles of varying shapes and sizes. J. Colloid Interface Sci. 584, 360–371 (2021)

22. Boo, Y.C.: Emerging strategies to protect the skin from ultraviolet rays using plant-derived materials. Antioxidants. 9, 637 (2020)

23. Chen, S., Liu, Y., Chen, S., Zhao, G., Wu, Y.: Triazole ultraviolet absorbers with enrichment performance for material surfaces protection from ultraviolet rays. Mater. Lett. 291, 129496 (2021)

24. Rohm, K., Manas-Zloczower, I.: A micromechanical approach to TPU mechanical properties: Framework and experimental validation. Mech. Mater. 180, 104627 (2023)

25. Li, B., Zhou, M., Huo, W., Cai, D., Qin, P., Cao, H., Tan, T.: Fractionation and oxypropylation of corn-stover lignin for the production of biobased rigid polyurethane foam. Ind. Crops Prod. 143, 111887

(2020)

26. Zhu, M., Ma, Z., Liu, L., Zhang, J., Huo, S., Song, P.: Recent advances in fire-retardant rigid polyurethane foam. J. Mater. Sci. Technol. 112, 315–328 (2022)

27. Parcheta, P., Głowińska, E., Datta, J.: Effect of bio-based components on the chemical structure, thermal stability and mechanical properties of green thermoplastic polyurethane elastomers. Eur. Polym. J. 123, 109422 (2020)

28. Cooper, S.L., Guan, J.: Advances in polyurethane biomaterials. Woodhead Publishing (2016)

29. Mohanty, S.R., Mohanty, S., Nayak, S.K., Samal, S.K.: Synthesis and evaluation of novel acrylic and ester-based polyols for transparent polyurethane coating applications. Mater. Today Commun. 27, 102228 (2021)

30. Liang, C., Gracida-Alvarez, U.R., Gallant, E.T., Gillis, P.A., Marques, Y.A., Abramo, G.P., Hawkins, T.R., Dunn, J.B.: Material flows of polyurethane in the United States. Environ. Sci. Technol. 55, 14215–14224 (2021)

31. Sinduja, P., Rajeshkumar, S., Priyadharshini, R., Divyashri, S.: Comparative Anti Inflammatory Activity of Hexane and Aqueous Extract of Mucuna pruriens. J. Pharm. Res. Int. 1156–1166 (2021)

32. Naeem, M.H., Al-Nesrawy, S.H.H.: Preparation of (Rubber Blend/Oyster Shell Powder) Composites and Study Rheological Properties. (2019)

33. Roudbari, M.A., Jorshari, T.D., Lü, C., Ansari, R., Kouzani, A.Z., Amabili, M.: A review of size-dependent continuum mechanics models for micro-and nano-structures. Thin-Walled Struct. 170, 108562 (2022)

34. Guruswamy, S.: Engineering properties and applications of lead alloys.

CRC Press (1999)

35. Ma, Z., Xue, R., Li, J., Zhao, Y., Xue, Q., Chen, Z., Wang, Q., Poon, C.S.: Use of thermally modified waste concrete powder for removal of Pb (II) from wastewater: Effects and mechanism. Environ. Pollut. 277, 116776 (2021)

36. Ossola, G., Wojcik, A.: UV modification of tire rubber for use in cementitious composites. Cem. Concr. Compos. 52, 34–41 (2014)

37. Al-Nesrawy, S.H., Al-Maamori, M., Hassani, A.S., Jaafar, H.I.: Effect of blend of Reclaimed tire and Carbon Black Percent on the Mechanical properties of SBR/NR blends. Int. J. Adv. Res. 2, 234–243 (2014)

38. Shi, G., Zhao, Z., Pai, J., Lee, I., Zhang, L., Stevenson, C., Ishara, K., Zhang, R., Zhu, H., Ma, J.: Highly sensitive, wearable, durable strain sensors and stretchable conductors using graphene/silicon rubber composites. Adv. Funct. Mater. 26, 7614–7625 (2016)

39. Seyedmehdi, S.A., Zhang, H., Zhu, J.: Influence of production method, silicone type and thickness on silicon rubber superhydrophobic coatings. Prog. Org. Coatings. 90, 291–295 (2016)

40. Hashim, A., Hadi, A.: Novel lead oxide polymer nanocomposites for nuclear radiation shielding applications. Ukr. J. Phys. 62, 978 (2017)

41. Yang, H., Yao, X., Zheng, Z., Gong, L., Yuan, L., Yuan, Y., Liu, Y.: Highly sensitive and stretchable graphene-silicone rubber composites for strain sensing. Compos. Sci. Technol. 167, 371–378 (2018)

42. Ersundu, A.E., Büyükyıldız, M., Ersundu, M.Ç., Şakar, E., Kurudirek, M.: The heavy metal oxide glasses within the WO3-MoO3-TeO2 system to investigate the shielding properties of radiation applications. Prog. Nucl. Energy. 104, 280–287 (2018)

43. Toyen, D., Rittirong, A., Poltabtim, W., Saenboonruang, K.: Flexible,

lead-free, gamma-shielding materials based on natural rubber/metal oxide composites. Iran. Polym. J. 27, 33–41 (2018)

44. Cataldo, F., Prata, M.: New composites for neutron radiation shielding. J. Radioanal. Nucl. Chem. 320, 831–839 (2019). https://doi.org/10.1007/s10967-019-06526-5

45. Wortmann, M., Frese, N., Keil, W., Brikmann, J., Biedinger, J., Brockhagen, B., Reiss, G., Schmidt, C., Gölzhäuser, A., Moritzer, E.: The deterioration mechanism of silicone molds in polyurethane vacuum casting. ACS Appl. Polym. Mater. 2, 4719–4732 (2020)

46. Liu, J., Yao, Y., Chen, S., Li, X., Zhang, Z.: A new nanoparticle-reinforced silicone rubber composite integrating high strength and strong adhesion. Compos. Part A Appl. Sci. Manuf. 151, 106645 (2021)

47. El-Agawany, F.I., Mahmoud, K.A.-A., Akyildirim, H., Yousef, E.-S., Tekin, H.O., Rammah, Y.S.: Physical, neutron, and gamma-rays shielding parameters for Na2O–SiO2–PbO glasses. Emerg. Mater. Res. 10, 227–237 (2021)

48. Aboud, H., Aldhuaibata, M.J.R., Alajermi, Y.: Radiation shielding traits of bismuth–cadmium–barium-borate glasses: Role of lead activation. J. Phys. Chem. Solids. 164, 110597 (2022)

49. Kilicoglu, O., More, C. V, Akman, F., Dilsiz, K., Oğul, H., Kaçal, M.R., Polat, H., Agar, O.: Micro Pb filled polymer composites: Theoretical, experimental and simulation results for γ-ray shielding performance. Radiat. Phys. Chem. 194, 110039 (2022)

50. Rajabimashhadi, Z., Naghizadeh, R., Zolriasatein, A., Bagheri, S., Mele, C., Esposito Corcione, C.: Hydrophobic, Mechanical, and Physical Properties of Polyurethane Nanocomposite: Synergistic Impact of Mg (OH) 2 and SiO2. Polymers (Basel). 15, 1916 (2023)

51. Al-Samed, H.A., Al-maamori, M., Hussein, A.A.: The Effect of Reinforcement PolySilicon Rubber with Foam Liner on Tensile Set and Hardness. J. Surv. Fish. Sci. 10, 5976–5986 (2023)

52. Shit, S.C., Shah, P.: A Review on Silicone Rubber. Natl. Acad. Sci. Lett. 36, 355–365 (2013). https://doi.org/10.1007/s40009-013-0150-2

53. Manshaie, R., Khorasani, S.N., Veshare, S.J., Abadchi, M.R.: Effect of electron beam irradiation on the properties of natural rubber (NR)/styrene–butadiene rubber (SBR) blend. Radiat. Phys. Chem. 80, 100–106 (2011)

54. Kumar, V., Sehgal, R., Gupta, R.: Blends and composites of polyhydroxyalkanoates (PHAs) and their applications. Eur. Polym. J. 161, 110824 (2021)

55. Dorigato, A.: Recycling of polymer blends. Adv. Ind. Eng. Polym. Res. 4, 53–69 (2021)

56. Al-Nesrawya, S.H., Mohseenb, M.J., Al-Bermany, E.: Reinforcement the mechanical properties of (NR50/SBRs50/OSP) composites with oyster shell powder and carbon black. In: IOP Conference Series: Materials Science and Engineering. p. 12060. IOP Publishing (2020)

57. Thaptong, P., Sae-Oui, P., Jittham, P., Sirisinha, C.: Optimization of highly dispersible silica/carbon black hybrid filler ratio for tire tread based on solution-and emulsion-styrene butadiene rubber. J. Appl. Polym. Sci. 139, e52608 (2022)

58. Bouab, M., Harit, A., Boufettal, H., Mahdaoui, S., Samouh, N.: Desmoid fibromatosis of the breast occurring after breast reduction surgery mimicking a carcinoma: A rare case report. Ann. Med. Surg. 77, 103526 (2022)

59. Jubinville, D., Esmizadeh, E., Saikrishnan, S., Tzoganakis, C.,

Mekonnen, T.: A comprehensive review of global production and recycling methods of polyolefin (PO) based products and their post-recycling applications. Sustain. Mater. Technol. 25, e00188 (2020)

60. Krauklis, A.E., Karl, C.W., Gagani, A.I., Jørgensen, J.K.: Composite material recycling technology—state-of-the-art and sustainable development for the 2020s. J. Compos. Sci. 5, 28 (2021)

61. Bussetta, P., Correia, N.: Numerical forming of continuous fibre reinforced composite material: A review. Compos. Part A Appl. Sci. Manuf. 113, 12–31 (2018)

62. Tong, X.C.: Thermally Conductive Polymer Matrix Composites. Adv. Mater. Therm. Manag. Electron. Packag. 201–232 (2011)

63. Fan, Y., Fowler, G.D., Zhao, M.: The past, present and future of carbon black as a rubber reinforcing filler–A review. J. Clean. Prod. 247, 119115 (2020)

64. Oladele, I.O., Omotosho, T.F., Adediran, A.A.: Polymer-based composites: an indispensable material for present and future applications. Int. J. Polym. Sci. 2020, (2020)

65. Chang, I., Lee, M., Tran, A.T.P., Lee, S., Kwon, Y.-M., Im, J., Cho, G.-C.: Review on biopolymer-based soil treatment (BPST) technology in geotechnical engineering practices. Transp. Geotech. 24, 100385 (2020)

66. Zheng, J., Han, J., Liu, Z., Xia, W., Zhang, X., Li, L., Liu, X., Bian, R., Cheng, K., Zheng, J.: Biochar compound fertilizer increases nitrogen productivity and economic benefits but decreases carbon emission of maize production. Agric. Ecosyst. Environ. 241, 70–78 (2017)

67. Ye, H., Zheng, G., Yang, X., Zhang, D., Zhang, Y., Yan, S., You, L., Hou, S., Huang, Z.: Application of different carbon-based transition metal oxide composite materials in lithium-ion batteries. J. Electroanal. Chem.

898, 115652 (2021)

68. Onan, A.: Bidirectional convolutional recurrent neural network architecture with group-wise enhancement mechanism for text sentiment classification. J. King Saud Univ. Inf. Sci. 34, 2098–2117 (2022)

69. Al-Haija, Q.A., McCurry, C.D., Zein-Sabatto, S.: Intelligent self-reliant cyber-attacks detection and classification system for IoT communication using deep convolutional neural network. In: International Networking Conference. pp. 100–116. Springer (2021)

70. Guðlaugsson, B., Fazeli, R., Gunnarsdóttir, I., Davidsdottir, B., Stefansson, G.: Classification of stakeholders of sustainable energy development in Iceland: Utilizing a power-interest matrix and fuzzy logic theory. Energy Sustain. Dev. 57, 168–188 (2020)

71. Kohjiya, S., Ikeda, Y.: A short history of natural rubber research. In: Chemistry, Manufacture, and Application of Natural Rubber. pp. 407–427. Elsevier (2021)

72. Yoon, J.J., Park, T.G.: Degradation behaviors of biodegradable macroporous scaffolds prepared by gas foaming of effervescent salts. J. Biomed. Mater. Res. An Off. J. Soc. Biomater. Japanese Soc. Biomater. Aust. Soc. Biomater. Korean Soc. Biomater. 55, 401–408 (2001)

73. Xiao, H., Xu, C., Wang, R., Yu, P., Zhou, J., Bai, J.: A Nonlinear Model and Parameter Identification Method for Rubber Isolators under Shock Excitation in Underwater Vehicles. J. Mar. Sci. Eng. 9, 1282 (2021)

74. Wang, Q., Chen, X., Huang, X., Muhammad, A., Shi, Y., Dai, C., Ren, N., Paramane, A.: Tailoring Electric Field Distortion in High-Voltage Power Modules Utilizing Epoxy Resin/Silicon Carbide Whisker Composites with Field-Dependent Conductivity. ACS Appl. Electron. Mater. 4, 478–493 (2022)

75. Ramini, M., Agnelli, S., Ramorino, G.: Applications of shear heating parameter for injection molding process optimization of AEM rubber compounds. Express Polym. Lett. 16, 354–367 (2022)

76. Zeng, X., Li, G., Zhu, J., Sain, M., Jian, R.: NBR/CR-Based High-Damping Rubber Composites Containing Multiscale Structures for Tailoring Sound Insulation. Macromol. Mater. Eng. 2200464 (2022)

77. Santamaria, A.: Historical overview of nanotechnology and nanotoxicology. Nanotoxicity. 1–12 (2012)

78. Abid, N., Khan, A.M., Shujait, S., Chaudhary, K., Ikram, M., Imran, M., Haider, J., Khan, M., Khan, Q., Maqbool, M.: Synthesis of nanomaterials using various top-down and bottom-up approaches, influencing factors, advantages, and disadvantages: A review. Adv. Colloid Interface Sci. 300, 102597 (2022)

79. Mazari, S.A., Ali, E., Abro, R., Khan, F.S.A., Ahmed, I., Ahmed, M., Nizamuddin, S., Siddiqui, T.H., Hossain, N., Mubarak, N.M.: These nanomaterials are synthesized through methods, depending upon the end-user property demand. Synthesis of nanomaterials has two major approaches, one is top-down, in which the size of larger molecules makes smaller to nanoscale and the other is a bot. J. Environ. Chem. Eng. 9, 105028 (2021)

80. Assad, H., Fatma, I., Kumar, A., Kaya, S., Vo, D.-V.N., Al-Gheethi, A., Sharma, A.: An overview of MXene-Based nanomaterials and their potential applications towards hazardous pollutant adsorption. Chemosphere. 134221 (2022)

81. Kumar, A.P., Depan, D., Tomer, N.S., Singh, R.P.: Nanoscale particles for polymer degradation and stabilization—trends and future perspectives. Prog. Polym. Sci. 34, 479–515 (2009)

82. Hu, T., Gu, Z., Williams, G.R., Strimaite, M., Zha, J., Zhou, Z., Zhang, X., Tan, C., Liang, R.: Layered double hydroxide-based nanomaterials for biomedical applications. Chem. Soc. Rev. (2022)

83. Chinnasamy, B.: Mapping of quantitative analysis of research trend in nanomaterials. Mater. Today Proc. 49, 2922–2927 (2022)

84. Ali, E.S., Sharker, S.M., Islam, M.T., Khan, I.N., Shaw, S., Rahman, M.A., Uddin, S.J., Shill, M.C., Rehman, S., Das, N.: Targeting cancer cells with nanotherapeutics and nanodiagnostics: Current status and future perspectives. In: Seminars in cancer biology. pp. 52–68. Elsevier (2021)

85. Jiang, Z., Li, L., Huang, H., He, W., Ming, W.: Progress in Laser Ablation and Biological Synthesis Processes:“Top-Down” and “Bottom-Up” Approaches for the Green Synthesis of Au/Ag Nanoparticles. Int. J. Mol. Sci. 23, 14658 (2022)

86. Deng, J., Wang, J., Shi, J., Li, H., Lu, M., Fan, Z., Gu, Z., Cheng, H.: Tailoring the physicochemical properties of nanomaterials for immunomodulation. Adv. Drug Deliv. Rev. 180, 114039 (2022)

87. Saha, S., Bansal, S., Khanuja, M.: Classification of nanomaterials and their physical and chemical nature. In: Nano-enabled Agrochemicals in Agriculture. pp. 7–34. Elsevier (2022)

88. Balazs, A.C., Emrick, T., Russell, T.P.: Nanoparticle polymer composites: where two small worlds meet. Science (80-.). 314, 1107–1110 (2006)

89. Singh, V., Yadav, P., Mishra, V.: Recent advances on classification, properties, synthesis, and characterization of nanomaterials. Green Synth. Nanomater. bioenergy Appl. 83–97 (2020)

90. Saleh, T.A.: Nanomaterials: Classification, properties, and environmental

toxicities. Environ. Technol. Innov. 20, 101067 (2020)

91. Darwish, M.S.A., Mostafa, M.H., Al-Harbi, L.M.: Polymeric nanocomposites for environmental and industrial applications. Int. J. Mol. Sci. 23, 1023 (2022)

92. Fang, Y.-S., Yuan, J., Liu, T.-T., Wang, Q.-Q., Cao, W.-Q., Cao, M.-S.: Clipping electron transport and polarization relaxation of Ti3C2Tx based nanocomposites towards multifunction. Carbon N. Y. 201, 371–380 (2023)

93. Idumah, C.I.: Recently emerging trends in flame retardancy of phosphorene polymeric nanocomposites and applications. J. Anal. Appl. Pyrolysis. 105855 (2023)

94. Mohammadpour-Haratbar, A., Zare, Y., Rhee, K.Y.: Electrochemical biosensors based on polymer nanocomposites for detecting breast cancer: Recent progress and future prospects. Adv. Colloid Interface Sci. 102795 (2022)

95. Perera, K.Y., Jaiswal, S., Jaiswal, A.K.: A review on nanomaterials and nanohybrids based bio-nanocomposites for food packaging. Food Chem. 376, 131912 (2022)

96. Van Nguyen, S., Lee, B.-K.: PVA/CNC/TiO2 nanocomposite for food-packaging: Improved mechanical, UV/water vapor barrier, and antimicrobial properties. Carbohydr. Polym. 298, 120064 (2022)

97. Olayil, R., Prabu, V.A., DayaPrasad, S., Naresh, K., Sreekanth, P.S.R.: A review on the application of bio-nanocomposites for food packaging. Mater. Today Proc. 56, 1302–1306 (2022)

98. Friedrich, K.: Wear of reinforced polymers by different abrasive counterparts. In: Composite Materials Series. pp. 233–287. Elsevier (1986)

99. Xu, L., Di, Z., Chen, J., Shi, J., Yang, C.: Evolutionary game analysis on behavior strategies of multiple stakeholders in maritime shore power system. Ocean Coast. Manag. 202, 105508 (2021)

100. Arulrajah, A., Disfani, M.M., Haghighi, H., Mohammadinia, A., Horpibulsuk, S.: Modulus of rupture evaluation of cement stabilized recycled glass/recycled concrete aggregate blends. Constr. Build. Mater. 84, 146–155 (2015)

101. Yang, H., Li, Y., Zhou, F.: Propagation of stress pulses in a Rayleigh-Love elastic rod. Int. J. Impact Eng. 153, 103854 (2021)

102. Pei, X., Li, X., Zhao, S., Dong, P., Liu, X., Xie, M.: Low cycle fatigue evaluation of welded structures with arbitrary stress-strain curve considering stress triaxiality effect. Int. J. Fatigue. 162, 106969 (2022)

103. Do Kweon, H., Kim, J.W., Song, O., Oh, D.: Determination of true stress-strain curve of type 304 and 316 stainless steels using a typical tensile test and finite element analysis. Nucl. Eng. Technol. 53, 647–656 (2021)

104. Wick, C.D., Peters, A.J., Li, G.: Quantifying the contributions of energy storage in a thermoset shape memory polymer with high stress recovery: a molecular dynamics study. Polymer (Guildf). 213, 123319 (2021)

105. Lutzer, A., Nagel, C., Murphy, B.A., Aurich, J., Wulf, M., Gautier, C., Aurich, C.: Effects of blue monochromatic light directed at one eye of pregnant horse mares on gestation, parturition and foal maturity. Domest. Anim. Endocrinol. 78, 106675 (2022)

106. Siemer, J., Hilbert, A., Wolf, T., Hart, N., Müller, A., Schild, R.L.: Gender-specific weight estimation of fetuses between 2,501 and 3,999 g–new regression formulae. Fetal Diagn. Ther. 24, 304–309 (2008)

107. Kwak, H., Lis, J.T.: Control of transcriptional elongation. Annu. Rev. Genet. 47, 483–508 (2013)

108. Alaylar, B., Aygün, B., Turhan, K., Karadayi, G., Şakar, E., Singh, V.P., Sayyed, M.I., Pelit, E., Karabulut, A., Güllüce, M.: Characterization of gamma-ray and neutron radiation absorption properties of synthesized quinoline derivatives and their genotoxic potential. Radiat. Phys. Chem. 184, 109471 (2021)

109. Elanchezhian, C., Ramnath, B.V., Ramakrishnan, G., Rajendrakumar, M., Naveenkumar, V., Saravanakumar, M.K.: Review on mechanical properties of natural fiber composites. Mater. Today Proc. 5, 1785–1790 (2018)

110. Tadmor, Z., Gogos, C.G.: Principles of polymer processing. John Wiley & Sons (2006)

111. Treloar, L.R.G.: Stress-strain data for vulcanized rubber under various types of deformation. Rubber Chem. Technol. 17, 813–825 (1944)

112. Katman, H.Y.B., Khai, W.J., Bheel, N., Kırgız, M.S., Kumar, A., Khatib, J., Benjeddou, O.: Workability, strength, modulus of elasticity, and permeability feature of wheat straw ash-incorporated hydraulic cement concrete. Buildings. 12, 1363 (2022)

113. Van Nguyen, M., Lai, V.D., Veyseh, A.P. Ben, Nguyen, T.H.: Trankit: A light-weight transformer-based toolkit for multilingual natural language processing. arXiv Prepr. arXiv2101.03289. (2021)

114. Harkins, W.D., Brown, F.E.: The determination of surface tension (free surface energy), and the weight of falling drops: the surface tension of water and benzene by the capillary height method. J. Am. Chem. Soc. 41, 499–524 (1919)

115. Weymann, R.: The energy spectrum of radiation in the expanding universe. Astrophys. J. 145, 560 (1966)

116. Aim-O, P., Klinkhieo, S., Sophon, M., Sumano, N., Phacheerak, W.,

Phanak, M., Ruangvittayanon, A.: Performance of CsI (Tl) photodiode with optic fiber wire for Gamma-rays and X-rays detection. In: Journal of Physics: Conference Series. p. 12013. IOP Publishing (2022)

117. Abdullah, M.A.H., Rashid, R.S.M., Amran, M., Hejazii, F., Azreen, N.M., Fediuk, R., Voo, Y.L., Vatin, N.I., Idris, M.I.: Recent trends in advanced radiation shielding concrete for construction of facilities: materials and properties. Polymers (Basel). 14, 2830 (2022)

118. Dong, C., Zheng, W., Wang, L., Zhen, W., Zhao, L.: Insight into glass transition temperature and mechanical properties of PVA/TRIS functionalized graphene oxide composites by molecular dynamics simulation. Mater. Des. 206, 109770 (2021)

119. Ninich, O., Et-Tahir, A., Kettani, K., Ghanmi, M., Aoujdad, J., El Antry, S., Ouajdi, M., Satrani, B.: Plant sources, techniques of production and uses of tar: A review. J. Ethnopharmacol. 285, 114889 (2022)

120. Mengesha Medibew, T.: A comprehensive review on the optimization of the fused deposition modeling process parameter for better tensile strength of PLA-printed parts. Adv. Mater. Sci. Eng. 2022, (2022)

121. Cheewasukhanont, W., Siengsanoh, K., Limkitjaroenporn, P., Chaiphaksa, W., Kothan, S., Intachai, N., Kim, H.J., Kaewkhao, J.: The properties of silicate glass specimens for photon, neutron, and charged particles shielding: The roles of Bi2O3. Radiat. Phys. Chem. 201, 110385 (2022)

122. Gulihonenahali Rajkumar, A., Hemath, M., Kurki Nagaraja, B., Neerakallu, S., Thiagamani, S.M.K., Asrofi, M.: An artificial neural network prediction on physical, mechanical, and thermal characteristics of giant reed fiber reinforced polyethylene terephthalate composite. J. Ind. Text. 51, 769S-803S (2022)

123. Yuan, D., Liu, Q.: Photon energy and photon behavior discussions. Energy Reports. 8, 22–42 (2022)

124. Wang, H., Soldemo, M., Degerman, D., Lömker, P., Schlueter, C., Nilsson, A., Amann, P.: Direct Evidence of Subsurface Oxygen Formation in Oxide-Derived Cu by X-ray Photoelectron Spectroscopy. Angew. Chemie Int. Ed. 61, e202111021 (2022)

125. Kabir, Z.: X-r ay Photoconductivity and Typical Large-Area X-r ay Photoconductors. Photocond. Photocond. Mater. Fundam. Tech. Appl. 2, 613–641 (2022)

126. Abdelhamied, M.M., Atta, A., Abdelreheem, A.M., Farag, A.T.M., El Sherbiny, M.A.: Oxygen ion induced variations in the structural and Linear/Nonlinear optical properties of the PVA/PANI/Ag nanocomposite film. Inorg. Chem. Commun. 133, 108926 (2021)

127. Hong, S., Son, G.: Numerical modelling of acoustic cavitation threshold in water with non-condensable bubble nuclei. Ultrason. Sonochem. 83, 105932 (2022)

128. Zemlianskaya, D., Stadnichuk, E., Svechnikova, E.: Influence of hydrometeors on relativistic runaway electron avalanches. arXiv Prepr. arXiv2210.01916. (2022)

129. Akhmeteli, A.: Some Classical Models of Particles and Quantum Gauge Theories. Quantum Reports. 4, 486–508 (2022)

130. Georges, F., Rashad, M.N.H., Stefanko, A., Dlamini, M., Karki, B., Ali, S.F., Lin, P.J., Ko, H.S., Israel, N., Adikaram, D.: Deeply Virtual Compton Scattering Cross Section at High Bjorken x B. Phys. Rev. Lett. 128, 252002 (2022)

131. Wu, J., Wu, B., Wang, Z., Wu, X.: Strong nonreciprocal thermal radiation in Weyl semimetal-dielectric multilayer structure. Int. J. Therm. Sci. 181,

107788 (2022)

132. Le Bourvellec, C., Renard, C.: Interactions between polyphenols and macromolecules: Quantification methods and mechanisms. Crit. Rev. Food Sci. Nutr. 52, 213–248 (2012)

133. Barman, R., Hossain, M.S., Das, A., Rabby, M.K.A.: Investigation of radiation shielding characteristic features of different wood species. Radiat. Phys. Chem. 192, 109927 (2022)

134. ALMisned, G., Bilal, G., Baykal, D. Sen, Ali, F.T., Kilic, G., Tekin, H.O.: Bismuth (III) oxide and boron (III) oxide substitution in bismuth-boro-zinc glasses: A focusing in nuclear radiation shielding properties. Optik (Stuttg). 272, 170214 (2023)

135. Shareef, S.: The influence of greenery and landscape design on solar radiation and UHI mitigation: a case study of a boulevard in a hot climate. World. 3, 175–205 (2022)

136. Hugonin, J.-P., Besbes, M., Ben-Abdallah, P.: Fundamental limits for light absorption and scattering induced by cooperative electromagnetic interactions. Phys. Rev. B. 91, 180202 (2015)

137. Lie, J.L.: Survival analysis of GRID irradiated A549 cells in vitro, (2022)

138. Bordalo, P., Conlon, J.J., Gennaioli, N., Kwon, S.Y., Shleifer, A.: Memory and probability. Q. J. Econ. 138, 265–311 (2023)

139. Baur, M., Uhlmann, N., Pöschel, T., Schröter, M.: Correction of beam hardening in X-ray radiograms. Rev. Sci. Instrum. 90, 25108 (2019)

140. Gao, P.F., Yan, X.G., Li, F.G., Zhan, M., Ma, F., Fu, M.W.: Deformation mode and wall thickness variation in conventional spinning of metal sheets. Int. J. Mach. Tools Manuf. 173, 103846 (2022)

141. Han, L., Shen, J.-F., Liu, Y.-B.: Searching for a vector-like B quark

through a tW decay channel at future electron–positron colliders. Eur. Phys. J. C. 82, 637 (2022)

142. Rammah, Y.S., Olarinoye, I.O., El-Agawany, F.I., Ahmed, E.M., Salem, W.M.: Influence of Sm2O3 content on photon and fast neutron interaction parameters of zinc-tellurite glasses. Radiat. Phys. Chem. 192, 109914 (2022)

143. Shen, Y., Lin, Z., Wei, J., Xu, Y., Wan, Y., Zhao, T., Zeng, X., Hu, Y., Sun, R.: Facile synthesis of ultra-lightweight silver/reduced graphene oxide (rGO) coated carbonized-melamine foams with high electromagnetic interference shielding effectiveness and high absorption coefficient. Carbon N. Y. 186, 9–18 (2022)

144. Külekçi, G.: Investigation of gamma ray absorption levels of composites produced from copper mine tailings, fly ash, and brick dust. J. Mater. Cycles Waste Manag. 24, 1934–1947 (2022)

145. Casasanta, G., Falcini, F., Garra, R.: Beer–Lambert law in photochemistry: A new approach. J. Photochem. Photobiol. A Chem. 432, 114086 (2022)

146. Tousi, E.T.: Monte Carlo simulation of the mass attenuation coefficient and effective atomic number of the Eremurus-Rhizophora ssp. particleboard phantom at the mammography energy range. Prog. Nucl. Energy. 149, 104281 (2022)

147. Shi, C., Cheng, M., Guo, L., Li, R., Li, J.: Attenuation characteristics of Bessel Gaussian vortex beam by a wet dust particle. Opt. Commun. 514, 128138 (2022)

148. Zali, N.M., Yazid, H., Ahmad, M.H.A.R.M.: Neutron shielding behavior of thermoplastic natural rubber/boron carbide composites. In: IOP Conference Series: Materials Science and Engineering. p. 12018. IOP

Publishing (2018)

149. Mutlak, D.A., Ruhaima, A.A.K., Ibrahim, I.T., Mohammed, I.M.: Theoretical Calculation for Pure Epoxy and Lead by Monte Carlo. Pakistan J. Med. Heal. Sci. 17, 585 (2023)

150. Li, J., Carlson, B.E., Yung, Y.L., Lv, D., Hansen, J., Penner, J.E., Liao, H., Ramaswamy, V., Kahn, R.A., Zhang, P.: Scattering and absorbing aerosols in the climate system. Nat. Rev. Earth Environ. 3, 363–379 (2022)

151. Sadeq, M.S., Bashter, I.I., Salem, S.M., Mansour, S.F., Saudi, H.A., Sayyed, M.I., Mostafa, A.G.: Enhancing the gamma-ray attenuation parameters of mixed bismuth/barium borosilicate glasses: using an experimental method, Geant4 code and XCOM software. Prog. Nucl. Energy. 145, 104124 (2022)

152. Sankaran, S., Deshmukh, K., Ahamed, M.B., Pasha, S.K.K.: Recent advances in electromagnetic interference shielding properties of metal and carbon filler reinforced flexible polymer composites: a review. Compos. Part A Appl. Sci. Manuf. 114, 49–71 (2018)

153. Hodge, A.M., Biener, J., Hayes, J.R., Bythrow, P.M., Volkert, C.A., Hamza, A. V: Scaling equation for yield strength of nanoporous open-cell foams. Acta Mater. 55, 1343–1349 (2007)

154. Pejović, M.M.: Influence of low dose rate gamma radiation on breakdown voltage and electrical breakdown time delay of working gas Geiger-Muller chamber. Vacuum. 201, 111116 (2022)

155. Khorasani, A., Gibson, I., Awan, U.S., Ghaderi, A.: The effect of SLM process parameters on density, hardness, tensile strength and surface quality of Ti-6Al-4V. Addit. Manuf. 25, 176–186 (2019)

156. Guo, C.-Y., Lin, T.-L., Hsieh, T.-L.: A Solar-Rechargeable Radiation

Dosimeter Design for Radiation Hazard Zone Located with LoRa Network. Quantum Beam Sci. 6, 27 (2022)

157. Alshabatat, N., Abouel-Kasem, A.: The Effects of Sulfur Content on the Mechanical Properties of Nitrile Butadiene Rubber with Different Aging Conditions. Jordan J. Mech. Ind. Eng. 15, (2021)

158. Riaz, T., Zeeshan, R., Zarif, F., Ilyas, K., Muhammad, N., Safi, S.Z., Rahim, A., Rizvi, S.A.A., Rehman, I.U.: FTIR analysis of natural and synthetic collagen. Appl. Spectrosc. Rev. 53, 703–746 (2018)

159. Kushwaha, A., Rani, R., Patra, J.K.: Adsorption kinetics and molecular interactions of lead [Pb(II)] with natural clay and humic acid. Int. J. Environ. Sci. Technol. 17, 1325–1336 (2020). https://doi.org/10.1007/s13762-019-02411-6

160. Pashaei, S., Hosseinzadeh, S.: Investigation on physicomechanical, thermal, and morphological of dipodal silane-modified walnut shell powder-filled polyurethane green composites and their application for removal of heavy metal ions from water. Polym. Plast. Technol. Eng. 57, 1197–1208 (2018)

161. Mostafa, A., Abouel-Kasem, A., Bayoumi, M.R., El-Sebaie, M.G.: Effect of carbon black loading on the swelling and compression set behavior of SBR and NBR rubber compounds. Mater. Des. 30, 1561–1568 (2009)

162. Mittelman, A., Roman, I.: Tensile properties of real unidirectional Kevlar/epoxy composites. Composites. 21, 63–69 (1990)

163. Wang, Q., Chen, S., Wang, T.: Synthetic Rubber-based IPNs. Micro-and Nano-structured Interpenetr. Polym. Networks From Des. to Appl. 69–107 (2016)

164. Mitić, Ž., Cakić, M., Nikolić, G.: Fourier-Transform IR spectroscopic investigations of Cobalt (II)–dextran complexes by using D 2O isotopic

exchange. Spectroscopy. 24, 269–275 (2010)

165. Mahmood, A., Alam, S.: Performance and degradation analysis of HTV-SiR polymeric composites under the influence of bipolar DC voltages along with multiple stresses. Polym. Bull. 80, 11069–11089 (2023). https://doi.org/10.1007/s00289-022-04592-6

166. Edraki, M., Sheydaei, M., Zaarei, D., Salmasifar, A., Azizi, B.: Protective Nanocomposite Coating Based on Ginger Modified Clay and Polyurethane: Preparation, Characterization and Evaluation Anti-Corrosion and Mechanical Properties. Polym. Sci. Ser. B. 64, 756–764 (2022). https://doi.org/10.1134/S1560090422700531

167. Khorasani, M.T., MoemenBellah, S., Mirzadeh, H., Sadatnia, B.: Effect of surface charge and hydrophobicity of polyurethanes and silicone rubbers on L929 cells response. Colloids Surfaces B Biointerfaces. 51, 112–119 (2006)

168. Zheng, B., Wang, F., Dong, S., Huang, F.: Supramolecular polymers constructed by crown ether-based molecular recognition. Chem. Soc. Rev. 41, 1621–1636 (2012)

169. Rao, C.R.K., Narayan, R., Raju, K.: Interpenetrating and Semi-interpenetrating Polymer Networks of Polyurethane. Micro-and Nano-structured Interpenetr. Polym. Networks From Des. to Appl. 259–282 (2016)

170. Han, I., Aygun, M., Demir, L., Narmanlı, E.: A study on the mean free path and half value layer at various alloys for different photon energies. J. Xray. Sci. Technol. 19, 501–508 (2011)

171. Buyuk, B., Tugrul, A.B.: Gamma and neutron attenuation behaviours of boron carbide–silicon carbide composites. Ann. Nucl. Energy. 71, 46–51 (2014)

الخلاصة

تتضمن هذه الدراسة تحضير عجنات مطاطية بوليمرية تستخدم بشكل رئيسي في إنتاج البدلة الواقية للوقاية من الإشعاع. تم اختيار مطاط السيليكون (SiR) كمادة أساسية في العمل مع البولي يوريثان (PU) بنسب وزنية مختلفة (١٠٠:٠، ٩٠:١٠، ٨٠:٢٠، ٧٠:٣٠، ٦٠:٤٠، ٥٠:٥٠، ٤٠:٦٠، ٣٠:٧٠، ٢٠:٨٠، و١٠٠:٠) pphr مع المصلدات بنسبة 1:1

تم فحص الخواص الميكانيكية مثل قوة الشد، الاستطالة، الصلابة، ومعامل المرونة للخليط المطاطي (SiR:PU). تم قياس الصلابة باستخدام stand ASTM-D1415 (Shore A)، وتم إجراء اختبار الشد باستخدام stand ASTM-D 412-88 (T10-Tensometer). كانت العينة (SiR80:PU20) هي الأكثر ملائمة للخواص الميكانيكية.

تمت إضافة مسحوق الرصاص المايكروي إلى مزيج المطاط ($SiR_{80}:PU_{20}$) كمادة تقوية بنسب تحميل مختلفة هي (٠، ٢٠، ٤٠، ٦٠، ٨٠، ١٠٠، ١٥٠، ٢٠٠، ٢٥٠ و ٣٠٠) جزء في الساعة لكل ($SiR_{80}:PU_{20}$) مزيج مطاطي.

تم إجراء قياس طيف الأشعة تحت الحمراء (FTIR) على الخلائط المطاطية، كما تم إجراء الفحص المجهري الإلكتروني (SEM)، حيث تم توزيع الرصاص المايكروي بالتساوي على المتراكب SiR:PU/micro-Pb. ثم تم فحص الخواص الميكانيكية المتمثلة في الصلابة، قوة الشد، الاستطالة، ومعامل المرونة. تم تقديم العينات لفحص خواص الإشعاع باستخدام عداد كايكر باستخدام عنصري الإشعاع (Cs^{137}) و(Co^{60}) . تم اختيار العينة $SiR_{80}:PU_{20}/micro\text{-}Pb_{300}$ لتكون الأكثر ملائمة.

تم صب المركبات المطاطية ($SiR_{80}:PU_{20}/micro\text{-}Pb_{300}$) باستخدام طريقة الصب، ومن ثم تم استخدام مادة الرصاص النانوية كمادة داعمة بنسب وزنية متعددة (٠، ٠,٢، ٠,٤، ٠,٦، و٠,٨) pphr. تم تشخيص العينات بواسطة FTIR و SEM . كما تم فحص العينات لمعرفة الخواص الميكانيكية والخواص الإشعاعية باستخدام عداد جيجر باستخدام عنصري الإشعاع (Cs^{137}) و (Co^{60}). وفقا لنتائج معامل الامتصاص الخطي (μ) ، ومعامل الامتصاص الكتلي (μ_m)، وسمك النصف ($X_{1/2}$) ، فإن نسبة التحميل لمسحوق الرصاص النانوي والمايكروي في الهكسان تزيد من معاملات الامتصاص الخطي والكتلي وتقلل من سمك النصف. وهذا ينطبق على جميع المصادر المشعة.

وقد أثبت المتراكب النانوي ($SiR_{80}:PU_{20}:Micro\text{-}Pb_{300}:Nano\text{-}Pb_{0.8}$) ذو كفاءة عالية لتوهين الاشعاع مقارنتا بالعينات الاخرى، مما يجعله مناسبًا للاستخدام في تطبيقات الدروع الواقية لحماية العاملين في المجالات الطبية والصناعية.

جمهورية العراق
وزارة التعليم العالي والبحث العلمي
جامعة بابل
قسم الفيزياء

تحضير متراكب مطاط السليكون-بولي يورثان-رصاص لتوهين الاشعاع النووي

أطروحة مقدمة إلى مجلس كلية التربية للعلوم الصرفة -جامعة بابل كجزء من متطلبات نيل شهادة الدكتوراه فلسفة في التربية / الفيزياء

من قبل

موسى هاون نعيم نوفل

بكالوريوس تربية فيزياء
(جامعة بغداد ٢٠٠٣)
ماجستير تربية فيزياء
(جامعة بابل ٢٠١٩)

بأشراف

أ.د. سمير حسن هادي النصراوي
أ.د. محمد حمزه المعموري

١٤٤٥هـ
٢٠٢٣م